

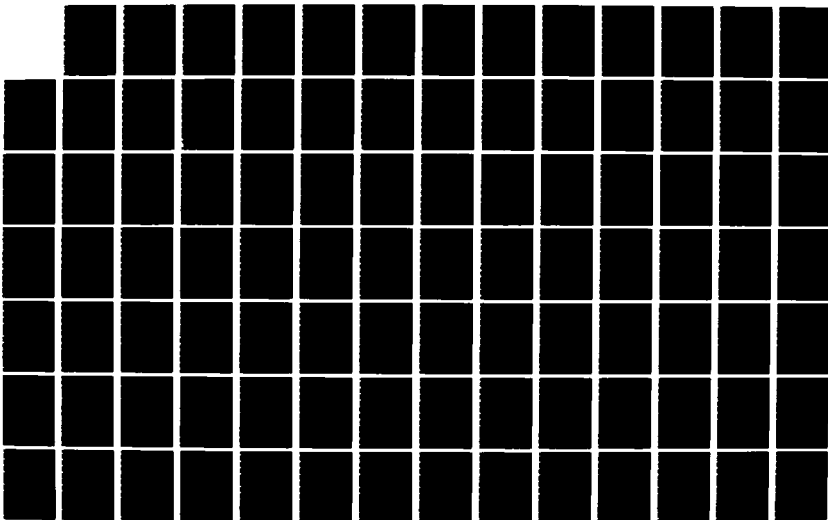
AD-A172 448

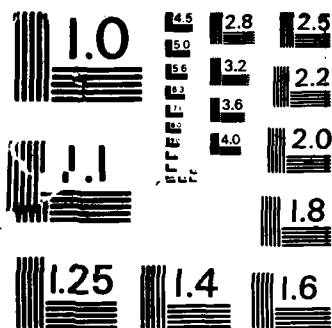
THE COLLAPSE OF COMPOSITE CYLINDRICAL PANELS WITH
VARIOUS CUTOUT LOCATION (U) AIR FORCE INST OF TECH
WRIGHT-PATTERSON AFB OH SCHOOL OF ENGI M F HERMSEN
MAR 86 AFIT/GAE-86M-2 F/G 11/4

1/2

UNCLASSIFIED

NL





MICROCOPY RESOLUTION TEST CHART
NATIONAL BUREAU OF STANDARDS-1963-A

AD-A172 440

DTIC FILE COPY



THE COLLAPSE OF
COMPOSITE CYLINDRICAL PANELS
WITH VARIOUS CUTOUT LOCATIONS
CONSIDERING MATERIAL DEGRADATION

THESIS

MICHAEL F. HERMSEN
First Lieutenant, USAF

This document has been approved
for public release and its
distribution is unlimited

DEPARTMENT OF THE AIR FORCE
AIR UNIVERSITY

AIR FORCE INSTITUTE OF TECHNOLOGY

Wright-Patterson Air Force Base, Ohio

DTIC
ELECTED
OCT 2 1966
A

AFIT/GAE-86M-2

THE COLLAPSE OF
COMPOSITE CYLINDRICAL PANELS
WITH VARIOUS CUTOUT LOCATIONS
CONSIDERING MATERIAL DEGRADATION

THESIS

MICHAEL F. HERMSEN
First Lieutenant, USAF

AFIT/GAE-86M-2

DTIC
ELECTE

OCT 2 1986

Approved for public release; distribution unlimited

AFIT/GAE-86M-2

THE COLLAPSE OF COMPOSITE CYLINDRICAL PANELS
WITH VARIOUS CUTOUT LOCATIONS
CONSIDERING MATERIAL DEGRADATION

THESIS

Presented to the Faculty of the School of Engineering
of the Air Force Institute of Technology
Air University
In Partial Fulfillment of the
Requirements for the Degree of
Master of Science in Aeronautical Engineering

Michael F. Hermsen, B.S.
First Lieutenant, USAF

March 1986

Approved for public release; distribution unlimited



ACKNOWLEDGEMENTS

I would like to express my sincere gratitude to Dr. Anthony Palazotto for his professional guidance and instruction in helping me complete this thesis. My thanks also go to Capt. Ronald Hinrichsen and Major Terry Hinnerichs, my committee members, for their advice and valuable suggestions.

I wish to thank Dr. Khot of the Air Force Flight Dynamics Laboratory, for sponsoring this work and providing the computer funds necessary to conduct the computer analysis.

A special thanks also goes to my parents, Ronald and Charolette Hermsen, for the guidance and support during the early years of my life.

Most of all, I would like to thank my wife, LeaAnn, for her love, support, and understanding throughout this endeavor.

Table of Contents

	Page
Acknowledgements	ii
List of Figures	iv
List of Tables	vii
Symbols	viii
Abstract	1
I. Introduction	2
Background	2
Objective	4
Approach	4
II. Theory	8
Classical Lamination Theory	8
STAGS-C1 Theory	16
Material Degradation Influence on Composites	20
III. Finite Element Modeling	24
Panel Properties	24
Element Selection - 411 Element	26
Grid Sizing	28
IV. Discussion and Results	30
Cutout Location Study	30
Material Degradation Study	65
V. Conclusions	80
VI. Recommendations and Suggestions	82
Appendix A: Miscellaneous Plots	83
Bibliography	139
Vita	142

List of Figures

Figure	Page
1.1 STAGSC-1 Cylindrical Shell Geometry	5
1.2 Cutout Locations within the Composite Cylindrical Panel . .	6
2.1 Definition of Coordinate System	9
2.2 Geometry of an N-Layered Laminate	9
2.3 Forces and Moments on a Laminate	13
3.1 Panel Notation and Material Properties	25
3.2 Quadrilateral 411 Plate Element	27
4.1 Radial Displacement Contour Plot for 2" x 2" Cutout at Collapse Load of 199.4 lbs/in (0/+45/-45/90)s, Cutout A . .	32
4.2 Radial Displacement Contour Plot for 2" x 2" Cutout at Collapse Load of 199.4 lbs/in (0/-45/+45/90)s, Cutout A . .	33
4.3 Eigenvector Contour Plot for 2" x 2" Cutout (0/+45/-45/90)s, Cutout A	35
4.3.1 Linear Radial Displacement Contour Plot for 2" x 2" Cutout Prior to Bifurcation Buckling, (0/+45/-45/90)s, Cutout A . .	36
4.4 Radial Displacement Contour Plot for 2" x 2" Cutout at 50% of Collapse Load, 101 lbs/in, (0/+45/-45/90)s, Cutout A . .	37
4.5 Load Displacement Curve, Linear and Collapse Analysis, for 2" x 2" Cutout and a 4" x 4" Cutout Located at Cutout Position A	38
4.5.1 Load Displacement Curve Taken At a Point Halfway Down the Left Side of the 2" x 2" Cutout Located at Position A . . .	40
4.5.2 Load Displacement Curve Taken At a Point Halfway Down the Left Side of the 4" x 4" Cutout Located at Position A . . .	41
4.6 Eigenvector Contour Plot for 2" x 2" Cutout (0/-45/+45/90)s, Cutout A	42
4.7 Radial Displacement Contour Plot for 4" x 4" Cutout at Collapse Load of 90.0 lbs/in (0/+45/-45/90)s, Cutout A . .	45
4.8 Eigenvector Contour Plot for 4" x 4" Cutout (0/+45/-45/90)s, Cutout A	46

Figure		Page
4.8.1	Linear Radial Displacement Contour Plot for 4" x 4" Cutout Prior to Bifurcation Buckling, (0/+45/-45/90)s, Cutout A . .	48
4.9	Radial Displacement Contour Plot for 2" x 2" Cutout at Collapse Load of 201.2 lbs/in (0/+45/-45/90)s, Cutout B . .	50
4.10	Eigenvector Contour Plot for 2" x 2" Cutout (0/+45/-45/90)s, Cutout B	51
4.11	Radial Displacement Contour Plot for 2" x 2" Cutout at Collapse Load of 147.2 lbs/in (0/+45/-45/90)s, Cutout C . .	53
4.12	Radial Displacement Contour Plot for 2" x 2" Cutout at Collapse Load of 178.6 lbs/in (0/-45/+45/90)s, Cutout C . .	54
4.13	Eigenvector Contour Plot for 2" x 2" Cutout (0/+45/-45/90)s, Cutout C	55
4.14	Eigenvector Contour Plot for 2" x 2" Cutout (0/-45/+45/90)s, Cutout C	56
4.15	Loading Edge Displacement, U, versus Axial Loading for Cutout A and Cutout C	58
4.16	Radial Displacement Contour Plot for 4" x 4" Cutout at Collapse Load of 66.0 lbs/in (0/+45/-45/90)s, Cutout C . .	59
4.17	Radial Displacement Contour Plot for 4" x 4" Cutout at Collapse Load of 66.0 lbs/in (0/-45/+45/90)s, Cutout C . .	60
4.18	Radial Displacement Contour Plot for 2" x 2" Cutout at Collapse Load of 178.6 lbs/in (0/+45/-45/90)s, Cutout C . .	62
4.19	Radial Displacement Contour Plot for 2" x 2" Cutout at Collapse Load of 147.2 lbs/in (0/-45/+45/90)s, Cutout C . .	63
4.20	Moisture Concentration Distribution for Unsymmetric and Symmetric Moisture Conditions	66
4.21	E _z and G ₁₂ Degradation vs Temperature at Constant Values of Moisture Concentration	67
4.22	Degradation in N _x for Unsymmetric Moisture Condition . . .	70
4.23	Degradation in N _x for Symmetric Moisture Condition	71
4.24	Radial Displacement Contour Plot for 2" x 2" Cutout at Collapse Load of 198.5 lbs/in (0/+45/-45/90)s, Cutout A and Symmetric Moisture Distribution, t*=0.001, and Room Temperature (80 °F)	74

Figure		Page
4.25	Radial Displacement Contour Plot for 2" x 2" Cutout at Collapse Load of 169.8 lbs/in (0/+45/-45/90)s, Cutout A and Symmetric Moisture Distribution, $t^*=0.5$, and High Temperature (250 °F)	75
4.26	Radial Displacement Contour Plot for 4" x 4" Cutout at Collapse Load of 82.25 lbs/in (0/+45/-45/90)s, Cutout A and Symmetric Moisture Distribution, $t^*=0.5$, and High Temperature (250 °F)	76
4.27	Reduction in Collapse Load - Symmetric Moisture Condition .	78
4.28	Reduction in Collapse Load - Unsymmetric Moisture Condition	79
A1.1 - A1.3	Radial Displacement as a Function of Location taken 3, 6, and 9 inches from the Loading Edge . . .	85
A1.4 - A1.12	Moment Profiles as a Function of Panel Location taken 3, 6, and 9 inches from the Loading Edge . . .	88
A2.1 - A2.3	Loading Edge Displacement vs Applied Load, Cutout A for +45, -45, and both +45 and -45 Second Ply . . .	98
A2.4 - A2.6	Loading Edge Displacement vs Applied Load, Cutout C for +45, -45, and both +45 and -45 Second Ply . . .	101
A2.7 - A2.9	Loading Edge Displacement vs Applied Load, Cutout D for +45, -45, and both +45 and -45 Second Ply . . .	104
A3.1 - A3.6	W Profiles at 4.5 and 5.0 inches from the Loading Edge as a function of Location, for Cutouts A, C, and D; +45 and -45 Second Ply	108
A4.1 - A4.18	Moment Profiles at $x=4.750$ and $x=7.250$ inches from the Loading Edge for Cutout A, C, and D	115
A4.19 - A4.24	N_x at the Loading Edge of the Panel at Collapse Load for Cutout A, C and D; +45 and -45 Second Ply .	133

List of Tables

Table		Page
3.1	Mesh Refinement Results for a 2" x 2" Cutout	29
4.1	Ply Layup, Cutout Size, and Cutout Location	31
4.2	Discontinuity Location Study Results	64
4.3	Moisture Conditions	68
4.4	Relation Between Real and Dimensionless Time	68
4.5	Environmental Effects Study Results	77

Symbols

A_{ij}	Extensional stiffnesses
B_{ij}	Coupling stiffnesses
C	Moisture concentration
C_0, C_1, C_2	Moisture concentration initial conditions
D_{ij}	Bending stiffnesses
E_1	Longitudinal modulus of elasticity
E_2	Transverse modulus of elasticity
F	Degrees Fahrenheit
G_{12}	Shear modulus of elasticity
h	Laminate thickness
K	Diffusion coefficient
K_x, K_y, K_{xy}	Curvatures
M_x, M_y, M_{xy}	Moment resultants
N_x, N_y, N_{xy}	Force resultants
N_x	Bifurcation load for axial loading
N_{x-orig}	Original bifurcation load
\bar{Q}_{ij}	Reduced stiffnesses
$\bar{\bar{Q}}_{ij}$	Transformed reduced stiffnesses
R, r	Panel's radius
R_U, R_V, R_W	Rotations about the x, y, and z coordinate axes
t	Time
t^*	Dimensionless time
T_g	Glass transition temperature
u, v, w	Displacements in the x, y, and z directions
U, V, W	Displacements in the X, Y, and Z directions

x, y, z	Spacial coordinates
X, Y, Z	Structural coordinate directions
$1, 2, 3$	Lamina principle axis directions
β, ϕ	Rotation
γ	Shear strain
ϵ	Normal strain
θ	Ply orientation
ν	Poisson's ratio
σ	Normal stress
τ	Shear stress
∂	Partial derivative
A_{rs}	System's linear stiffness matrix
$N1_{rs}$	Linear displacement matrix
$N2_{rs}$	Quadratic displacement matrix
q	Displacement vector
R_s	Surface force vector
$()_s$	Denotes a ply orientation that is symmetric with respect to the middle surface
$()^0$	Zero superscript denotes a middle surface value

ABSTRACT

An analytical study, using the STAGSC-1 computer code, was conducted on a graphite/epoxy (AS4/3501) composite cylindrical panel acting under compressive loading considering cutouts positioned at critical locations within the panels surface area. The study also investigated the material degradation effects of temperature and moisture on the collapse load of these cylindrical panels. Two temperatures (80 and 250 °F), in both a symmetric and unsymmetric moisture condition, were investigated. The overall material degradation characteristics were investigated by degrading the E_2 and G_{12} moduli of the individual plies.

It was found that the effects of moisture and temperature (material degradation effects) can greatly reduce the collapse load of the cutout panel. A 15% decrease in the collapse load occurred at the saturated moisture conditions and elevated temperatures. The material degradation effects were found to produce the same results no matter where the cutout was located. The panel with cutouts was less effected, at the saturated moisture condition and elevated temperature, then that of a panel with no cutout.

It was also found that the collapse load, as expected, was dependent upon the location of the cutout within the panel. There was a decrease in the collapse load by as much as 26.2% when the cutout was moved from the center of the panel to a position closer to the side edge. There was very little change, 1%, when the cutout was positioned closer to the loading edge of the panel. Ply layup was also of great importance. There was a 21.3% increase or decrease in the collapse load if a certain ply layup (0/±45/90)s, (symmetrically exchanging of the second and third plies) was chosen for the cutout positioned near the side supports.

I. INTRODUCTION

Background

Large, lightweight shell structures are used extensively in aircraft for both strength and stability. These shell structures are greatly influenced by either reinforced or nonreinforced cutouts and material degradation conditions. Due to these influences and with the recent advances, a vast number of these shells are made from composite materials. The composite materials are desired because of the high strength to weight ratio when compared to conventional materials. Therefore, from a practical point of view, there is a need for further research into composite shell structures and the effect of cutouts and material degradation conditions on the stability of the shell structures.

Very few references can be found dealing with buckling of composite panels and plates under axial compression with cutouts. In contrast, numerous studies have been carried out on isotropic plates and cylindrical panels without cutouts [1-6]. These studies centered around various boundary conditions and their affect on the buckling load. If one considered the area of axially loaded isotropic panels with cutouts [7-11], mainly, centered circular cutouts were analyzed numerically by finite difference techniques to determine the buckling and bifurcation loads.

As mentioned earlier, composite panels have become an important part of aerospace structures due to their excellent strength to weight ratio. Composite cylindrical panels without cutouts have been studied [12-16],

but very little work can be found dealing with composite panels with cutouts. Janisse [17] and Lee [18] are two authors who have studied the problem of cutouts in composite cylindrical panels. Janisse [17] found that the collapse characteristics of composite cylindrical panels are dependent on ply layup and size of the cutout. Lee [18], in a follow-up investigation, studied the effects of the cutout aspect ratio and concluded that as the surface area of the cutout increased the buckling load decreased with the effects of nonlinearity becoming more pronounced. These are the only studies which deal specifically with composite cylindrical panels containing cutouts. This shows that very little is known about the effect of cutouts and further study into this area is needed.

Temperature and moisture, the main emphasis of an environmental study, is another important area of interest in composite shell structures. Snead [19], while examining the effects of moisture and temperature on the instability of cylindrical composite panels, concluded that there was a definite degradation of the bifurcation load due to elevated temperatures and moisture exposure. Various other authors [20-23] have looked at the environmental effects and have come to the same conclusion. There is, however, a lack of research into how elevated temperature and moisture exposure (material degradation effects) relates to the collapse of a composite cylindrical panel with a cutout.

With a need for faster, lighter aircraft and the increasing interest in space, a better understanding of composite cylindrical shells with cutouts is needed. All of the previous cutout studies that were found dealt with centrally located cutouts and standard conditions. This

thesis addresses the issue of eccentrically located cutouts in composite cylindrical panels, and the effect of material degradation due to temperature and moisture on the collapse load of an axially loaded panel.

Objective

The major purpose of this thesis is to study the effects of material degradation on panels with cutouts. To observe this effect, one first has to establish the critical positions of specific size cutouts within the panel. In order to do this, the effect of a cutout located at different positions within the composite cylindrical panel subjected to an axial loading will be studied analytically using the Structural Analysis of General Shells (STAGSC-1) computer program. Then secondly, material degradation effects due to temperature and moisture at the critical cutout locations will be analyzed. Upon completion, this thesis will allow for a better understanding of axially loaded composite cylindrical shells with cutouts under less than perfect conditions.

... Shell analysis, Finite elements.

Approach

Due to the presence of the geometric discontinuity (cutout), a nonlinear analysis was used. This nonlinear analysis is part of the STAGSC-1 finite element computer program [26-27], developed by Lockheed, which incorporates a modified Newton-Raphson iteration technique along

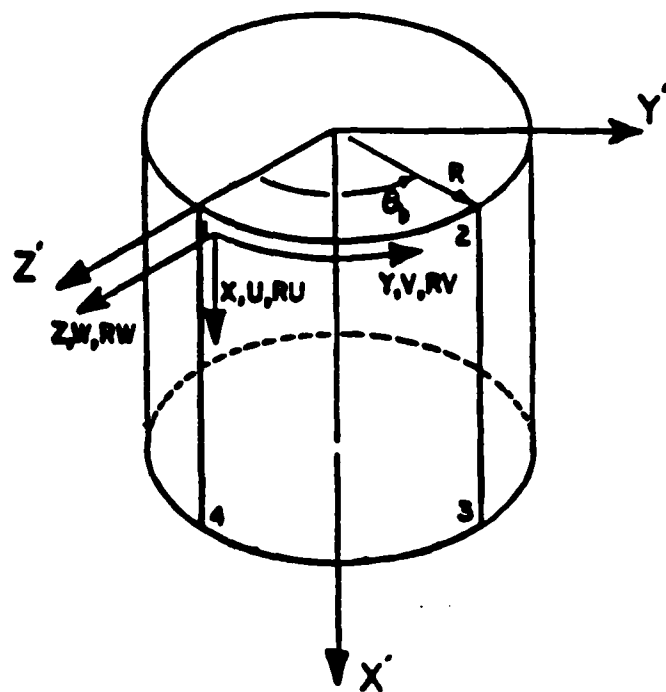


Fig. 1.1 STAGSC-1 Cylindrical Shell Geometry

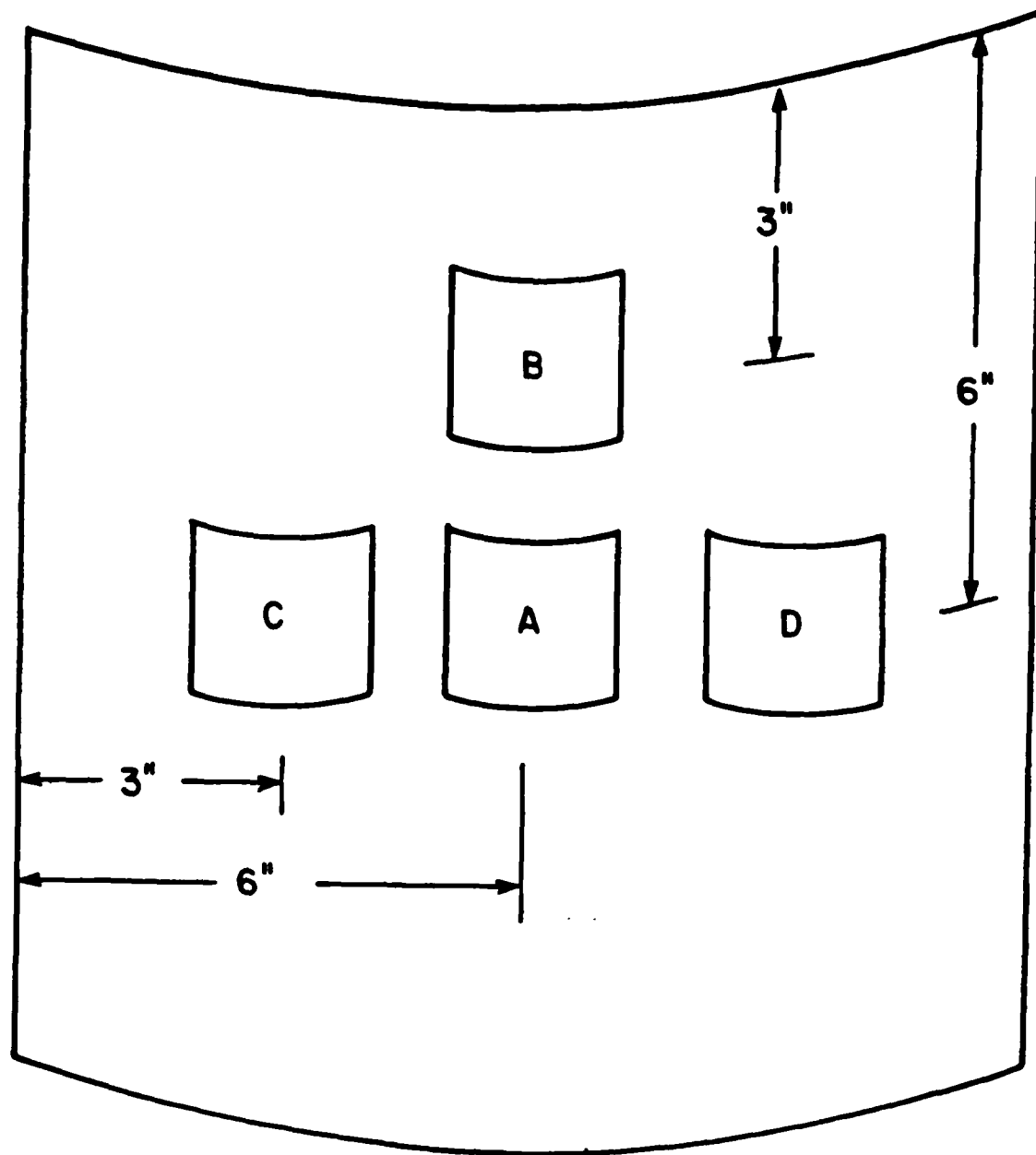


Fig. 1.2 Cutout Locations within the Composite Cylindrical Panel

with large displacement theory and moderate rotations to study the collapse of cylindrical panels with cutouts. The cylindrical shell geometry used by the STAGSC-1 computer program is shown in Fig 1.1.

Eccentrically located cutouts were investigated by positioning the cutout at four different locations as shown in Fig. 1.2. Both a 2" x 2" cutout (2.78% of panels total area) and a 4" x 4" cutout (11.1%) were examined along with the effect of interchanging ply positions.

Material degradation effects on a cutout located at different positions within the panel were also investigated. Cutout locations A and C, Fig. 1.2, were chosen for this analysis. For the cylindrical panel, a symmetric and a unsymmetric moisture concentration condition was used. Two time units were chosen for each of the moisture conditions; a steady state distribution and a near zero moisture absorption. These time units represent the two extremes of moisture conditions. Finally, two different temperatures were chosen, 80 °F (300 °K) and 250 °F (394 °K). The runs produced by the combination of the fore-mentioned conditions represents a near standard zero condition (room temperature and near zero moisture) and that of a high temperature and fully saturated moisture condition.

THEORY

Classical Lamination Theory

An in-depth understanding of composite laminae behavior is needed if one is going to analyze composite structures. Presented here, is a brief overview of the basic principles. The reader should refer to Ref. [24] and [25] for the in-depth development of these relations and a better understanding of Classical Lamination Theory.

For a lamina of orthotropic material, the plane stress constitutive relations in principal material coordinates are

$$\begin{Bmatrix} \sigma_1 \\ \sigma_2 \\ \tau_{12} \end{Bmatrix} = \begin{bmatrix} Q_{11} & Q_{12} & 0 \\ Q_{12} & Q_{22} & 0 \\ 0 & 0 & Q_{66} \end{bmatrix} \begin{Bmatrix} \epsilon_1 \\ \epsilon_2 \\ \gamma_{12} \end{Bmatrix} \quad (1)$$

and

$$\begin{aligned} Q_{11} &= E_1 / (1 - \nu_{12} \nu_{21}) \\ Q_{12} &= \nu_{12} E_2 / (1 - \nu_{12} \nu_{21}) = \nu_{21} E_1 / (1 - \nu_{12} \nu_{21}) \\ Q_{22} &= E_2 / (1 - \nu_{12} \nu_{21}) \\ Q_{66} &= G_{12} \end{aligned} \quad (2)$$

where Q_{ij} 's are the reduced stiffnesses in terms of the engineering constants and ϵ_1 and ϵ_2 are normal strains and γ_{12} is the shear strain for the lamina principle axes as shown in Fig. 2.1. Poisson's ratio, ν_{1j} , and shear modulus, G_{12} , for the 1-2 plane are defined as

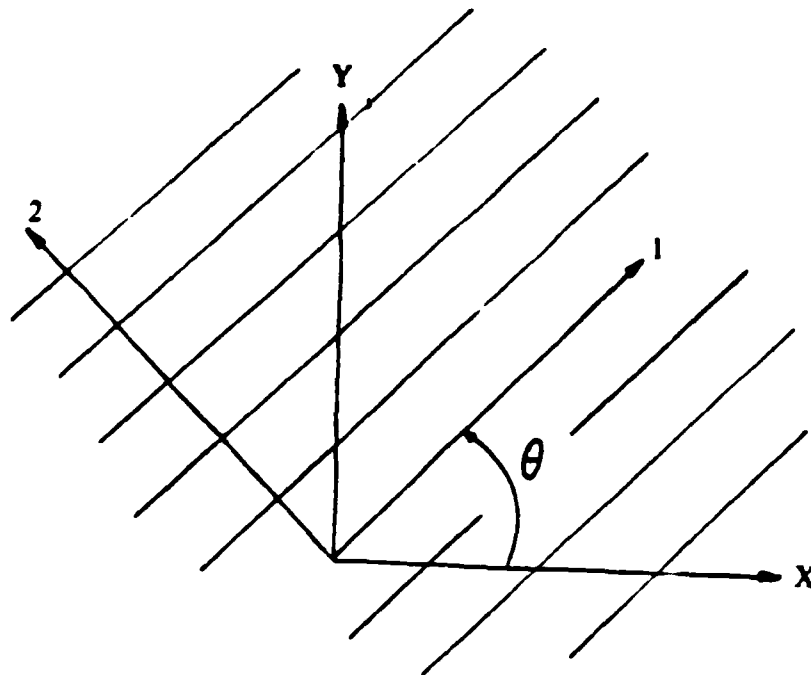


Fig. 2.1 Definition of Coordinate System

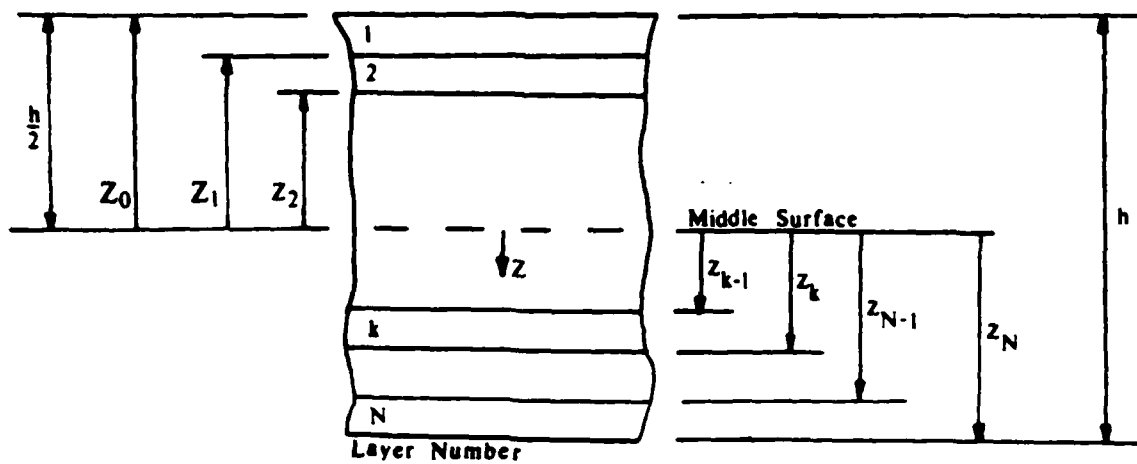


Fig. 2.2 Geometry of an N-Layered Laminate

$$\begin{aligned}
\nu_{12} &= -(\epsilon_2 / \epsilon_1) \\
\nu_{21} &= -(\epsilon_1 / \epsilon_2) \\
G_{12} &= (\tau_{12} / \gamma_{12})
\end{aligned}
\tag{3}$$

So far, orthotropic materials have been dealt with in their principal material directions. Expanding these relationships to cover any coordinate system, with the fiber axis oriented at some angle θ , (Fig. 2.1), the stresses become

$$\begin{Bmatrix} \sigma_x \\ \sigma_y \\ \tau_{xy} \end{Bmatrix} = \begin{bmatrix} Q_{11} & Q_{12} & Q_{16} \\ Q_{12} & Q_{22} & Q_{26} \\ Q_{16} & Q_{26} & Q_{66} \end{bmatrix} \begin{Bmatrix} \epsilon_x \\ \epsilon_y \\ \gamma_{xy} \end{Bmatrix}
\tag{4}$$

where

$$\begin{aligned}
Q_{11} &= Q_{11}\cos^4 \theta + 2(Q_{12} + 2Q_{66})\sin^2 \theta \cos^2 \theta + Q_{22}\sin^4 \theta \\
Q_{12} &= (Q_{11} + Q_{22} - 4Q_{66})\sin^2 \theta \cos^2 \theta + Q_{12}(\sin^4 \theta + \cos^4 \theta) \\
Q_{22} &= Q_{11}\sin^4 \theta + 2(Q_{12} + 2Q_{66})\sin^2 \theta \cos^2 \theta + Q_{22}\cos^4 \theta \\
Q_{16} &= (Q_{11} - Q_{12} - 2Q_{66})\sin \theta \cos^3 \theta + (Q_{12} - Q_{22} + 2Q_{66}) \\
&\quad \sin^3 \theta \cos \theta \\
Q_{26} &= (Q_{11} - Q_{12} - 2Q_{66})\sin^3 \theta \cos \theta + (Q_{12} - Q_{22} + 2Q_{66}) \\
&\quad \sin \theta \cos^3 \theta \\
Q_{66} &= (Q_{11} + Q_{22} - 2Q_{12} - 2Q_{66})\sin^2 \theta \cos^2 \theta + Q_{66}(\sin^4 \theta + \cos^4 \theta)
\end{aligned}
\tag{5}$$

The above equations are derived for individual lamina and in order to define the stress and strain variations through the thickness (Fig. 2.2), each k^{th} layer of the multilayered laminate can be written as

$$\{\sigma\}_k = [Q]_k \{\epsilon\}_k \quad (6)$$

By extending the stress-strain relationships to the multilayered laminate two assumptions are made. First, the laminate is presumed to consist of perfectly bonded laminae. These laminae are infinitesimally thin with the displacements continuous across the laminae so that no lamina can slip relative to another. Secondly, the Kirchhoff-Love hypothesis applies. This hypothesis states that normals to the mid-surface remain plane and normal to that surface after bending.

The middle surface strain-displacement relations for a cylindrical laminate with moderately large rotations of tangents to the panel reference are given by Sanders' kinematic relations without initial imperfections as

$$\begin{aligned} x^\circ &= u^\circ, x = u, x + 1/2 \phi_x^2 + 1/2 \phi^2 \\ y^\circ &= v^\circ, y = v, y + w/R + 1/2 \phi_y^2 - 1/2 \phi^2 \\ xy^\circ &= v, x + u, y + \phi_x \phi_y \end{aligned} \quad (7)$$

where u , v , and w denote the axial, circumferential, and radial components of the mid-surface displacement. The ϕ 's are the rotation components and in terms of displacement are

$$\begin{aligned} \phi_x &= -w, x \\ \phi_y &= -w, y + v/R \\ \phi &= 1/2(v, x - u, y) \end{aligned} \quad (8)$$

where R is the radius of curvature of the panel at the mid-surface.

The middle surface curvatures are then written as

$$\begin{aligned} \kappa_x &= \phi_{x,x} \\ \kappa_y &= \phi_{y,y} \\ 2 \kappa_{xy} &= 2 \kappa_{yx} = \phi_{y,x} + \phi_{x,y} + \phi/R \end{aligned} \quad (9)$$

Using the Kirchhoff-Love hypothesis with the known middle surface strains and curvatures, the strain-curvature relationship for a laminate becomes

$$\begin{Bmatrix} \epsilon_x \\ \epsilon_y \\ \gamma_{xy} \end{Bmatrix} = \begin{Bmatrix} \epsilon^0_x \\ \epsilon^0_y \\ \gamma^0_{xy} \end{Bmatrix} + z \begin{Bmatrix} \kappa_x \\ \kappa_y \\ 2 \kappa_{xy} \end{Bmatrix} \quad (10)$$

If the strain-curvature relationship, (Eqn. 10), which represents the strain variation through the thickness, is substituted into the stress-strain relations, (Eqn. 6), the stress for any k^{th} layer can be expressed in terms of the middle surface strains and curvatures as

$$\begin{Bmatrix} \sigma_x \\ \sigma_y \\ \gamma_{xy} \end{Bmatrix}_k = \begin{bmatrix} \bar{Q}_{11} & \bar{Q}_{12} & \bar{Q}_{16} \\ \bar{Q}_{12} & \bar{Q}_{22} & \bar{Q}_{26} \\ \bar{Q}_{16} & \bar{Q}_{26} & \bar{Q}_{66} \end{bmatrix}_k \left\{ \begin{Bmatrix} \epsilon^0_x \\ \epsilon^0_y \\ \gamma^0_{xy} \end{Bmatrix} + z \begin{Bmatrix} \kappa_x \\ \kappa_y \\ 2 \kappa_{xy} \end{Bmatrix} \right\} \quad (11)$$

By integrating the stresses of each laminate layer, the resultant forces and moments acting on a laminate become for example

$$\begin{Bmatrix} N_x \\ M_x \end{Bmatrix} = \int_{-t/2}^{t/2} \begin{Bmatrix} \sigma_x \\ \sigma_y \end{Bmatrix} z \, dz \quad (12)$$

where N_x and M_x are the force and moment per unit length of the cross section of the laminate as shown in Fig. 2.3.

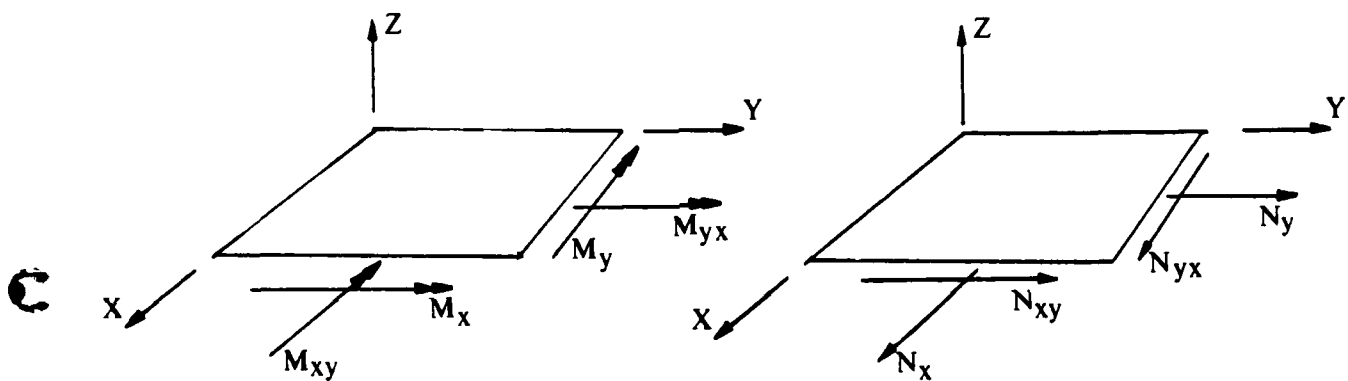


Fig. 2.3 Forces and Moments on a Laminate

If all the forces and moments for the N-layered laminate are collected, the result is

$$\begin{Bmatrix} N_x \\ N_y \\ N_{xy} \end{Bmatrix} = \int_{-t/2}^{t/2} \begin{Bmatrix} \sigma_x \\ \sigma_y \\ \tau_{xy} \end{Bmatrix} dz = \sum_{k=1}^N \int_{z_{k-1}}^{z_k} \begin{Bmatrix} \sigma_x \\ \sigma_y \\ \tau_{xy} \end{Bmatrix}_k dz \quad (13)$$

and

$$\begin{Bmatrix} M_x \\ M_y \\ M_{xy} \end{Bmatrix} = \int_{-t/2}^{t/2} \begin{Bmatrix} \sigma_x \\ \sigma_y \\ \tau_{xy} \end{Bmatrix} z dz = \sum_{k=1}^N \int_{z_{k-1}}^{z_k} \begin{Bmatrix} \sigma_x \\ \sigma_y \\ \tau_{xy} \end{Bmatrix}_k z dz \quad (13)$$

where the z_k and z_{k-1} layers are defined in Fig. 2.2.

Looking closely at Eqn. 13, and substituting in Eqn. 11 while also recalling the fact that the stiffness matrix, $[Q_{ij}]$, is constant within the lamina yields the following

$$\begin{Bmatrix} N_x \\ N_y \\ N_{xy} \end{Bmatrix} = \sum_{k=1}^N \begin{bmatrix} Q_{11} & Q_{12} & Q_{16} \\ Q_{12} & Q_{22} & Q_{26} \\ Q_{16} & Q_{26} & Q_{66} \end{bmatrix} \int_{z_{k-1}}^{z_k} \begin{Bmatrix} \epsilon^o_x \\ \epsilon^o_y \\ \gamma^o_{xy} \end{Bmatrix} dz + \int_{z_{k-1}}^{z_k} \begin{Bmatrix} \kappa_x \\ \kappa_y \\ \kappa_{xy} \end{Bmatrix} z dz \quad (14)$$

$$\begin{Bmatrix} M_x \\ M_y \\ M_{xy} \end{Bmatrix} = \sum_{k=1}^N \begin{bmatrix} Q_{11} & Q_{12} & Q_{16} \\ Q_{12} & Q_{22} & Q_{26} \\ Q_{16} & Q_{26} & Q_{66} \end{bmatrix} \int_{z_{k-1}}^{z_k} \begin{Bmatrix} \epsilon^o_x \\ \epsilon^o_y \\ \gamma^o_{xy} \end{Bmatrix} z dz + \int_{z_{k-1}}^{z_k} \begin{Bmatrix} \kappa_x \\ \kappa_y \\ \kappa_{xy} \end{Bmatrix} z^2 dz$$

Recalling that ϵ^o_x , ϵ^o_y , γ^o_{xy} , κ_x , κ_y , and κ_{xy} are not functions of z but are middle surface values so they can be removed from the summation signs and rewritten as

$$\begin{Bmatrix} N_x \\ N_y \\ N_{xy} \end{Bmatrix} = \begin{bmatrix} A_{11} & A_{12} & A_{16} \\ A_{12} & A_{22} & A_{26} \\ A_{16} & A_{26} & A_{66} \end{bmatrix} \begin{Bmatrix} \epsilon^o_x \\ \epsilon^o_y \\ \gamma^o_{xy} \end{Bmatrix} + \begin{bmatrix} B_{11} & B_{12} & B_{16} \\ B_{12} & B_{22} & B_{26} \\ B_{16} & B_{26} & B_{66} \end{bmatrix} \begin{Bmatrix} \kappa_x \\ \kappa_y \\ \kappa_{xy} \end{Bmatrix} \quad (15)$$

$$\begin{Bmatrix} M_x \\ M_y \\ M_{xy} \end{Bmatrix} = \begin{bmatrix} B_{11} & B_{12} & B_{16} \\ B_{12} & B_{22} & B_{26} \\ B_{16} & B_{26} & B_{66} \end{bmatrix} \begin{Bmatrix} \epsilon^o_x \\ \epsilon^o_y \\ \gamma^o_{xy} \end{Bmatrix} + \begin{bmatrix} D_{11} & D_{12} & D_{16} \\ D_{12} & D_{22} & D_{26} \\ D_{16} & D_{26} & D_{66} \end{bmatrix} \begin{Bmatrix} \kappa_x \\ \kappa_y \\ \kappa_{xy} \end{Bmatrix} \quad (15)$$

where

$$\begin{aligned} A_{ij} &= \sum_{k=1}^N (\bar{Q}_{ij})_k (z_k - z_{k-1}) \\ B_{ij} &= 1/2 \sum_{k=1}^N (\bar{Q}_{ij})_k (z_k^2 - z_{k-1}^2) \\ D_{ij} &= 1/3 \sum_{k=1}^N (\bar{Q}_{ij})_k (z_k^3 - z_{k-1}^3) \end{aligned} \quad (16)$$

The A_{ij} 's are called the extensional stiffnesses, the B_{ij} 's are called the coupling stiffnesses, and the D_{ij} 's are called the bending stiffnesses.

STAGSC-1 Theory

The Structural Analysis of General Shells (STAGSC-1) is a computer program developed by Lockheed Palo Alto Research Laboratory [26-27]. The program is an energy based finite element program that uses a Newton-Raphson nonlinear equation solver. STAGSC-1 is a general purpose, thin shell, structural analysis program used to analyze general shells under various static, thermal, and mechanical loadings. This nonlinear analysis, used to study the collapse of shells with cutouts, allows for the determination of the critical load.

According to the energy method, a system's total potential energy is used to derive its equilibrium equations from which stability can be determined by the solution to an eigenvalue problem. A shell's total potential energy is equal to its internal strain energy minus the product of the external forces and their respective deflections.

An element's strain energy is given by [13]:

$$U = 1/2 \int_{\text{area}} \{ \epsilon \}^T [N] \{ \epsilon \}_0 dA \quad (17)$$

where

$$[\epsilon]_0 = \begin{bmatrix} \epsilon_x \\ \epsilon_y \\ 2 \epsilon_{xy} \\ \kappa_x \\ \kappa_y \\ 2 \kappa_{xy} \end{bmatrix} \quad (18)$$

and

$$[N] = \begin{bmatrix} [A] & [B] \\ [B] & [D] \end{bmatrix} \quad (19)$$

The expressions for the mid-surface strains were presented in Eqn's. 7 and 9 and $[N]$ was given in Eqn's. 15 and 16. In general, the strain vector $[\epsilon]_0$ is a function of the mid-surface displacements u, v, w , the first order derivatives of u, v, w and the second derivative of w . Therefore, we can let a vector $[d]$ represent this functional dependence of $[\epsilon]_0$ on the displacement by

$$[d]^T = [u, u_x, u_y, v, v_x, v_y, w, w_x, w_y, w_{xx}, w_{xy}, w_{yy}] \quad (20)$$

By using vector $[d]$, Bauld [13] carried out the integration of Eqn. 17 and found that the expression for strain energy is comprised of three distinct parts. The first part is quadratic in displacements, the second cubic in displacements, and the third quartic in displacements. In a finite element analysis, vector $[d]$ is represented by an element's shape functions and nodal degrees of freedom. Thus, the strain energy can be expressed in terms of an element's degrees of freedom. An element's external potential energy is obtained by using a similar finite element analysis on its external forces. The strain energy and external potential energy are combined to give the total system's potential energy, V , and can be written in the form given by Bauld [13] as:

$$V = (1/2 A_{rs} + 1/6 N1_{rs} + 1/12 N2_{rs})q_r q_s - R_s q_s \quad (21)$$

A_{rs} is the system's linear stiffness matrix with no dependence on the displacement vector, q . $N1_{rs}$ and $N2_{rs}$ are matrices with linear and quadratic dependence, respectively, on displacement. R_s is the surface force vector.

The principle of total potential energy states that the equilibrium configuration of a conservative mechanical system corresponds to a stationary value of the total potential energy of the system. Therefore, taking the first variation of Eqn. 21 and setting it equal to zero, we have a set of nonlinear, algebraic equations of the form

$$(A_{rs} + 1/2 N1_{rs} + 1/3 N2_{rs})q_s - R_s = 0 \quad (22)$$

Loss of stability (collapse), results when the second variation of the system's total potential energy ceases to be positive definite, or

$$\text{DET} (A_{rs} + N1_{rs} + N2_{rs}) = 0 \quad (23)$$

Equation 23 is also used by STAGSC-1 to solve the eigenvalue problem of the form

$$[A] + \lambda[B] + \lambda^2[C] = 0 \quad (24)$$

where $[B]$ and $[C]$ represent nonlinear stiffness matrices in unknown

displacements and products of displacements, respectively. For a linear analysis the matrix C is neglected and λ is the proportionality constant of a convenient load level used in the equilibrium equations (Eqn's. 22) to solve for the unknown displacements. The quantities $[A]$ and $[B]$ or equivalently, A_{rs} and N_{lrs} are calculated once based on the equilibrium displacements. Finally, the load proportionality parameter, λ , is incremented until a sign change on the left side of Eqn. 23 occurs, signifying bifurcation.

MATERIAL DEGRADATION INFLUENCES ON COMPOSITES

Extreme temperature, near or beyond the polymer's glass transition temperature, and moisture (water absorbed by the polymer resin) can cause severe degradation of the superior properties of the composites. The degradation factors which influence the resin properties are increased with temperature, with the absorption by the polymeric resin material of a swelling agent such as water vapor, and with the sudden expansion of absorbed gases in the resin [21]. The composite fibers, on the other hand, which are typically graphite, are not affected by either moisture or temperature. Therefore, the resin which is influenced by temperature and moisture, plays the most important part in the changing of the composite's properties.

Temperature and moisture act on the polymeric resin in two ways. The first is that moisture absorption makes the resin swell, causing a change in the residual stresses of the composite and possibly micro-crack formation. This matrix swelling and the rapid heating eventually leads to surface cracks. Secondly, moisture absorbed in the resin results in plasticization of the resin, the result of the lowering of the glass transition temperature, T_g . The glass transition temperature is actually a temperature range below which the resin is essentially brittle and above which it behaves rubbery. As the resin changes, one observes a decrease in the tensile properties and a reduction in the shear moduli of the composite as well as a slight increase in the longitudinal elastic moduli [23].

The primary mechanism for absorption of moisture is through diffusion. In this analysis, Fick's second law of diffusion [28], which under certain circumstances has been shown to correlate with test data [23], was used. Fick developed this equation in 1855 by drawing an analogy between heat conduction in a solid and diffusion through the solid. Fick's equation can be written as

$$\partial C / \partial t = K (\partial^2 C / \partial z^2) \quad (25)$$

where C is a measure of moisture of the laminate as a function of time and distance through the thickness, z equals the space coordinate measured normal to the surface, K the diffusion constant, and t the time. C is expressed as a ratio of the gain in the weight of the laminate due to the absorption of moisture divided by the original weight of the laminate.

The solution to this partial differential equation (Eqn. 25) with boundary and initial conditions pertinent to the problem is shown below. This series solution in a slightly different form is found in Sec. 4.3.5 of Ref.[23]

$$C(z,t) = C_1 + (C_2 - C_1)*(z/h) + \quad (26)$$

$$\begin{aligned} & (z/\pi) \sum_{n=1}^{\infty} ((C_2 \cos n\pi - C_1)/n) * (\sin(n\pi z/h)) * (\exp(-Kn^2 \pi^2 t)/h^2) + \\ & (4C_0/\pi) \sum_{m=0}^{\infty} (1/2m+1) * (\sin((2m+1)\pi z/h)) * (\exp(-K(2m+1)^2 \pi^2 t)/h^2) \end{aligned}$$

where C is as previously defined, C_0 the initial, uniform moisture concentration through the thickness of the laminate, C_1 and C_2 the moisture concentration boundary conditions at the inside ($-z$) and the outside ($+z$) surfaces of the laminate, respectively, and h the thickness of the laminate.

This series solution, which is a combination of a steady state moisture effect and a transient moisture distribution, allows for the determination of the through the thickness moisture distribution. Because of a series solution, accuracy is dependent on the number of terms that are used. Snead [19] wrote a computer program which calculates the solution to the series approximation using the first 14 terms of the approximation, and thus the mechanical properties of each ply can be determined.

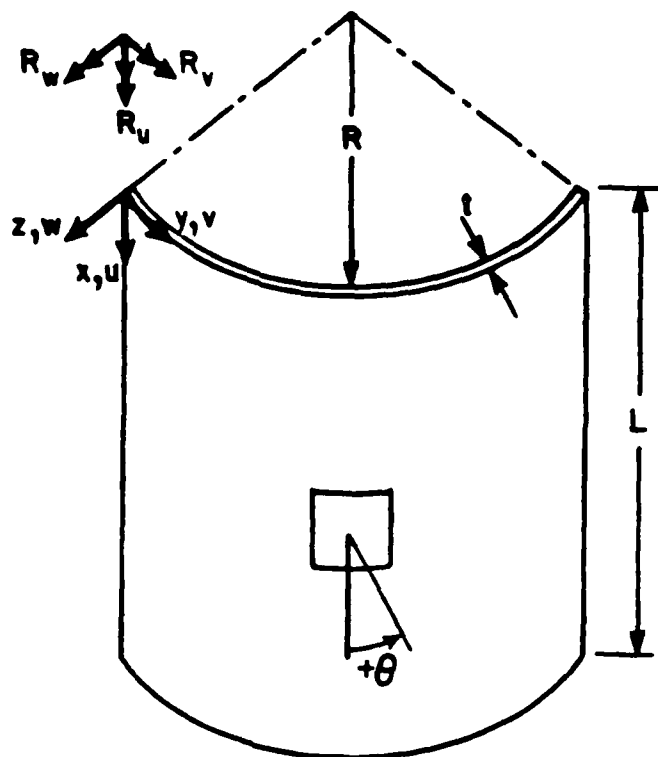
There are limitations on the application of Fick's equation. The series solution of Fick's equation assumes that the moisture diffusion coefficient K is constant (for this study K equals 0.52537×10^{-10} in²/sec [24]). In reality, the diffusion coefficient is a function of the laminates temperature and moisture concentration and a series solution to the Fick equation using this functional approach can be found in Ref. [29]. However, for composite material studies, the diffusion process may be assumed to take place at a constant temperature. This is true because moisture diffusion is a relatively slow process with many months and years required before the moisture concentration distribution through the laminate achieves equilibrium. Thus, K is considered to be a constant as is usually done when the Fick equation is incorporated into composite material studies [19,24].

Fick's equation to model moisture diffusion in composites is also affected by rapid temperature changes. Rapid thermal heating of the laminate near the materials' T_g has been found to increase the rate of moisture weight gain above that predicted by Fick's equation [23]. This increase is believed to be due to the development of surface crazing and cracking brought about by the rapid heating and resin swelling. With the restrictions of no rapid heating, no surface crazing or cracking, and assuming K to be constant, Fick's equation gives a good initial approximation of the moisture concentration distribution through a composite laminate [24].

III. FINITE ELEMENT MODELLING

Panel Properties

For the finite element analysis, a graphite epoxy composite panel that is 12 inches long, a circumferential length of 12 inches, and a radius of curvature of 12 inches was modeled. The panel's dimensions and material properties are shown in Fig. 3.1. The panel consists of eight 0.005 inch plies for a total thickness of 0.04 inches. Two different symmetric ply orientations were examined, (0/+45/-45/90/90/-45/+45/0) referred to as (0/+45/-45/90)s and (0/-45/+45/90)s. All the panels were loaded along the top edge which was clamped with the u displacement free. The vertical edges of the panel had u and v displacements (x and y direction displacements, respectively) and rotation about the x axis, R_u , free. The bottom of the panel was clamped with no free degrees of freedom (DOF).



DIMENSIONS AND MATERIAL PROPERTIES

MATERIAL: GRAPHITE-EPOXY

RADIUS: $R=12''$

LENGTH: $L=12''$

NUMBER OF PLIES: 8

ORIENTATION OF PLIES, θ : $(0/45/-45/90)_s$
 $(0/-45/+45/90)_s$

THICKNESS: 8 PLIES AT $0.005'' = 0.04''$

ELASTIC MODULI: $E_1 = 18850$ ksi, $E_2 = 1413.8$ ksi

SHEAR MODULUS: $G=855$ ksi

POISSON'S RATIO: $\nu_{12}=0.3$

x, y, z : STRUCTURAL COORDINATES

u, v, w : DISPLACEMENTS

R_u, R_v, R_w : ROTATIONS

Fig. 3.1 Panel Notation and Material Properties

Element Selection

For the finite element analysis, the element selected is a quadrilateral plate element referred to as the QUAF 411 in the STAGSC-1 documentation [26]. The QUAF 411 consists of three translational displacements, two in-plane rotations and two independent normal rotations at each corner node, plus tangential displacements at each of the four midside nodes for a total of 32 DOF. QUAF 411, shown in Fig. 3.2, was developed to remove the displacement incompatibilities which exist when flat shell elements do not lie in the same plane. The in-plane shape functions are represented by cubic polynomials and if the edge displacements are to be compatible, the transverse displacement shape functions must be of the same order. This is accomplished by the use of two normal rotations at each corner node and tangential displacements at mid-side nodes. The difference between these two rotations yields a shear strain at each corner node which is introduced as an extra degree of freedom. The shape functions for the u and v displacements within the QUAF 411 element are cubic polynomials parallel to the edge and quadratic perpendicular to the edge. Also, the bending shape functions are cubic in both directions.

This thesis requires a nonlinear collapse analysis to be carried out by the STAGSC-1 computer program and the QUAF 411 element was the best available element to use [26]. The drawback to the QUAF 411 element is that there is no transition element in the STAGSC-1 library so grid selection becomes very important.

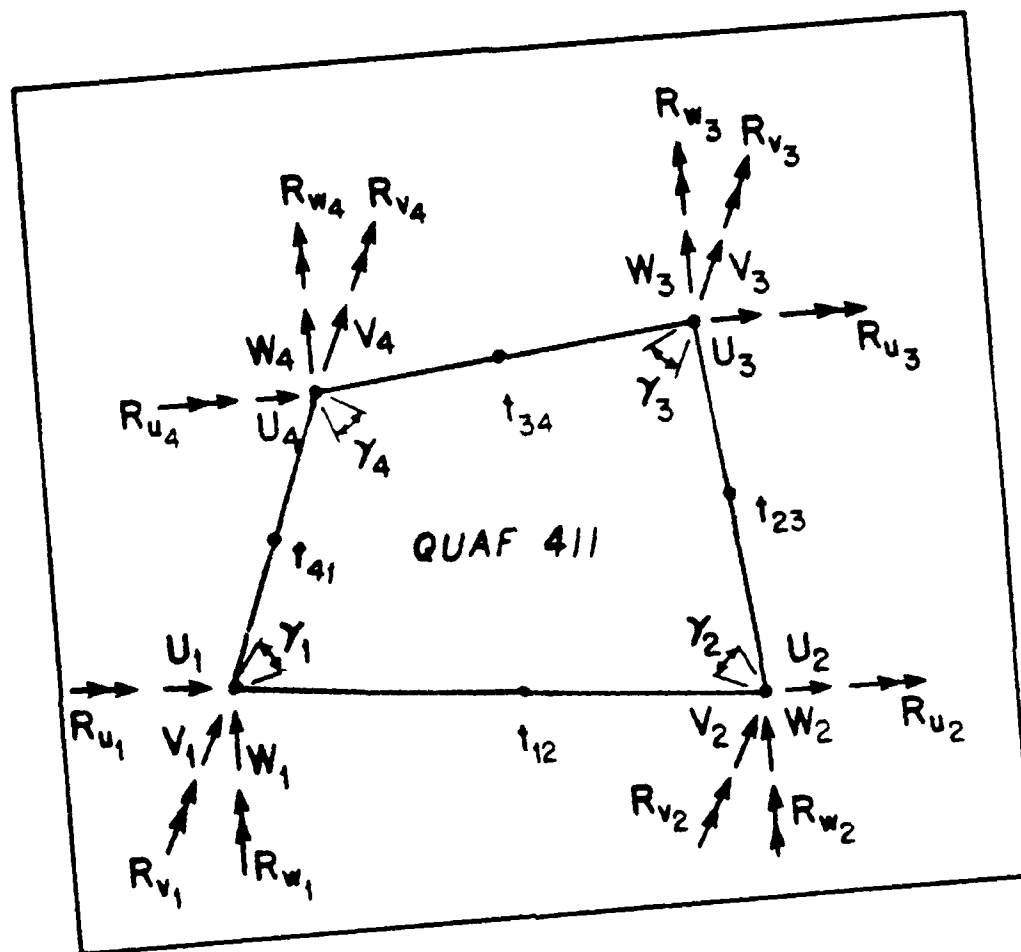


Fig. 3.2 Quadrilateral 411 Plate Element

Grid Sizing

Grid selection is a trade-off between cost and accuracy. Lee [18] pointed out that the elements should be as close to an aspect ratio (axial dimension divided by circumferential dimension) of unity as can possibly be achieved. Elements with an aspect ratio of 0.5 should be no closer than at least two inches from the cutout and elements with an aspect ratio of 2 should be no closer than at least one and one-half inches from the cutout considering cutout areas of up to 11% of the panels surface. These important parameters were used and an element mesh was constructed. The mesh used in this paper was refined around the cutout to obtain better accuracy.

The refined mesh that was chosen for the analysis was compared to the 17 x 19 grid of Lee [18] for a centrally located 2" x 2" cutout. The major difference between the two mesh models is located in the vicinity of the cutouts reentrant corners. The mesh used herein is 30% finer in these areas. Shown in Table 3.1 are the results of the comparison of the 17 x 19 grid of Lee with the refined 17 x 20 grid used in this analysis. As the table shows, the 17 x 20 grid gives excellent results. Therefore, since the grid refinement chosen compares favorably, it was used for the cutout and material degradation analysis.

Table 3.1: Mesh Refinement Results for a 2" x 2" Cutout

(Note- a different set of material properties
was used to match the published results)

<u>Published results</u> [18]	<u>Refined Grid</u>
17 x 19 grid	17 x 20 grid
2381 Active DOF	2556 Active DOF
208.1 lbs/in collapse load	208.7 lbs/in collapse load
26 incremental steps	24 incremental steps
--	0.3% difference

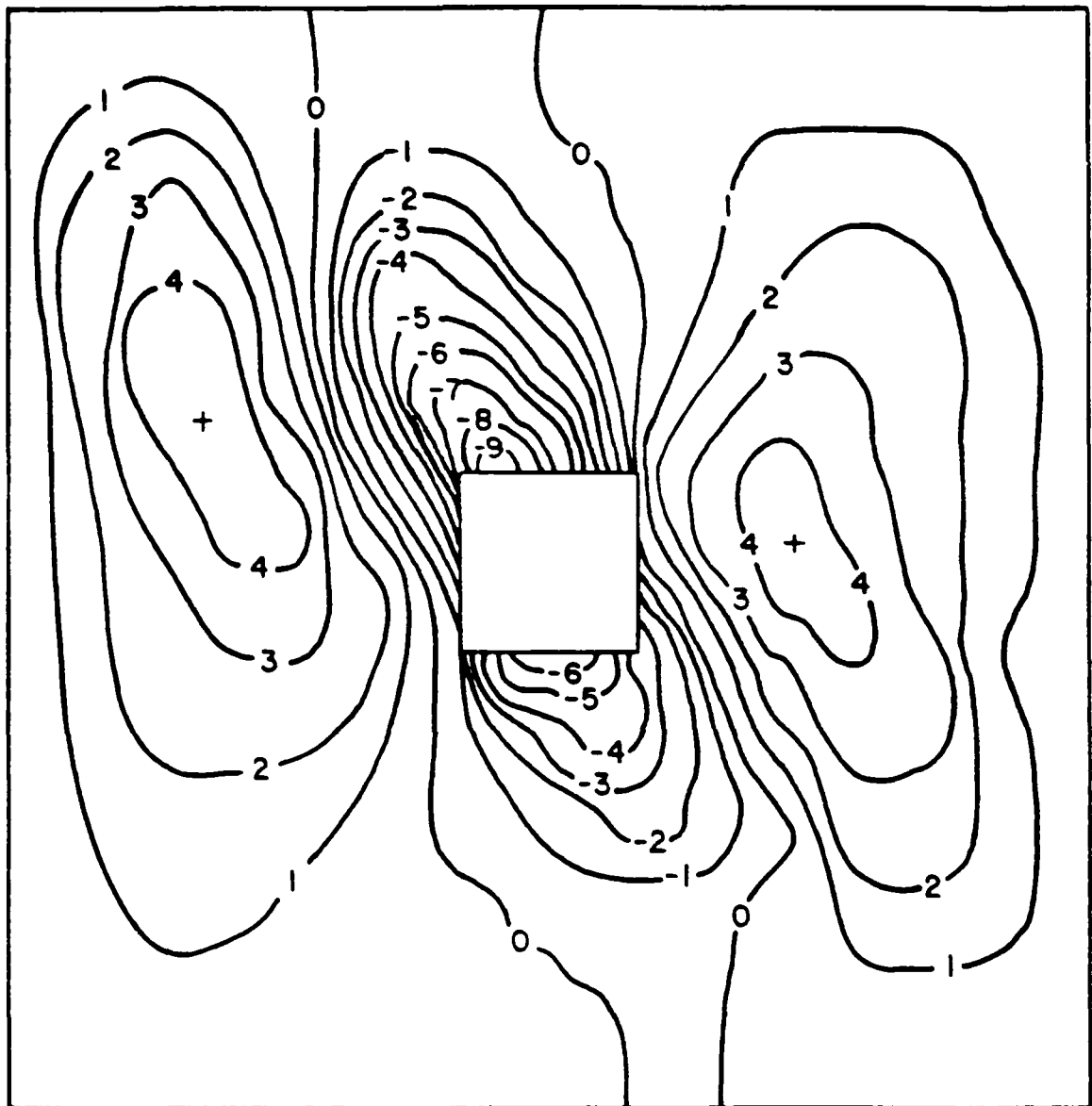
IV. DISCUSSION AND RESULTS

The main study area of this thesis is the material degradation effects considering cutout location. Thus, in order to establish the critical characteristics of the effect that a true geometric imperfection (cutout) has on a composite panel, a study of the effect of the discontinuity location in the panel has been carried out. The cutouts consisted of a 2" x 2" cutout which removed 2.78% of the panels total surface area and the 4" x 4" cutout which removed 11.1% of the total area. The different ply layups, different size cutouts and the cutout locations studied are shown in Table 4.1. The reader must recognize that the results presented within this thesis are based on a finite element study and no attempt has been made to compare the results with experimental values.

The first cutout considered was located in the middle of the panel, cutout location A (Fig. 1.2). A collapse analysis was completed on two symmetric ply orientations, (0/+45/-45/90)_s and (0/-45/+45/90)_s (collapse is considered the point in which the load can no longer increase with increased displacement). The different orientations had no effect on the collapse load of 199.4 lbs/in. However, there was a difference in the radial displacement contours as shown in Figs. 4.1 and 4.2. As can be seen in Fig. 4.1, at the final load level (collapse load), one can see the loss of symmetry and the formation of a trough of radial displacement that runs from the upper left of the panel to the lower right. In looking at Fig. 4.2, (for the (0/-45/+45/90)_s orientation) the trough of radial displacement runs from the upper right

Table 4.1: Ply Layup, Cutout Size, and Cutout Location

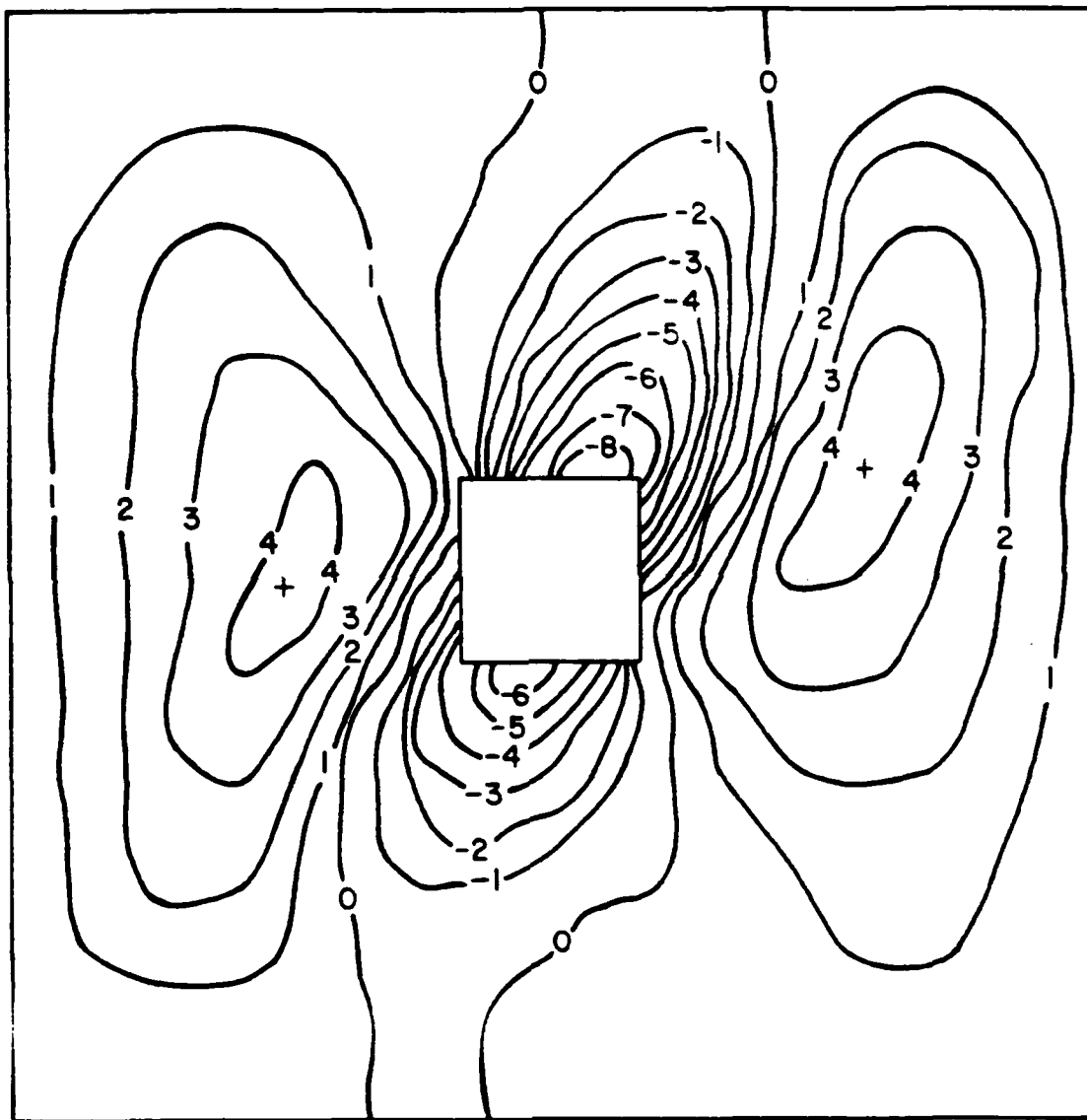
<u>Ply Layup</u>	<u>Cutout Size (inches)</u>		<u>Cutout Location (Fig. 1.2)</u>	
(0/+45/-45/90) _s	2 x 2	4 x 4	A	C
(0/-45/+45/90) _s	2 x 2	4 x 4	A	C
(0/+45/-45/90) _s	2 x 2		B	D
(0/-45/+45/90) _s	2 x 2		D	



$W_{max} = -0.046572$ inches

CONTOUR LEVELS ARE IN 10ths OF MAXIMUM DISPLACEMENTS

Fig. 4.1 Radial Displacement Contour Plot for 2" x 2" Cutout at Collapse Load of 199.4 lbs/in (0/+45/-45/90)s, Cutout A



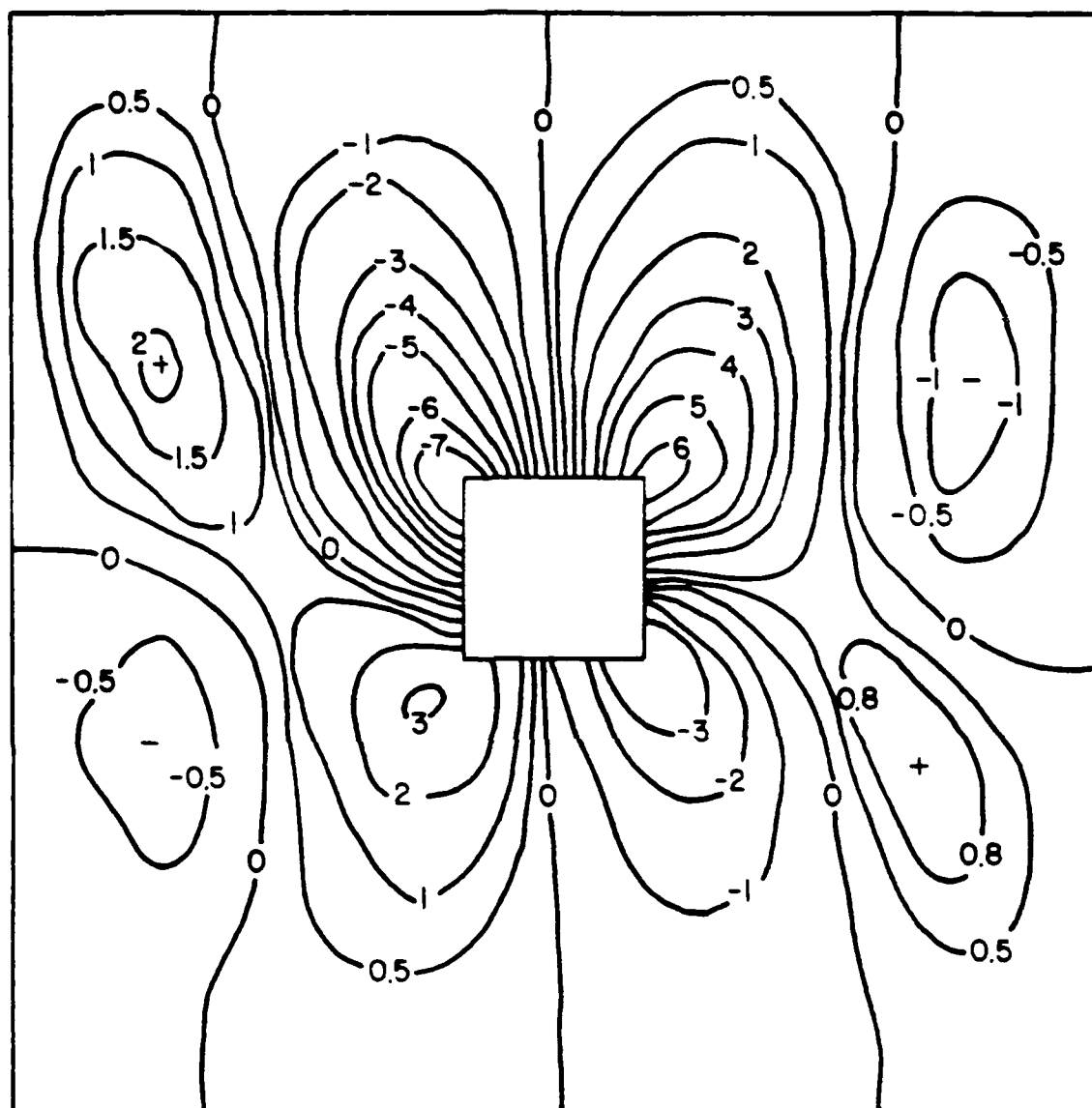
$W_{max} = -0.043796$ inches

CONTOUR LEVELS ARE IN 10ths OF MAXIMUM DISPLACEMENTS

Fig. 4.2 Radial Displacement Contour Plot for 2" x 2" Cutout at Collapse Load of 199.4 lbs/in (0/-45/+45/90)s, Cutout A

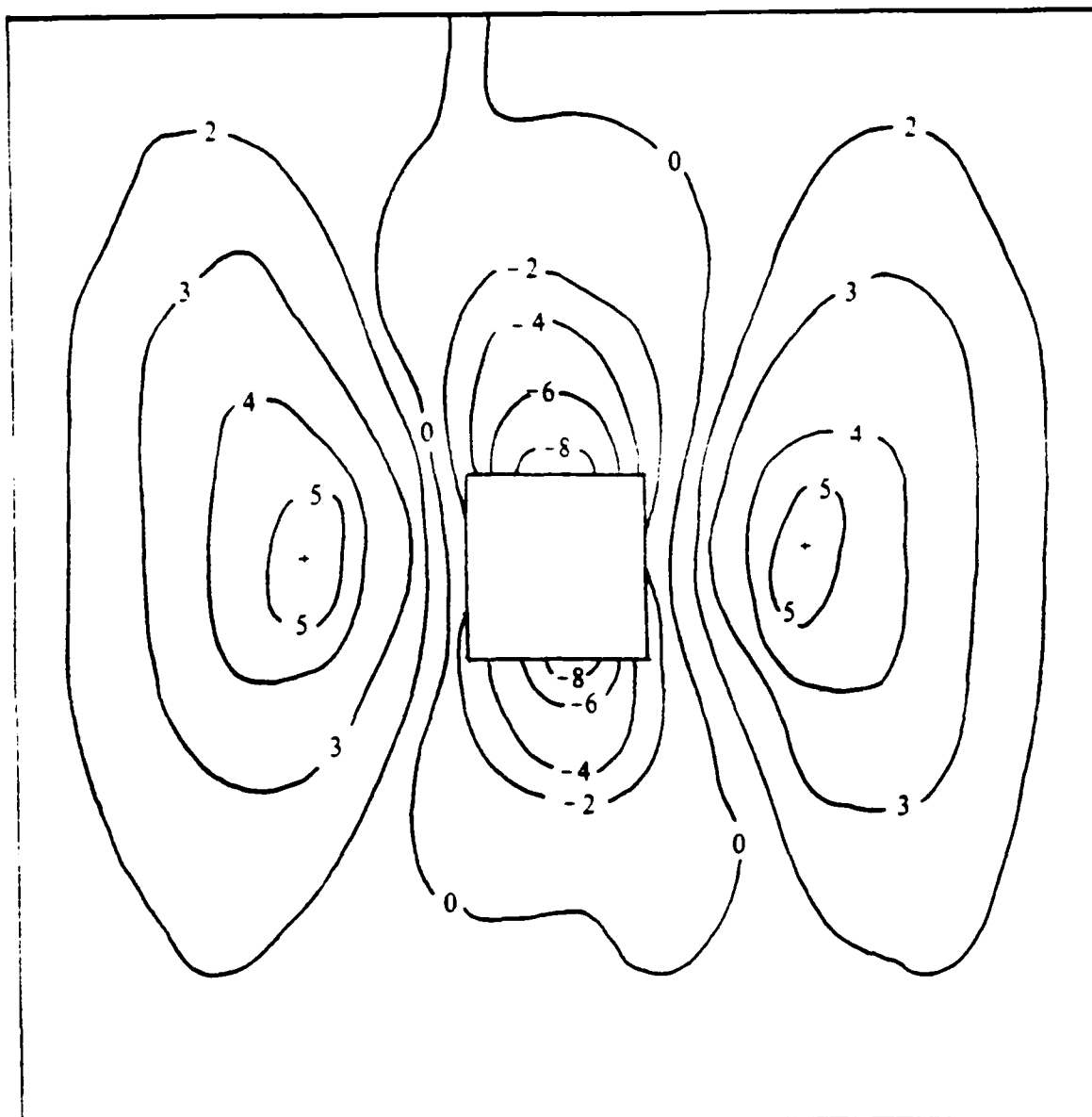
to the panel's lower left. This difference in the orientation of the troughs seems to be related to the orientation of the second ply (taken from the outer surface edge). A (0/+45/-45/90)s orientation produces a trough along the direction of the +45° ply (ply angle defined in Fig. 3.1) while a (0/-45/+45/90)s orientation produces a trough along the order of the -45° ply.

In order to explain the unexpected collapse displacement for the 2" x 2" cutout, a comparison was made between the eigenvector solution and the radial contour plot. Fig. 4.3 represents the eigenvector for the (0/+45/-45/90)s orientation, and one should observe that a trough similar to the panel's collapse mode is appearing. However, the overall eigenvector shape does not resemble that of the collapse mode. Further study into this area was required. Fig. 4.3.1 represents the total linear solution prior to the bifurcation (buckling) point and Fig. 4.4 represents the nonlinear 2" x 2" collapse analysis at 50% of the total collapse force. As the two plots show, the displacement contours are nearly identical. This clearly shows that the 2" x 2" nonlinear analysis closely followed the linear solution through the initial stages of loading. Further proof of this linear phenomena can be found in Fig. 4.5, the plot of the load displacement curves. As the plot shows, the 2" x 2" cutout closely followed the linear bifurcation plot. There is, however, a difference between the final bifurcation load point and the collapse load of roughly 13%. As the linear prebuckling contour indicates, a drastic change in the displacement function occurs at bifurcation in which the trough is developed. This shows that a greater force is needed to go from the linear displacement contour plot to the



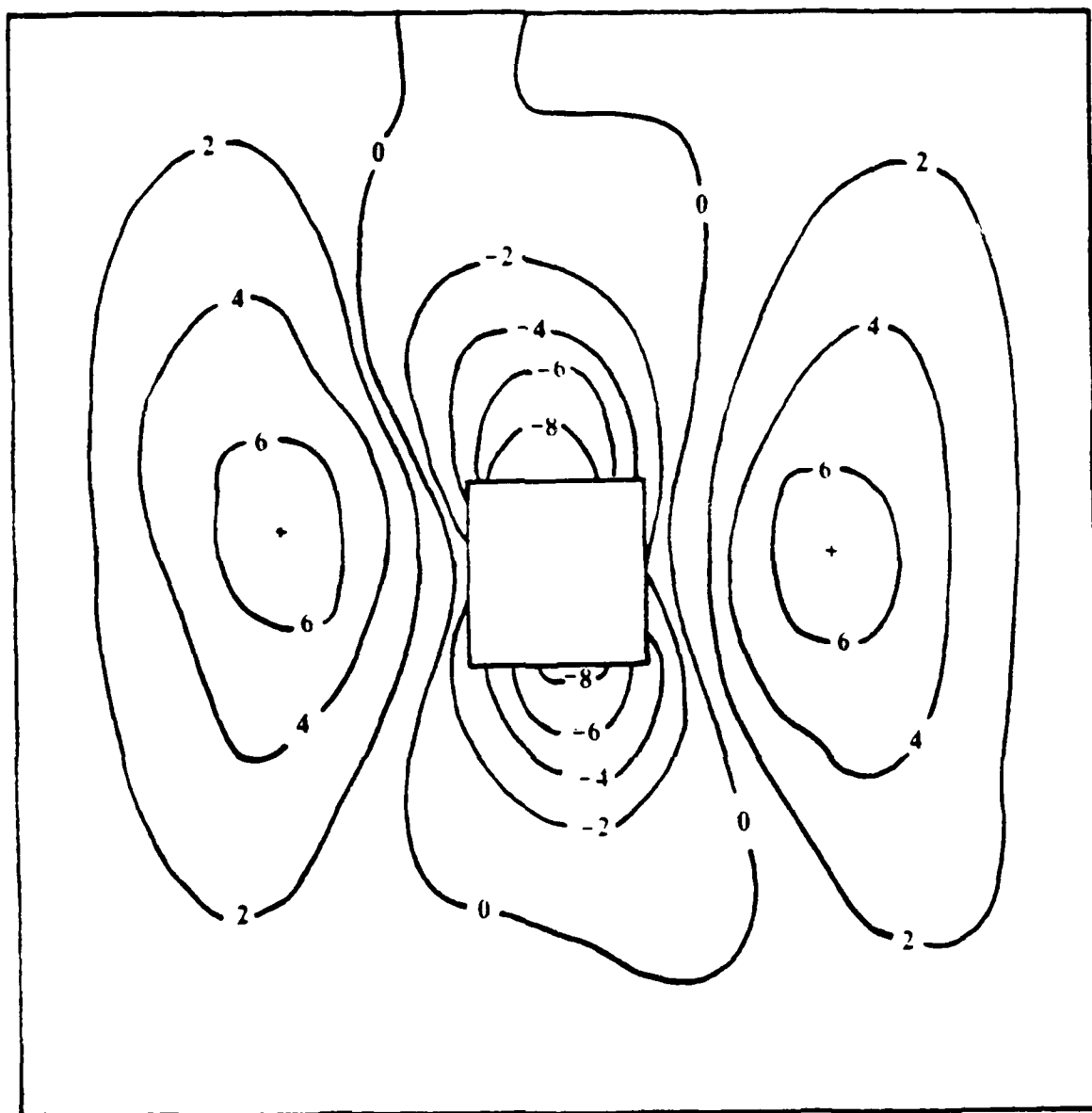
CONTOUR LEVELS ARE IN 10% OF MAXIMUM DISPLACEMENTS

Fig. 4.3 Eigenvector Contour Plot for 2" x 2" Cutout
(0/+45/-45/90)s, Cutout A



CONTOUR LEVELS ARE IN 10ths OF MAXIMUM DISPLACEMENTS

Fig. 4.3.1 Linear Radial Displacement Contour Plot for 2" x 2"
Cutout Prior to Bifurcation Buckling. (0/+45/-45/90)s,
Cutout Position A.



$$V_{max} = -0.01325 \text{ inches}$$

CONTOUR LEVELS ARE IN 10ths OF MAXIMUM DISPLACEMENTS

Fig. 4.4 Radial Displacement Contour Plot for 2" x 2" Cutout at 50% of Collapse Load, 101 lbs/in, (0/+45/-45/90)s, Cutout A

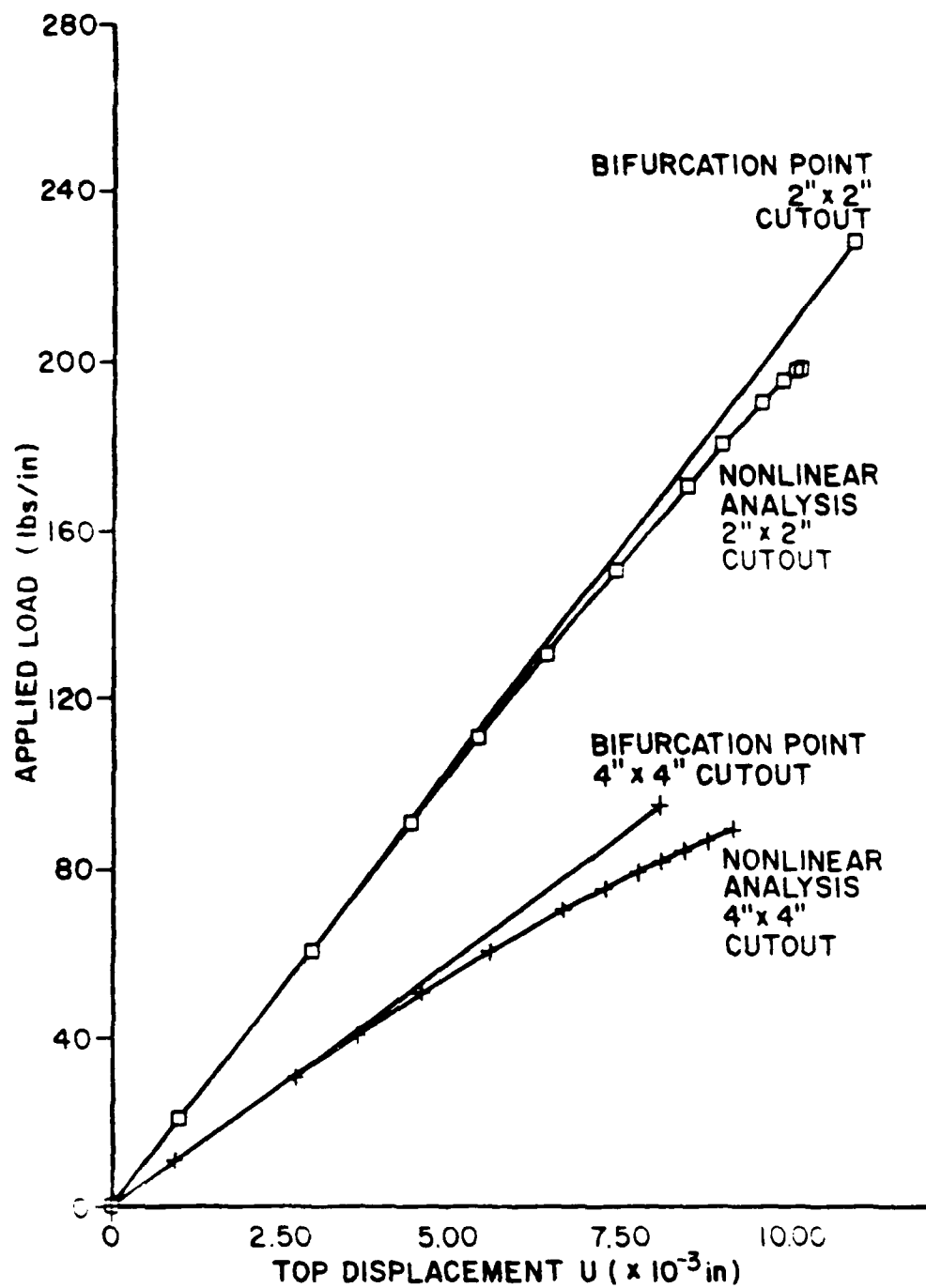


Fig. 4.5 Load Displacement Curve, Linear and Collapse Analysis, for 2" x 2" Cutout and a 4" x 4" Cutout Located at Cutout Position A

eigenvector then the force needed to collapse the panel, as would be expected. This is primarily true because the nonlinear collapse analysis contour plot responds gradually to the trough development. The collapse analysis is still a nonlinear phenomena even though it appears to follow the linear path. Shown in Fig. 4.5.1 is the load displacement curve for a point located halfway along the left side of the cutout. This curve shows that the solution does become nonlinear as collapse approaches. It can also be shown using this same analysis that for the $(0/-45/+45/90)_s$ panel the eigenvector is such that, as mentioned previously, the displacement trough is directed in an orientation taken on by a negative angle, Fig. 4.6.

A further description can be made relative to the radial displacement function. As pointed out previously, there was an initial surprise in seeing unsymmetric deflection movements. The symmetry was evident when the panel is looked at for lower load values or what is called the linear portion. In this linear portion, the different orientations, $(0/+45/-45/90)_s$ and $(0/-45/+45/90)_s$, did not matter in the solutions displacement contours as they were identical and symmetric. At the higher loadings the influence of the cutout comes into play and the final contour plot results in the unsymmetrical secondary loading arrangement (the eigenvectors) as previously mentioned. The question may be asked as to what feature of the stiffness coefficients could indicate an unsymmetrical and different displacement function within the shell by only changing the ply orientation (actually just switching the second and third plies) of the quasi-isotropic layup. The answer lies in the D_{16} and D_{26} terms of the bending stiffness parameter matrix since the other

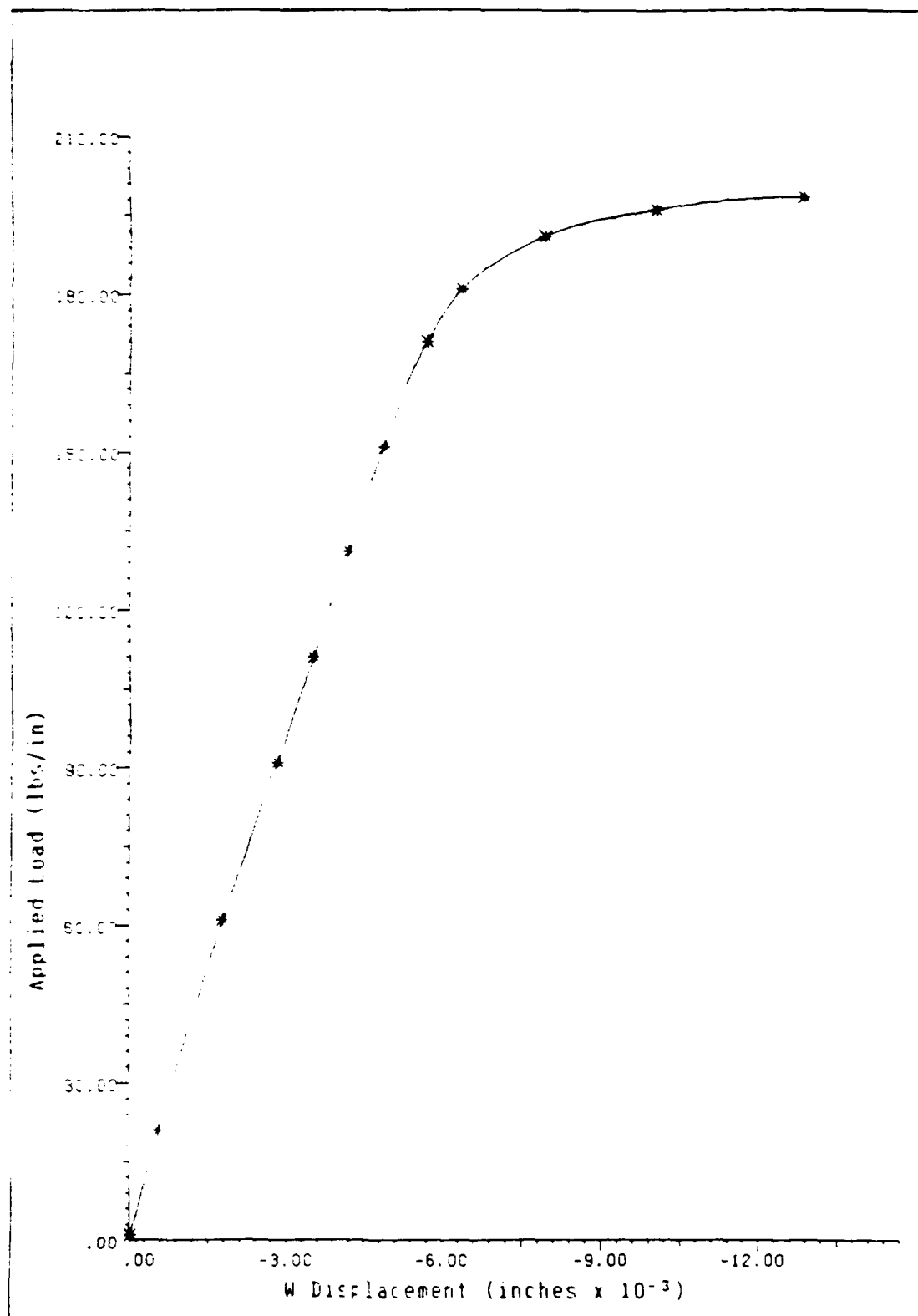


Fig. 4.5.1 Load Displacement Curve Taken At A Point Halfway Down the Left Side of the 2' x 2" Cutout Located at Cutout Position A.

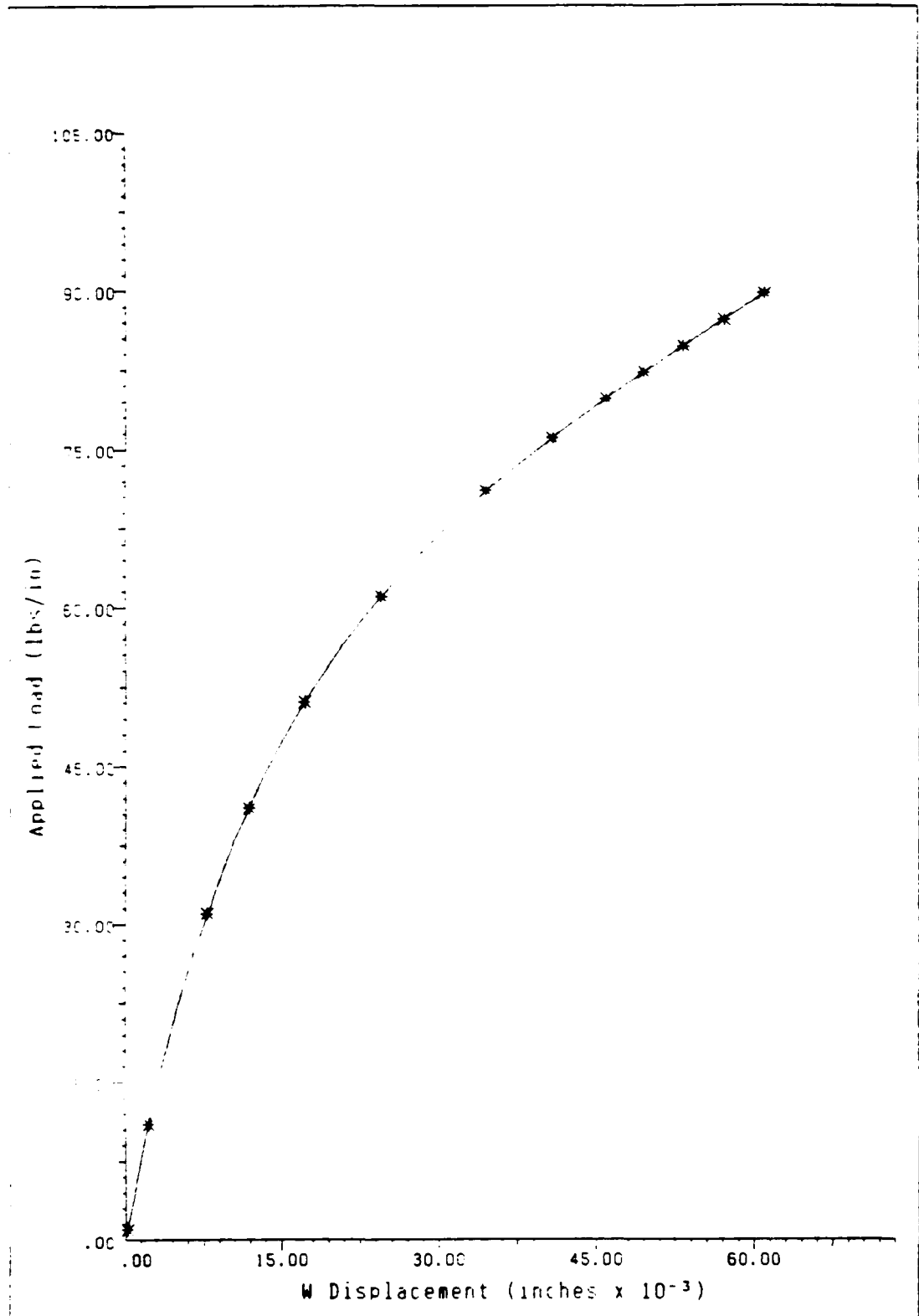
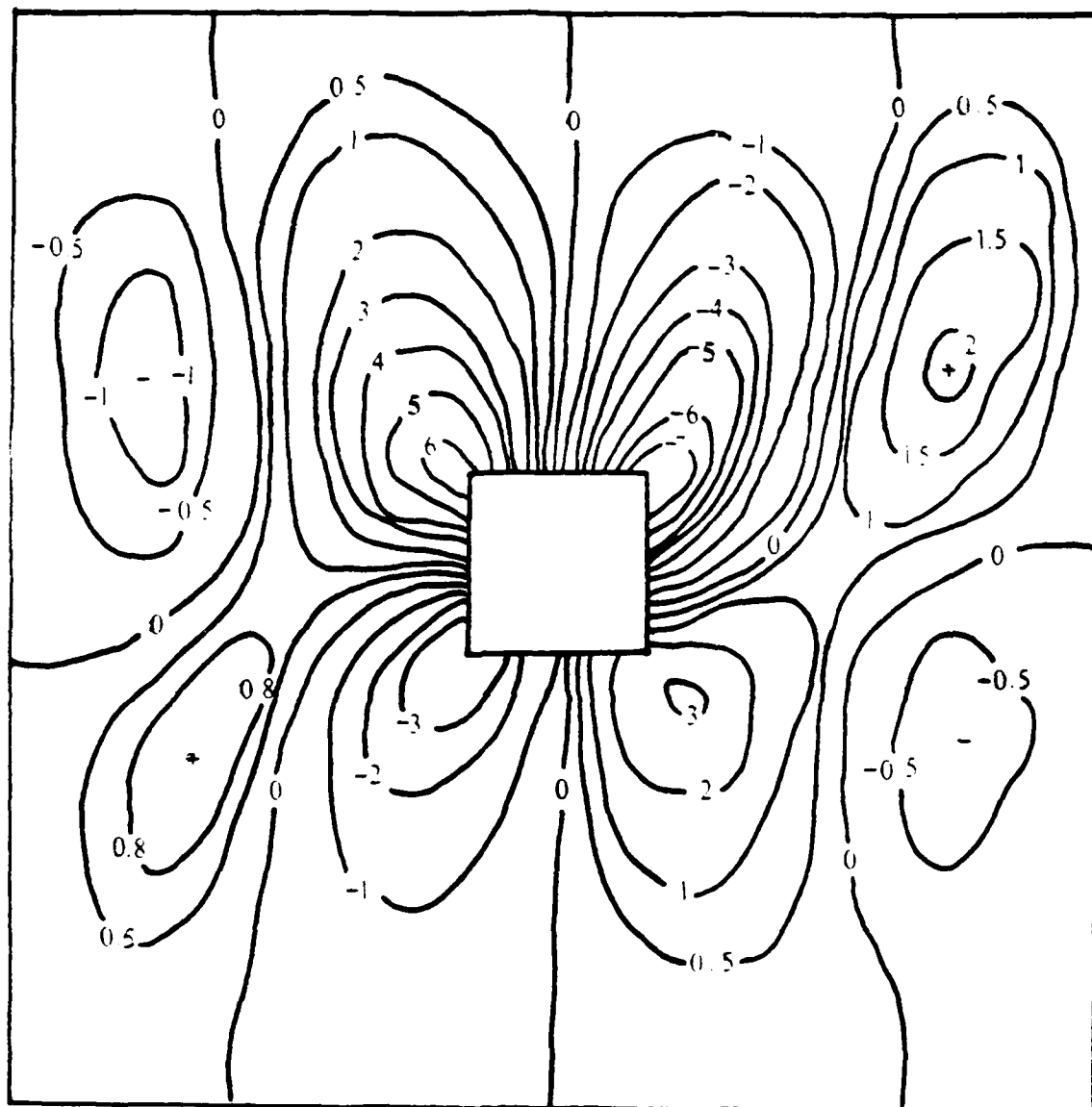


Fig. 4.5.2 Load Displacement Curve Taken At A Point Halfway Down the Left Side of the 4' x 4' Cutout Located at Cutout Position A.



CONTOUR LEVELS ARE IN 10ths OF MAXIMUM DISPLACEMENTS

Fig. 4.6 Eigenvector Contour Plot for 2" x 2" Cutout
(0/-45/+45/90)s, Cutout A

stiffness parameters are equal. These D_{ij} coefficients are related to the twisting moment, M_{xy} . The M_{xy} equation is written as

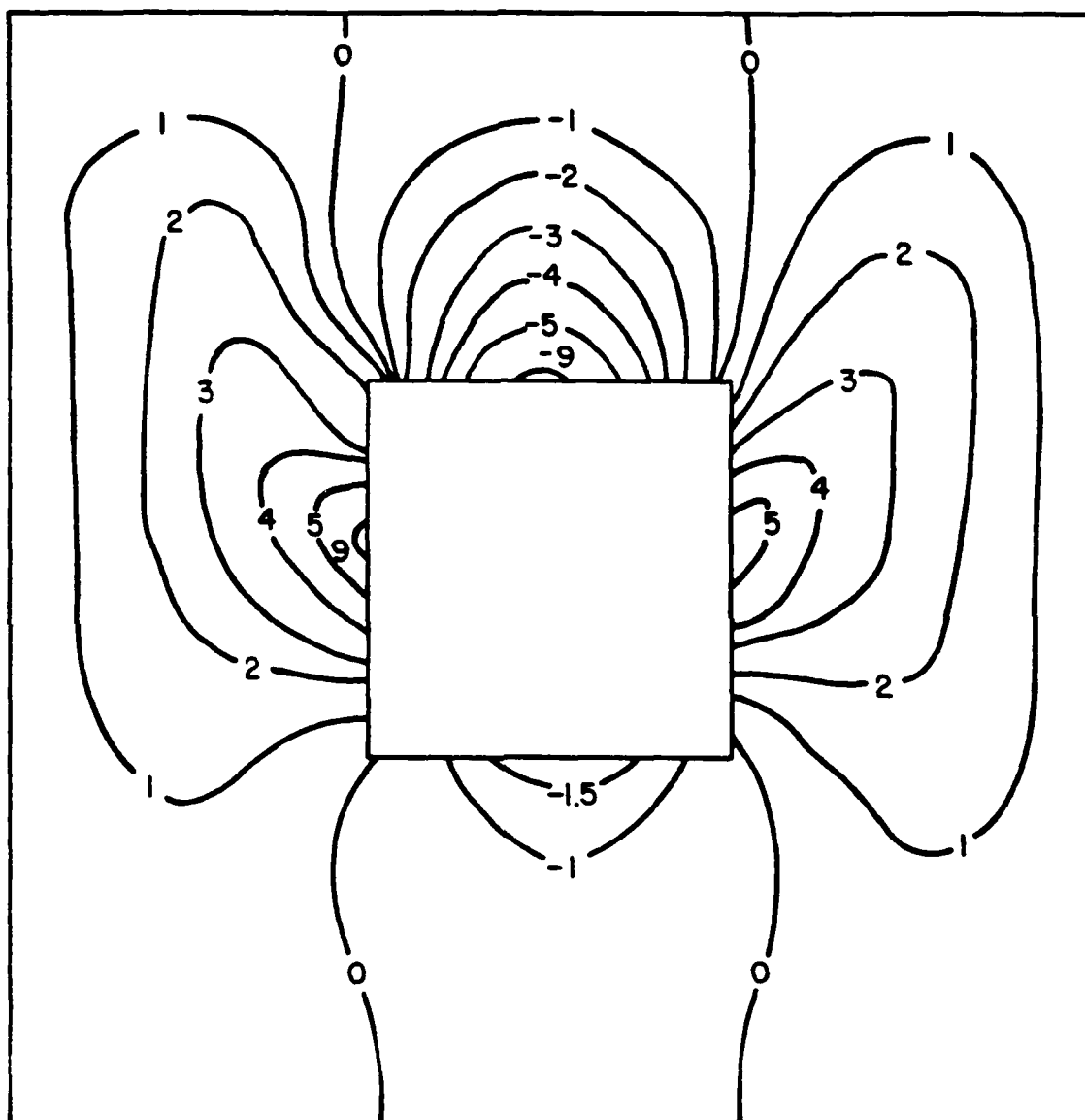
$$M_{xy} = D_{1\epsilon} \kappa_x + D_{2\epsilon} \kappa_y + D_{6\epsilon} \kappa_{xy} \quad (27)$$

where the κ 's are the changes in the surface curvatures and the D_{ij} 's are the bending stiffness elements [24,25]. In the (0/+45/-45/90)s arrangement the $D_{1\epsilon}$ and $D_{2\epsilon}$ are positive and in the (0/-45/+45/90)s ply orientation the terms have the same magnitude but are negative in sign. This means that M_{xy} will change with ply orientation and since this moment function dominates the collapse for the small 2" x 2" cutout, different contour arrangements are produced. Thus, there is a tie-in with the twisting moment, the curvature and the displacement w . However, in the linear loading portion, since there is very little bending moment the A_{ij} (extensional stiffness parameters) matrix dominates the solution and $D_{1\epsilon}$ and $D_{2\epsilon}$ can not affect the displacement contours. Therefore, at the lower loads (linear range) the displacement contours do not follow the second ply angle. In looking at the effect a 4" x 4" cutout had on the panel, one notices a difference from the 2" x 2" cutout. First, it can be noticed in Fig. 4.5, collapse load versus end shortening and in Fig. 4.5.2, load displacement curve of a point located halfway along the left side of the cutout, that the solution is totally nonlinear for the 4" x 4" cutout. This, as previously mentioned, is not true when considering the 2" x 2" cutout. Furthermore, it can be observed that collapse load and bifurcation load are very close. It becomes obvious that the nonlinearity surrounding the 4" x 4" cutout is associated with a larger

amount of bending which allows the collapse to seek a level similar to the linear load. Yet, this same phenomena is not true for the 2" x 2" cutout since it is depicting a linear relationship in the area surrounding the actual cutout. Linearity is not conducive to direct bending moment, such as M_x and M_y . Thus, the separation between bifurcation and collapse load is apparent when one considers the 2" x 2" cutout.

Once again, looking at the larger cutout (4" x 4"), the radial displacement contours are investigated. Fig. 4.7 represents the contour displacements for a collapse load of 90.0 lbs/in and a ply orientation of (0/+45/-45/90)s. For a ply orientation of (0/-45/+45/90)s (plot not shown) the same symmetric contour displacements can be seen with only a slight amount of non-symmetry that can be observed at the center of the cutout's vertical edges. In looking at the contour plot one can see that the displacement pattern at collapse is more symmetric about the circumferential and longitudinal axes than the similar panel with a smaller cutout. This is because the larger cutout produces the direct bending effect earlier and the moment change is more spread out, therefore, a more symmetric displacement pattern. It can also be seen that the larger (4" x 4") cutout does not display the inward displacement trough along the second ply angle as was seen in the smaller (2" x 2") cutout giving evidence the M_{xy} function is not as dominant relative to the other moment resultants.

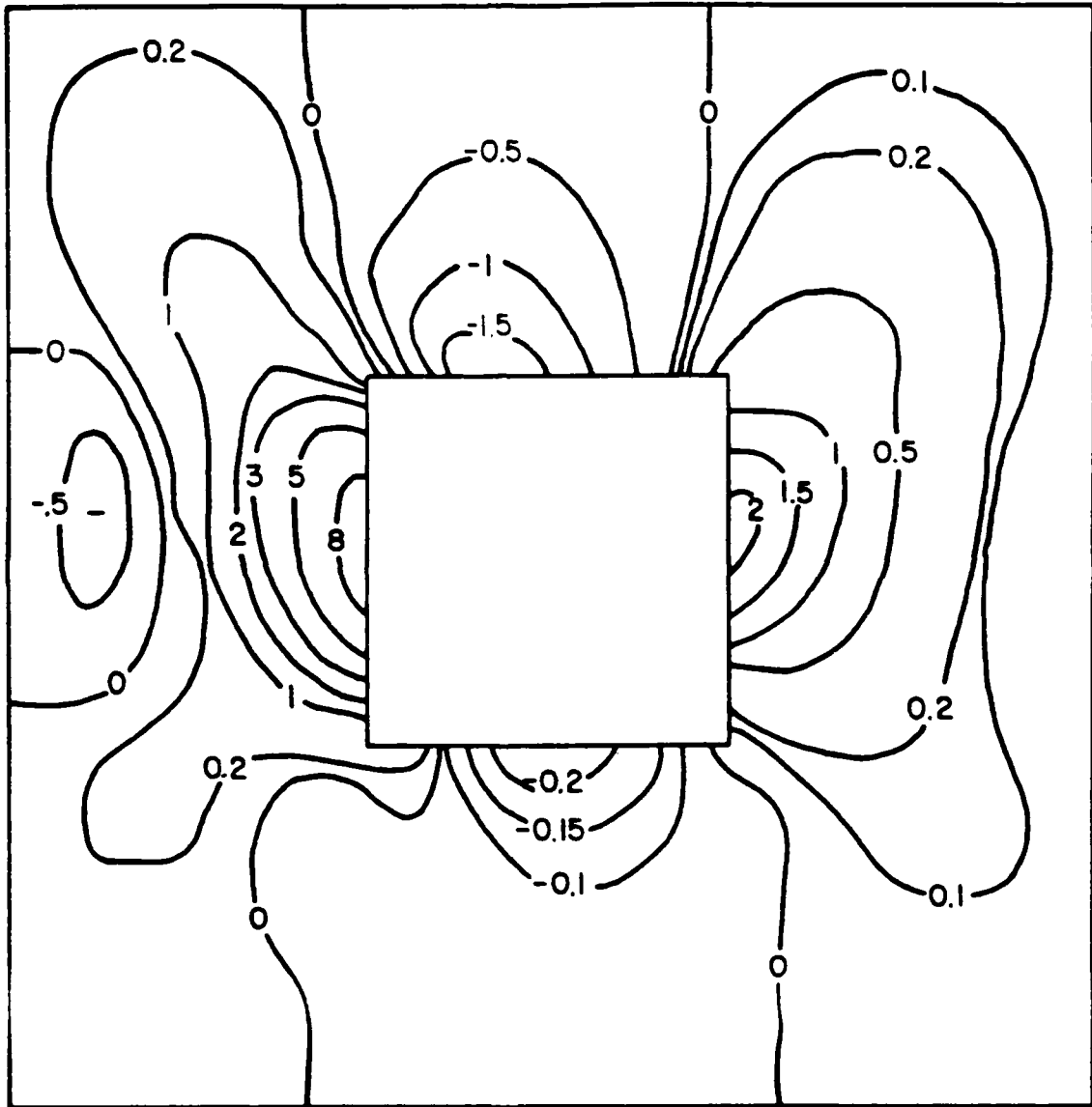
Fig. 4.8 is the radial component eigenvector contour plot of the (0/+45/-45/90)s panel with the larger cutout (4" x 4"). In comparing the eigenvector plot to the displacement contours at the collapse load, there



$W_{\max} = -0.063962$ inches

CONTOUR LEVELS ARE IN 10ths OF MAXIMUM DISPLACEMENTS

Fig. 4.7 Radial Displacement Contour Plot for 4" x 4" Cutout at Collapse Load of 90.0 lbs/in (0/+45/-45/90)s, Cutout A

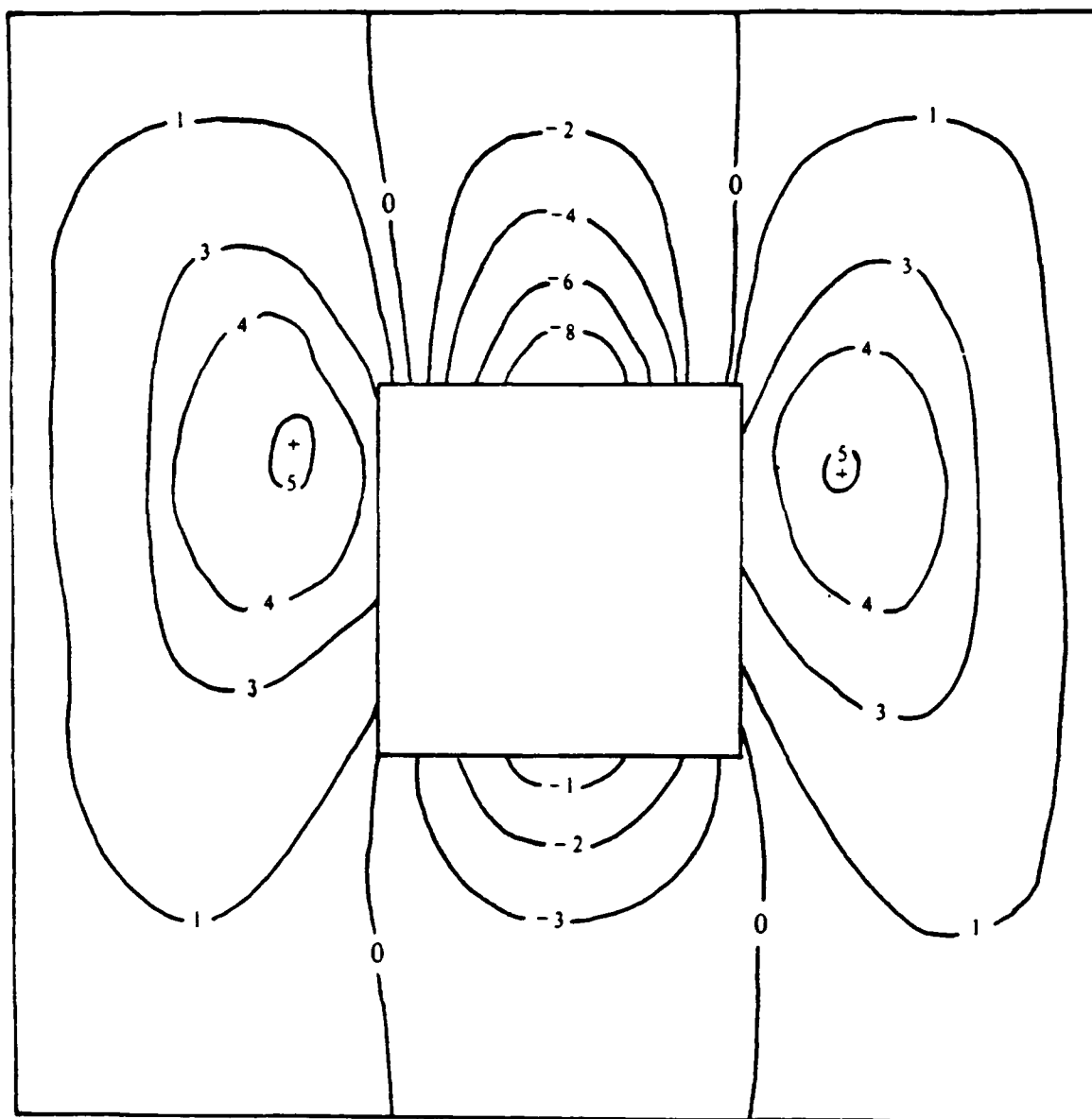


CONTOUR LEVELS ARE IN 10ths OF MAXIMUM DISPLACEMENTS

Fig. 4.8 Eigenvector Contour Plot for 4" x 4" Cutout
(0/+45/-45/90)s, Cutout A

is very little similarity. The radial displacement contour plot, Fig. 4.7, at collapse produces a symmetric displacement along a vertical centerline. On the other hand, the eigenvector plot, Fig. 4.8, has a displacement pattern that is slightly tilted and the overall pattern does not resemble the collapse displacement pattern. Fig. 4.8.1 represents the linear solution prior to bifurcation and closely resembles the nonlinear collapse analysis plot, Fig. 4.7. In essence, when the panel collapsed it did not go into the shape of the eigenvector as the panels with the smaller cutouts did. If the panel absorbs energy primarily through its axial stiffness (smaller cutout and uncut panel) then the displacement field at collapse is eigenvector oriented. However, if the panel absorbs energy through both the axial and bending stiffness then the displacement field is not eigenvector oriented. This difference can also be explained by comparing the amounts of radial displacement.

In looking at the radial displacements, the small cutouts had maximum radial displacements approximately equal to the panel thickness (0.04 inches). The largest radial displacement in the panels with small cutouts was 0.047 inches and that was on the panel of (0/+45/-45/90)s. On the other hand, the panels with the larger cutout (4" x 4") had radial displacements of 0.064 inches which is over one and one-half the panels thickness. Therefore, the displacement field generated by the 2" x 2" cutout is not going to have that great of an effect on the nonlinear collapse mode since the radial displacements are small (near the panel's thickness). Thus, at collapse the panel will behave almost linear and will have the shape of the linear bifurcation. Since the radial displacements for the panel with the large cutout are one and one-half



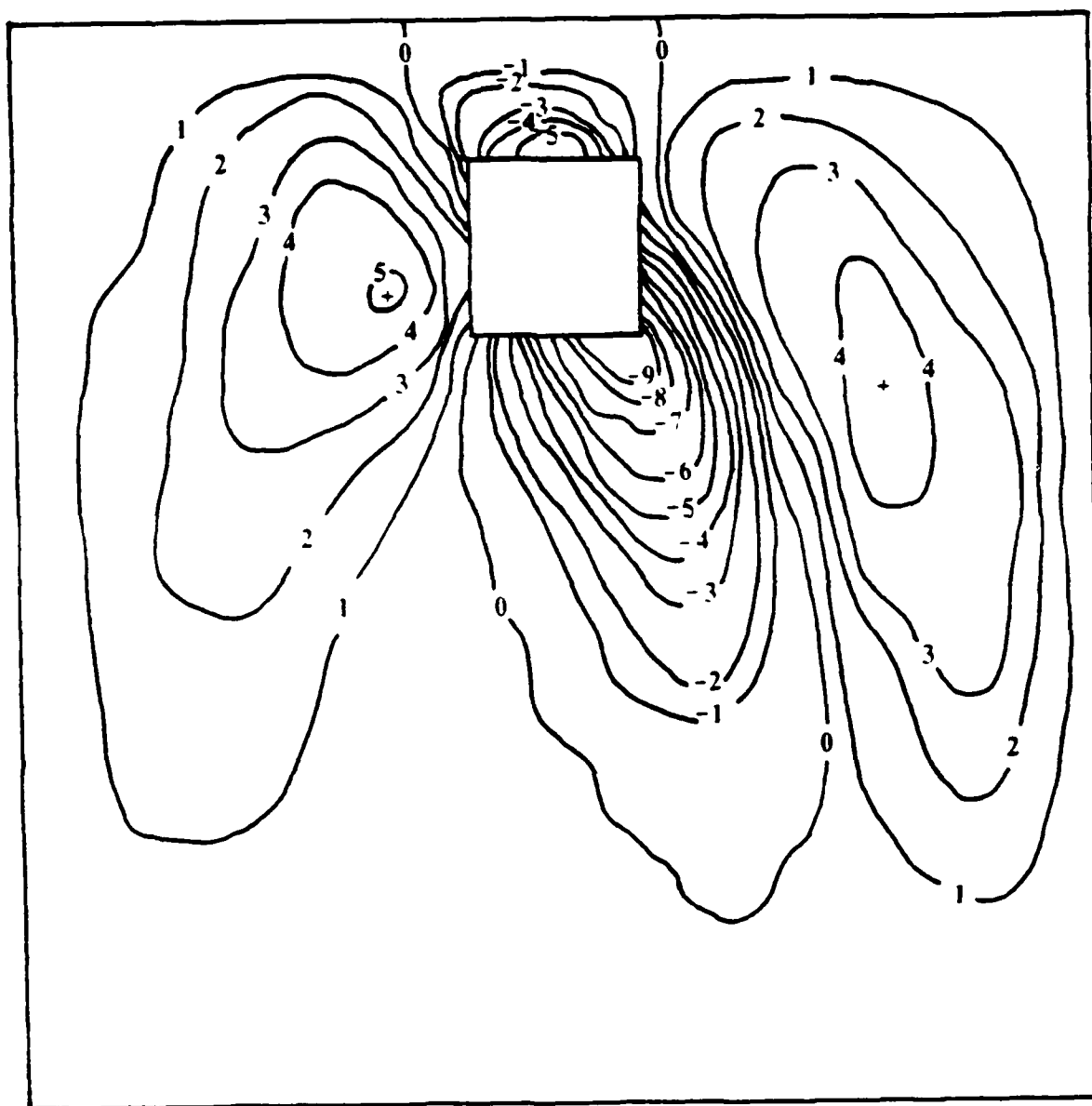
CONTOUR LEVELS ARE IN 10ths OF MAXIMUM DISPLACEMENTS

Fig. 4.8.1 Linear Radial Displacement Contour Plot for 4" x 4"
Cutout Prior to Bifurcation Buckling, (0/+45/-45/90)s,
Cutout Position A.

the panels thickness, their effect on the nonlinear collapse analysis will be greater. With these large displacements (greater than the panel's thickness) the nonlinear effect of the cutout on the collapse analysis dictates the collapse displacement pattern as discussed previously. This pattern is symmetric and there is no shift to the secondary loading path. The nonlinearity in the presence of the 4" x 4" cutout is felt by the panel throughout its loading history while the nonlinearity of the smaller 2" x 2" cutout does not effect the panel's displacement pattern as much.

To continue on with the cutout placement study, a (0/+45/-45/90)s ply orientation 2" x 2" cutout was placed near the top of the panel (cutout location B). This cutout location produced a collapse load of 201.15 lbs/in, or a 0.8% change from the 2" x 2" cutout located at the exact middle (cutout location A). The radial displacement contour plot, Fig. 4.9, looks exactly like the middle cutout (location A) except that the cutout is displaced upward. Fig.4.10 is the eigenvector plot for the cutout located on the top of the panel (location B). Once again we see that at collapse the contour plot has shifted into the secondary loading path (the eigenvector). Since the top cutout acts very nearly the same as the middle cutout, its analysis would yield the same interpretation as the middle cutout discussed earlier.

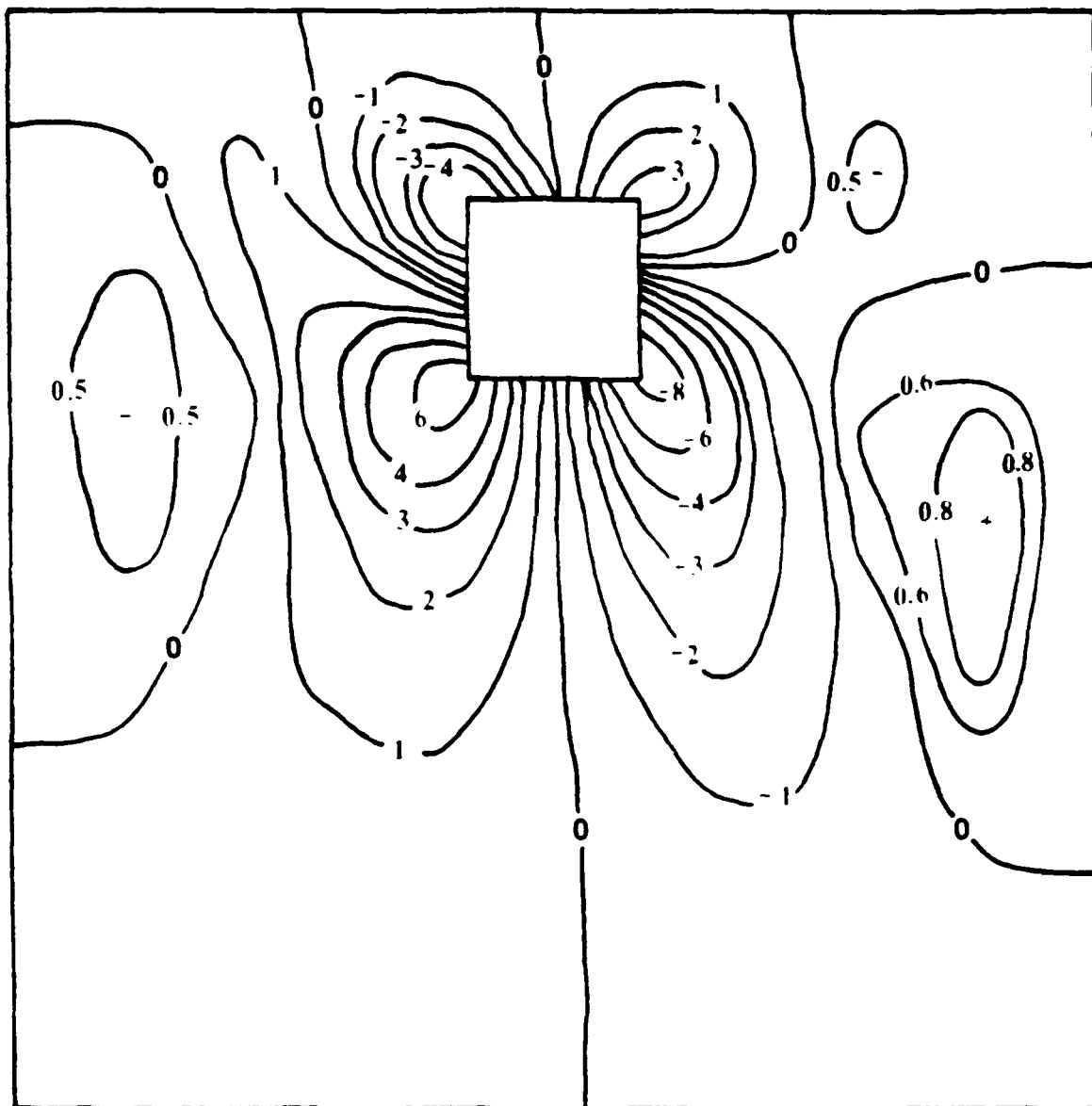
Next, if the 2" x 2" cutout is placed along one side, such as at location C, there is a unique dependence on the ply orientation. A ply orientation of (0/+45/-45/90)s produces a collapse load of 147.18 lbs/in or a 26.2% decrease from the 2" x 2" middle cutout. With a ply orientation of (0/-45/+45/90)s, a collapse load of 178.6 lbs/in is found,



$W_{max} = -0.0499$ inches

CONTOUR LEVELS ARE IN 10ths OF MAXIMUM DISPLACEMENTS

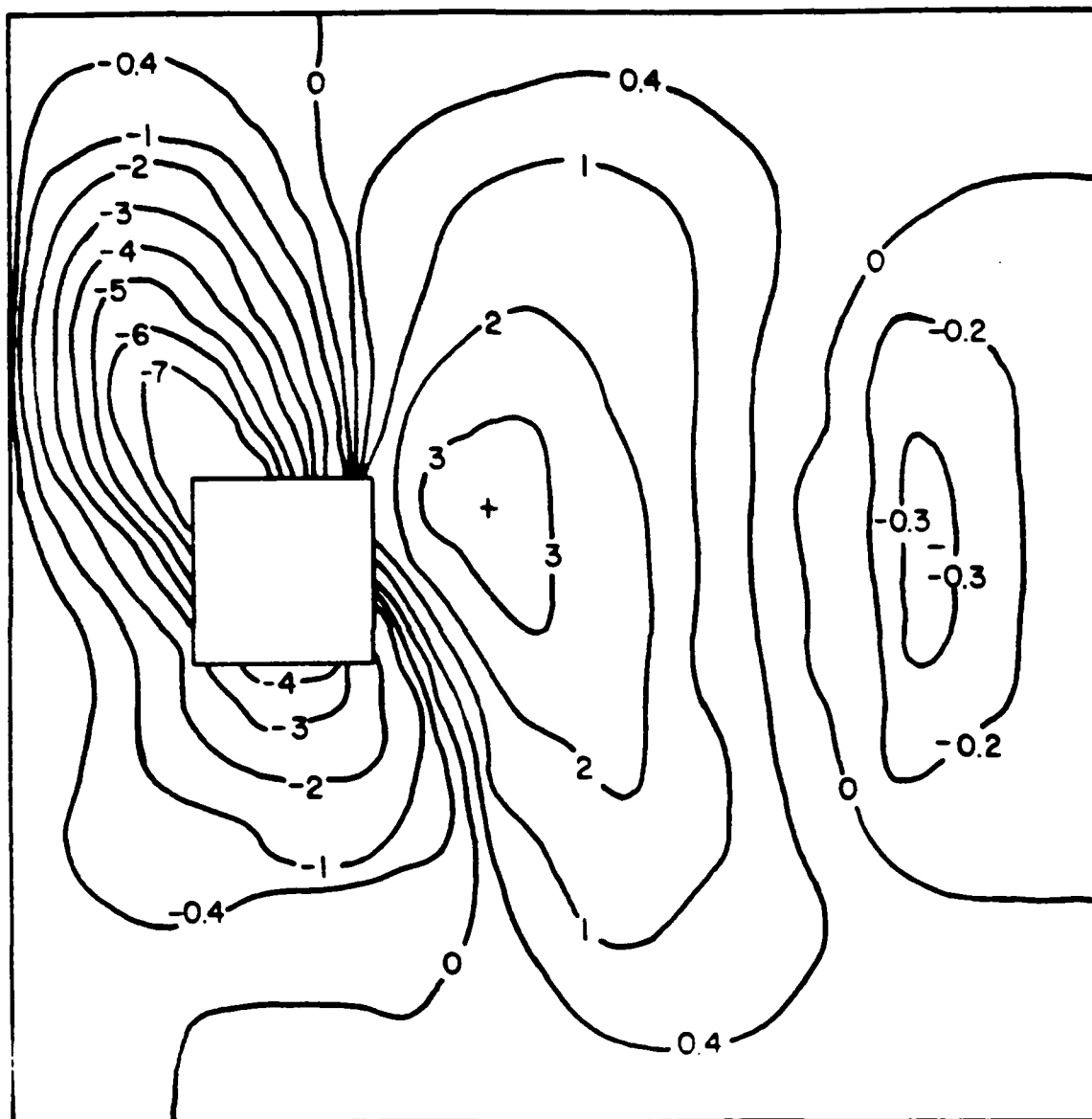
Fig. 4.9 Radial Displacement Contour Plot for 2" x 2" Cutout at Collapse Load of 201.2 lbs/in (0/+45/-45/90)s, Cutout 8



CONTOUR LEVELS ARE IN 10ths OF MAXIMUM DISPLACEMENTS

Fig. 4.10 Eigenvector Contour Plot for 2" x 2" Cutout
(0/+45/-45/90)s, Cutout B

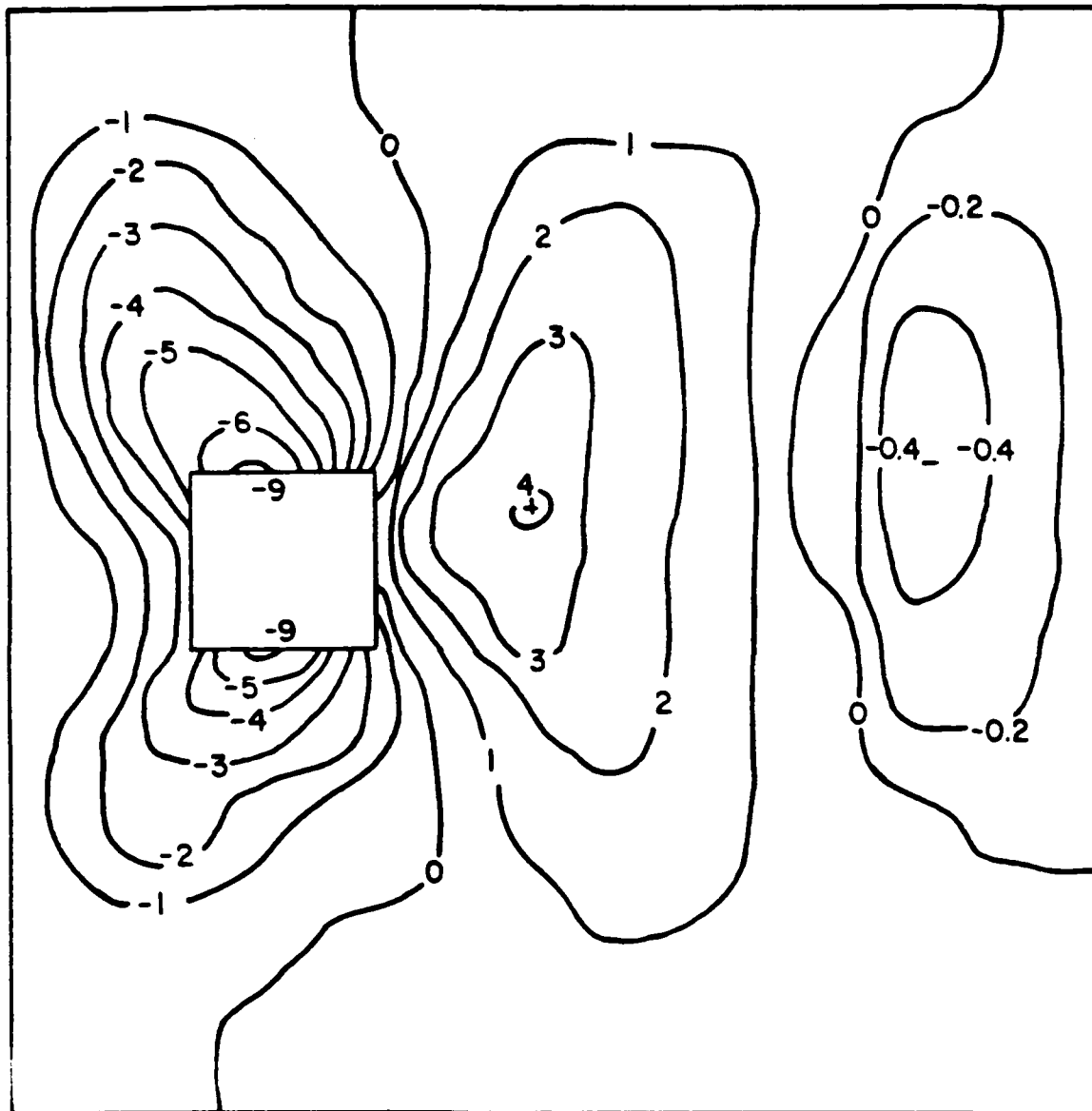
which is 10.4% less than the middle cutout collapse load and 17.6% more than the $(0/+45/-45/90)_s$ side cutout. Radial displacement contour plots are different for the $(0/+45/-45/90)_s$ and the $(0/-45/+45/90)_s$, Fig. 4.11 and 4.12 respectively. In looking at Fig. 4.11, the radial displacement contour plot for $(0/+45/-45/90)_s$, one observes again the inward displacement trough along a line near the second ply angle ($+45^\circ$). This trough runs along the same angle as that of the middle cutout (cutout A). A big difference is noticed when Fig. 4.12 is examined. This contour plot, if it were similar to the middle $(0/-45/+45/90)_s$, would have a trough along the -45° degree angle. However, there is no trough along the -45° degree angle as we had seen earlier. What is seen is a semicircular shaped trough that starts in the upper left and ends in the lower left. The semicircle trough allows for a greater curvature and the panel absorbs more energy and achieves a higher collapse load. Figs. 4.13 and 4.14 represent radial displacement eigenvector contour plots for the $(0/+45/-45/90)_s$ and $(0/-45/+45/90)_s$ respectively. In reviewing Fig. 4.11, one can see that at collapse the $(0/+45/-45/90)_s$ ply orientation has shifted to the secondary loading path (the eigenvector shown in Fig. 4.13). However, in reviewing Fig. 4.12 and 4.13 both plots of the $(0/-45/+45/90)_s$, one sees that at collapse the displacement contours are not in the secondary (eigenvector) mode. This associated phenomena can be explained again by looking at M_{xy} . A side cutout means that there is less material between the cutout and the edge. Therefore, loads build up at a higher rate between the cutout and the side edge. Since the cutout is closer to the edge, the values of $D_{1\epsilon}$ and $D_{2\epsilon}$ (Eqn. 27) and there positive or negative values depending on ply orientation, determine the



$W_{max} = -0.042972$ inches

CONTOUR LEVELS ARE IN 10ths OF MAXIMUM DISPLACEMENTS

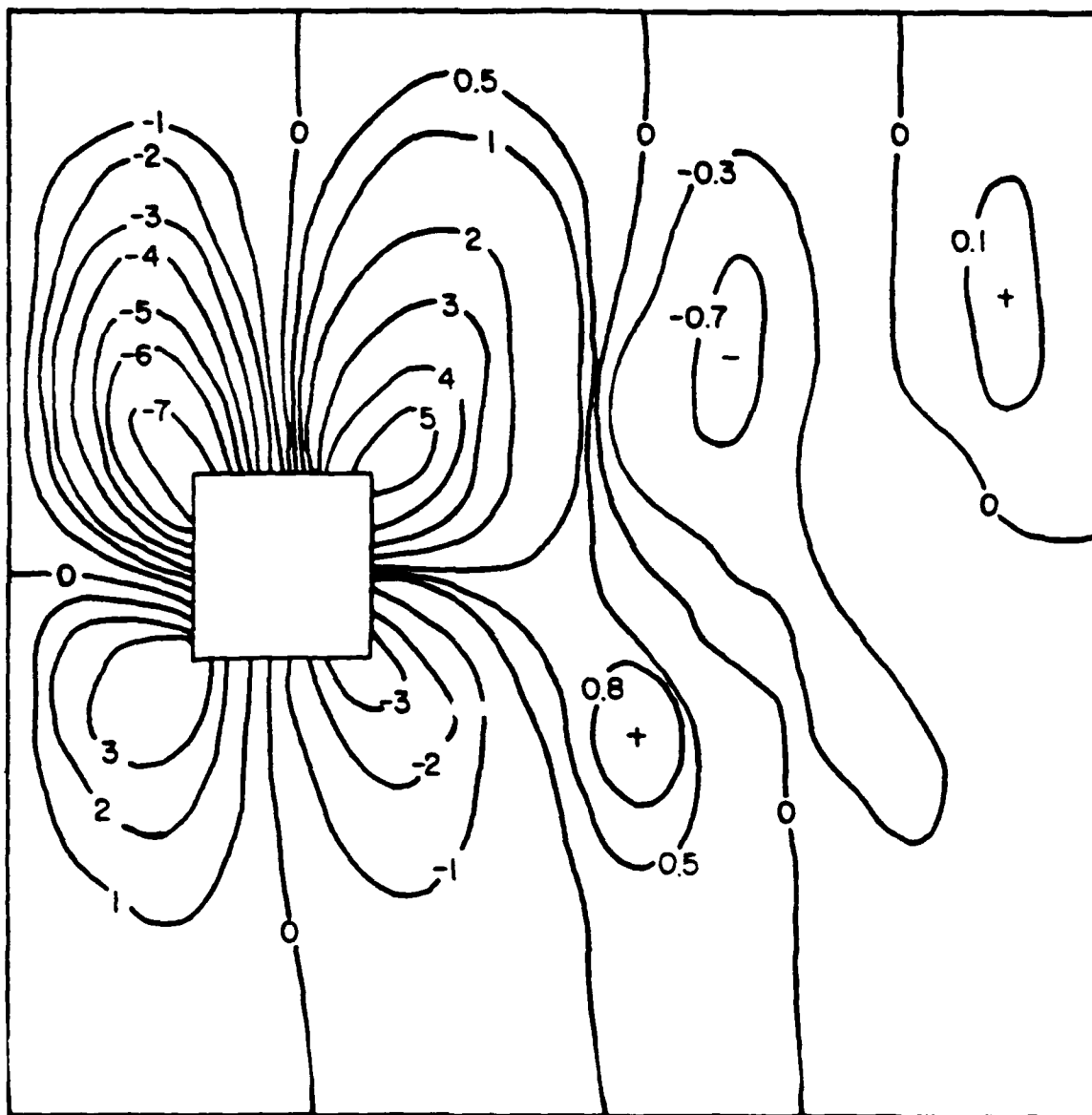
Fig. 4.11 Radial Displacement Contour Plot for 2" x 2" Cutout at Collapse Load of 147.2 lbs/in (0/+45/-45/90)s, Cutout C



$W_{max} = -0.035172$ inches

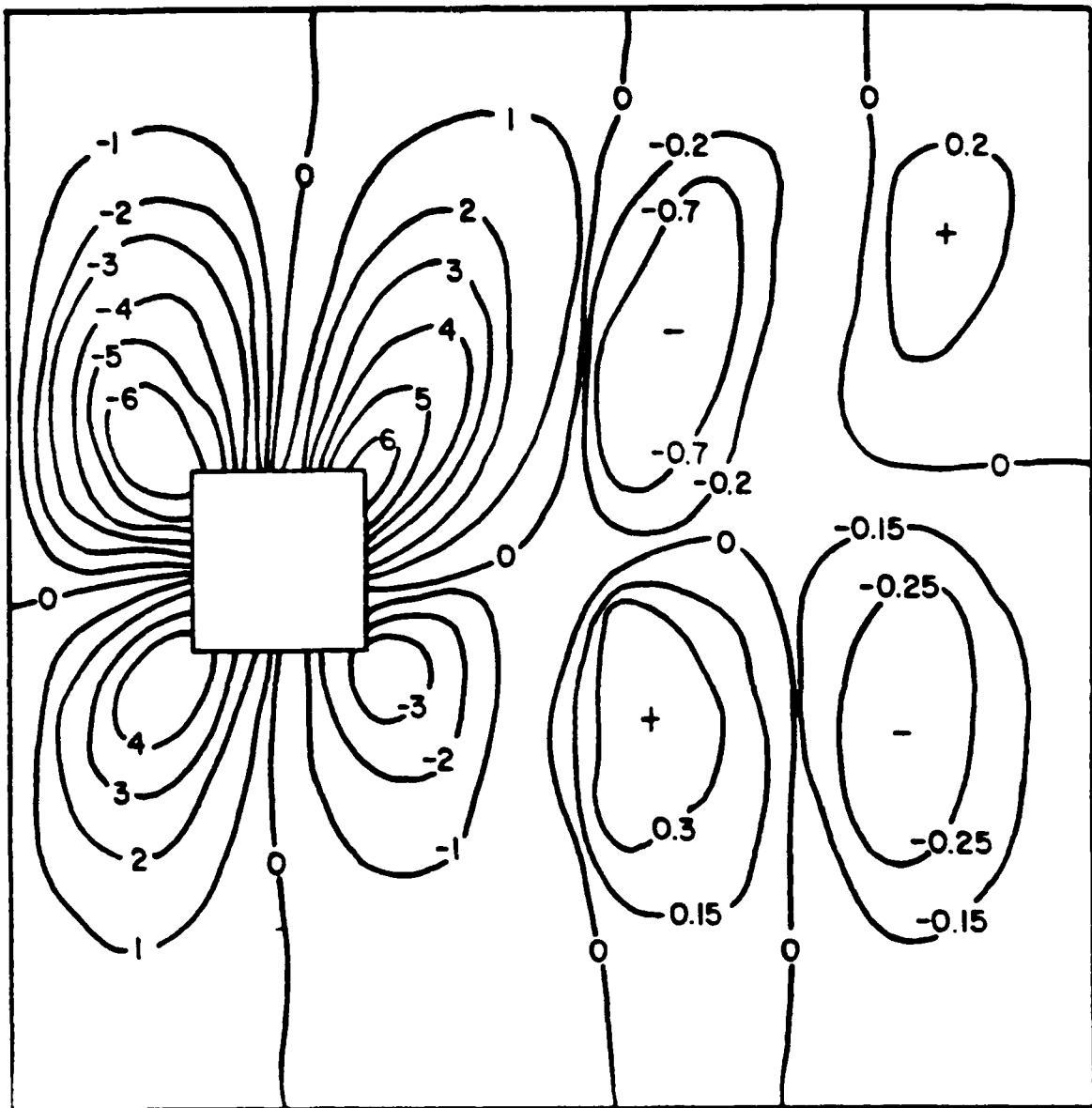
CONTOUR LEVELS ARE IN 10ths OF MAXIMUM DISPLACEMENTS

Fig. 4.12 Radial Displacement Contour Plot for 2° x 2° Cutout at Collapse Load of 178.6 lbs/in (0/-45/+45/90)s, Cutout C



CONTOUR LEVELS ARE IN 10ths OF MAXIMUM DISPLACEMENTS

Fig. 4.13 Eigenvector Contour Plot for 2" x 2" Cutout
(0/+45/-45/90)s, Cutout C



CONTOUR LEVELS ARE IN 10ths OF MAXIMUM DISPLACEMENTS

Fig. 4.14 Eigenvector Contour Plot for 2" x 2" Cutout
(0/-45/+45/90)s, Cutout C

amount of twisting moment, M_{xy} on the panel. The (0/+45/-45/90)s orientation, as seen earlier, has positive values for D_{16} and D_{26} and thus a greater twisting moment dominance and thus a lower collapse load. The opposite is true for the (0/-45/+45/90)s orientation. Here, since the D_{16} and D_{26} values are negative, the twisting moment is less and the panel can withstand a higher collapse load than the (0/+45/-45/90)s configuration.

Load displacement plots for cutout A and cutout C are shown in Fig. 4.15. This plot demonstrates the displacement in the direction of the load. The slight curvature near the collapse load expresses the fact that the problem is nonlinear. Since cutout C has a greater slope than cutout A, cutout C has greater axial stiffness.

Now a 4" x 4" cutout was placed along one side, cutout location C. The 4" x 4" cutout does not have a unique dependence on the ply orientation as was seen with the 2" x 2" cutout. A ply orientation of (0/+45/-45/90)s produces a collapse load of 66.0 lbs/in or a 26.7% decrease from the 4" x 4" middle cutout. Now, with a ply orientation of (0/-45/+45/90)s, a collapse load of 66.0 lbs/in was also obtained. The radial displacement contour plots are the same for the (0/+45/-45/90)s and the (0/-45/+45/90)s, Fig. 4.16 and 4.17 respectively. In looking at Fig. 4.16, the radial displacement contour plot for (0/+45/-45/90)s, one observes that the inward displacement trough is not along the second ply angle (+45°). The same displacement are noticed when Fig. 4.17 is also examined. As was the case with the middle 4" x 4" cutout, there is more symmetry about the circumferential and longitudinal axes than similar panels with cutouts. As mentioned previously, the larger cutout produces

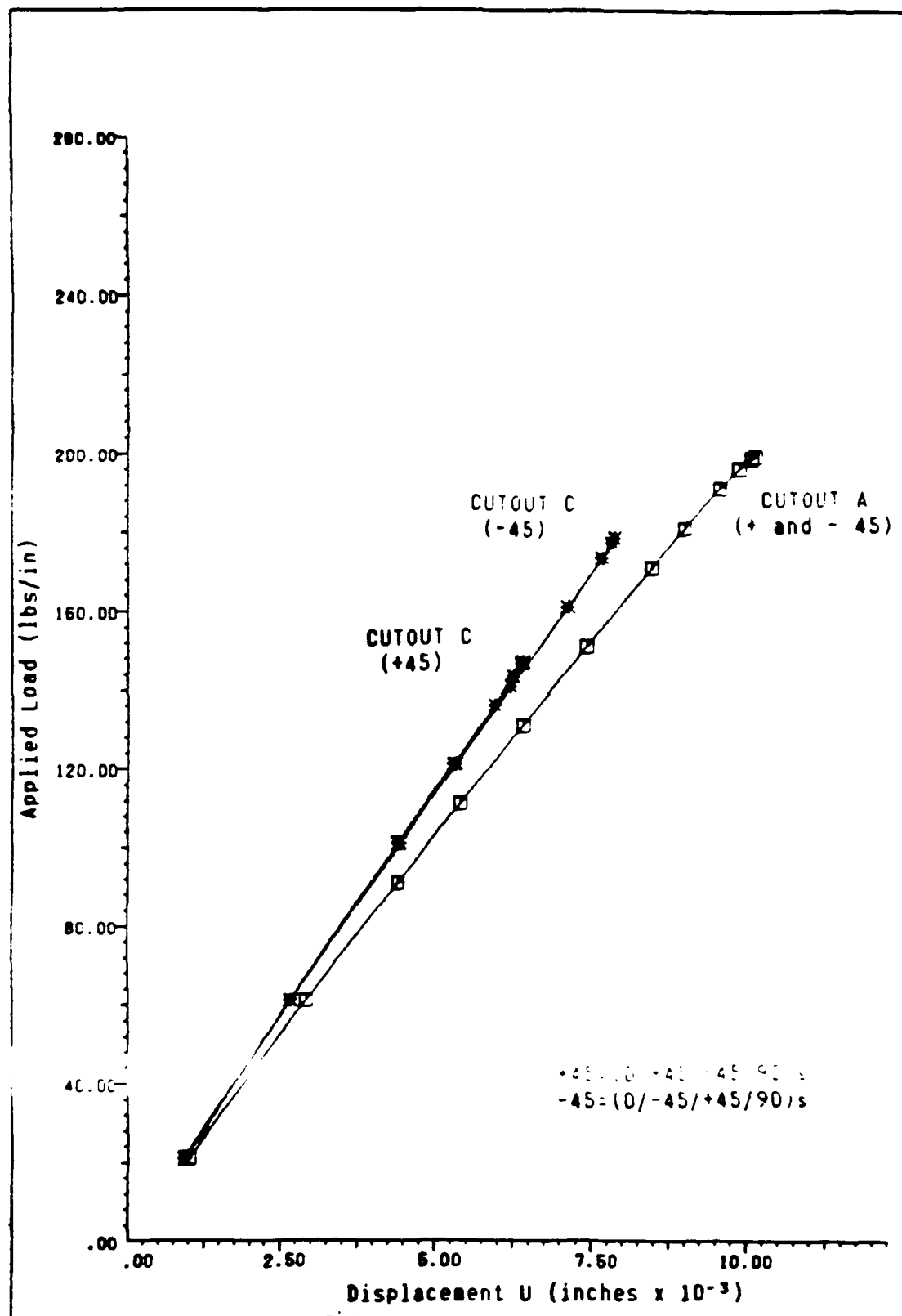
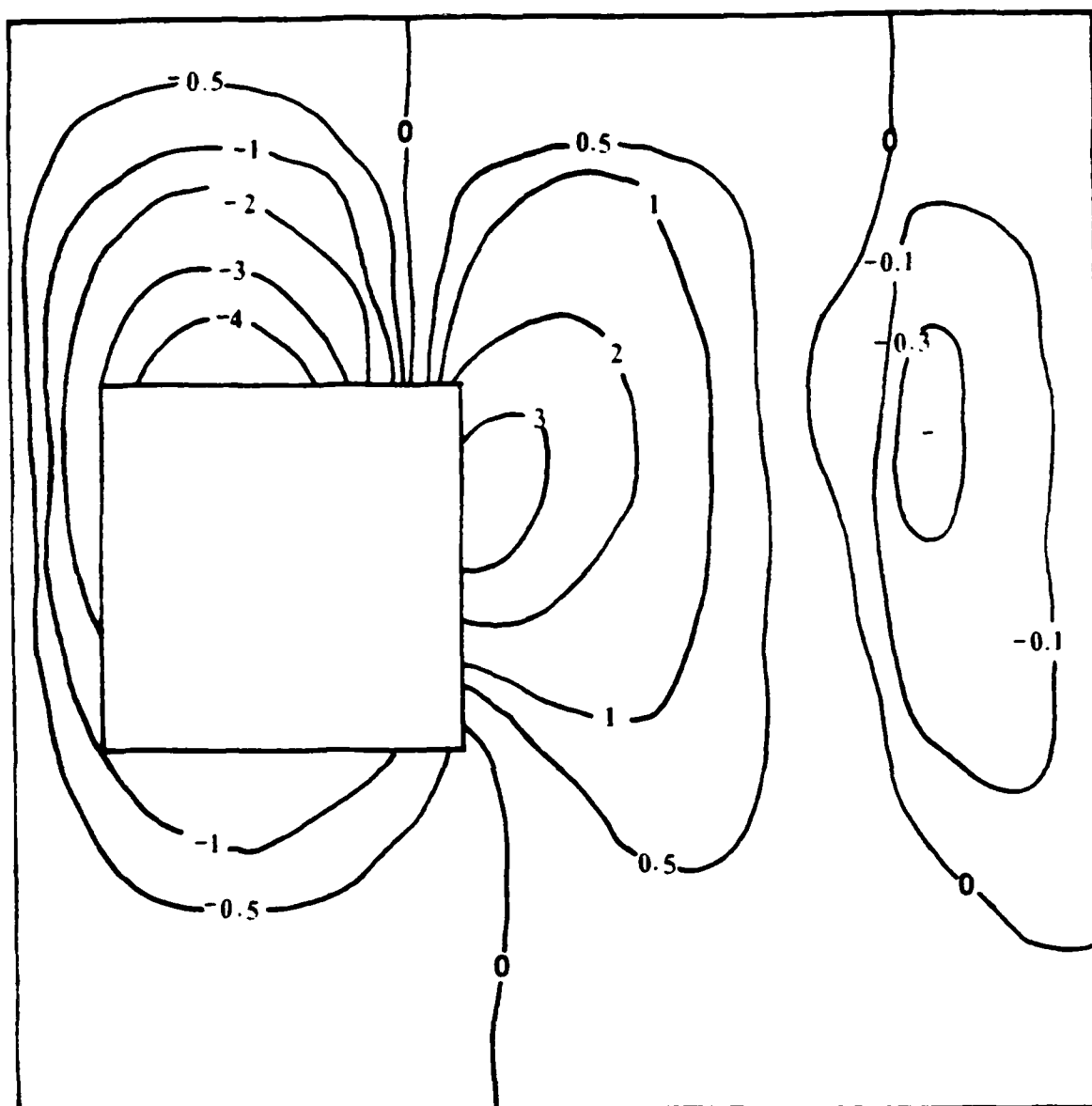


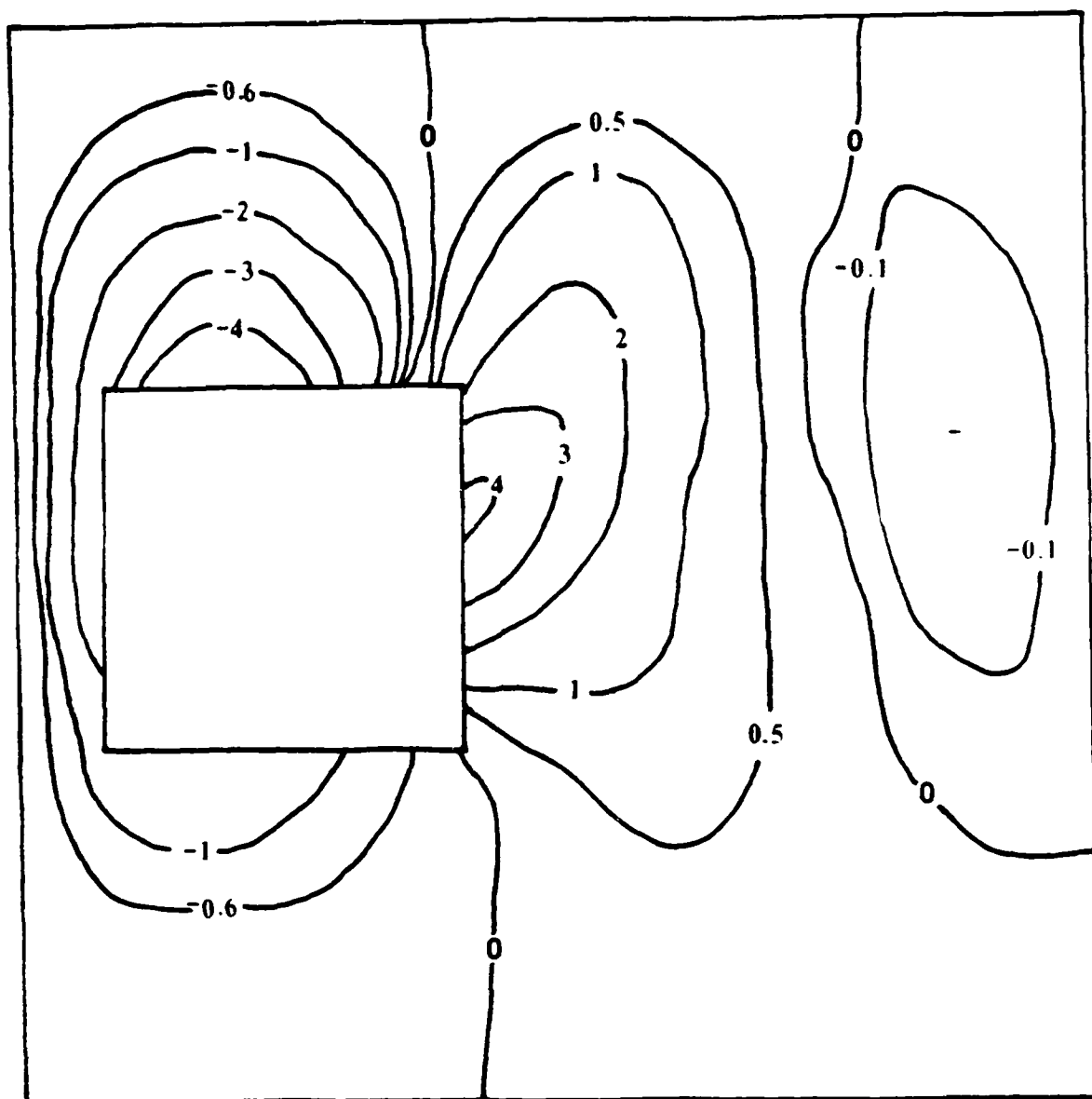
Fig. 4.15 Loading Edge Displacement, U, versus Axial Loading for Cutout A and Cutout C



$W_{max} = -0.0516$ inches

CONTOUR LEVELS ARE IN 10ths OF MAXIMUM DISPLACEMENTS

Fig. 4.16 Radial Displacement Contour Plot for 4" x 4" Cutout at Collapse Load of 66.0 lbs/in (0/+45/-45/90)s, Cutout C



$$W_{max} = -0.0506 \text{ inches}$$

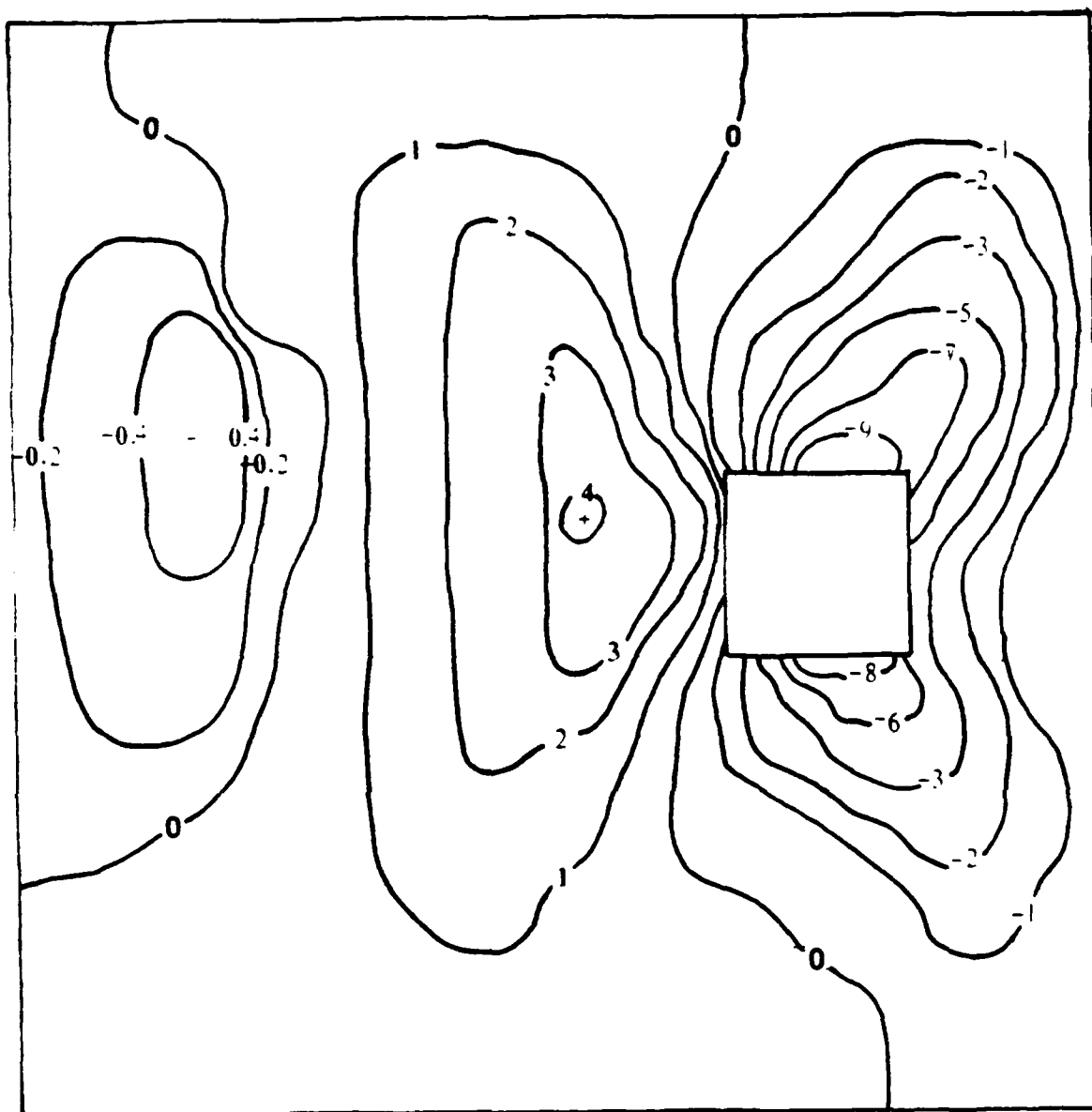
CONTOUR LEVELS ARE IN 10ths OF MAXIMUM DISPLACEMENTS

Fig. 4.17 Radial Displacement Contour Plot for 4" x 4" Cutout at Collapse Load of 66.0 lbs/in (0/-45/+45/90)s, Cutout C

the direct bending effect earlier and the moment change is more spread out, therefore, a more symmetric displacement pattern. As before, when the panels collapsed, they did not go into the shape of the eigenvector (plot not shown) as the panels with the smaller cutouts did.

This same phenomena that was observed for the cutout at location C can be seen for a cutout located along the right side, cutout location D (Fig. 1.2). There, however, is one slight change. Fig. 4.18 the cutout D (0/+45/-45/90)s ply orientation contour plot exhibits exactly the same characteristics as the (0/-45/+45/90)s ply orientation plot, Fig. 4.12, for cutout location C. The same is true for the cutout D (0/-45/+45/90)s plot, Fig. 4.19, and the cutout C (0/+45/-45/90)s plot, Fig. 4.11. That is, there is a swapping phenomena. The +45° second ply arrangement on the right side looks like and has the same collapse load as that of the -45° second ply arrangement of the left side cutout. Likewise, the -45° right side arrangement acts exactly like the +45° left side arrangement. Due to this special phenomena, the analysis of the right side would be exactly the same as its counterpart, the left side, as discussed earlier.

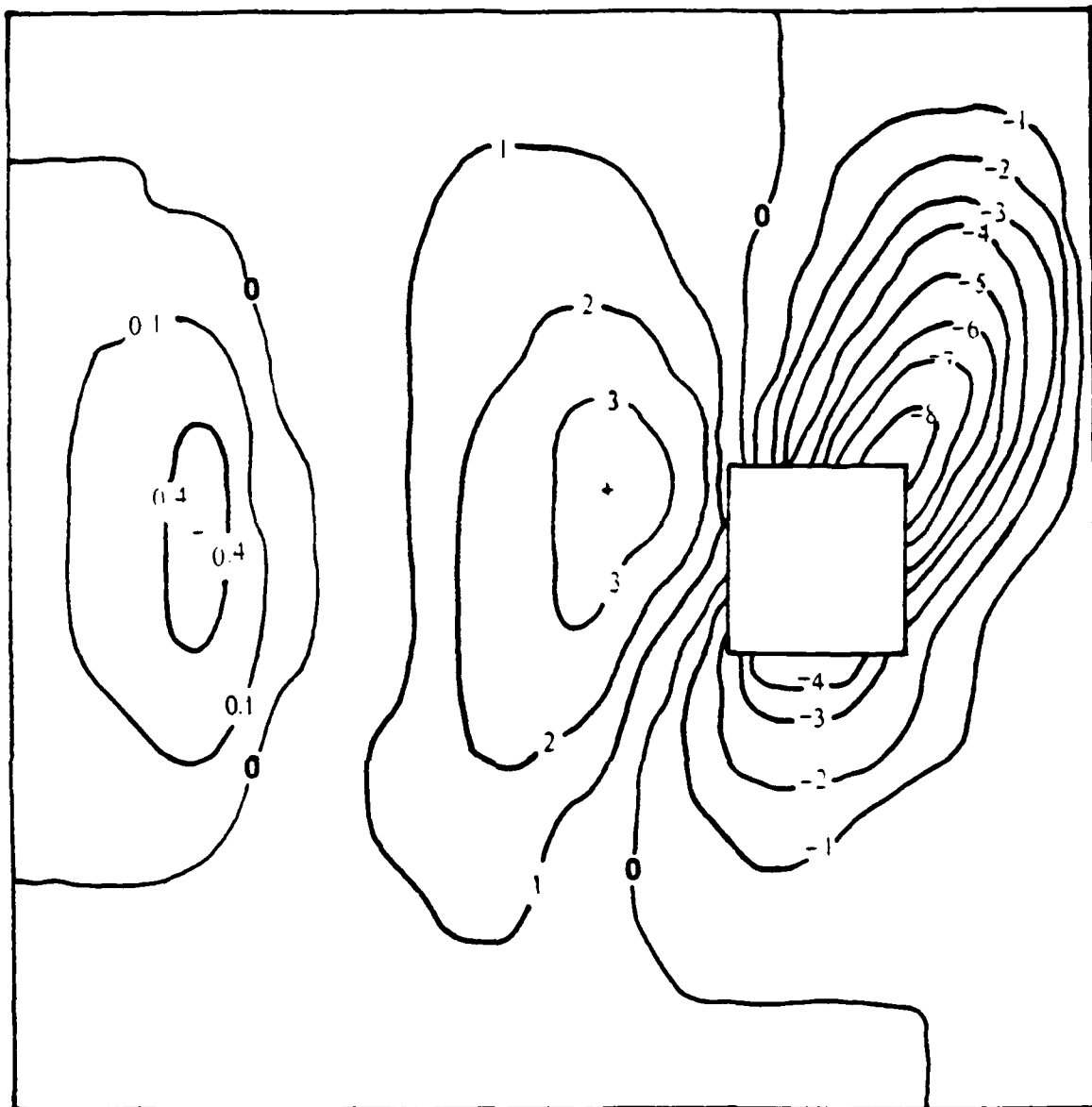
The results of the discontinuity location study is presented in Table 4.2. For the small cutout (2" x 2"), the different ply orientations really do not matter for cutouts located on the vertical axis of symmetry. However, if a cutout is repositioned to either side of this vertical axis of symmetry the ply orientation makes a significant difference. For the larger cutout (4" x 4") the ply orientation does not make a difference as the problem has become totally nonlinear.



$$W_{max} = -0.03507 \text{ inches}$$

CONTOUR LEVELS ARE IN 10ths OF MAXIMUM DISPLACEMENTS

Fig. 4.18 Radial Displacement Contour Plot for 2" x 2" Cutout at Collapse Load of 178.6 lbs/in (0/+45/-45/90)s, Cutout D



$$W_{max} = -0.0467 \text{ inches}$$

CONTOUR LEVELS ARE IN 10ths OF MAXIMUM DISPLACEMENTS

Fig. 4.19 Radial Displacement Contour Plot for 2" x 2" Cutout at Collapse Load of 147.2 lbs/in (0/-45/+45/90)s, Cutout D

Table 4.2: Discontinuity Location Study Results

Cutout	Ply	Collapse	Linear	percent of
<u>Location</u>	<u>Orientation</u>	<u>Load (lbs/in)</u>	<u>Bifurcation (lbs/in)</u>	<u>Collapse at A</u>

2" x 2"

A	(0/+45/-45/90),	199.4	229.014	--
A	(0/-45/+45/90),	199.4	229.014	--
B	(0/+45/-45/90),	201.15	222.035	0.9
B	(0/-45/+45/90),	201.15	222.035	0.9
C	(0/+45/-45/90),	147.18	198.479	-26.2
C	(0/-45/+45/90),	178.6	198.530	-10.4
D	(0/+45/-45/90),	178.6	198.530	-10.4
D	(0/-45/+45/90),	147.16	198.479	-26.2

4" x 4"

A	(0/+45/-45/90),	90.0	95.32	--
A	(0/-45/+45/90),	90.0	95.32	--
C	(0/+45/-45/90),	66.0	82.57	-26.7
C	(0/-45/+45/90),	66.0	82.57	-26.7

Material Degradation Effects Study

The previous study indicated that the critical cutout locations for establishing upper and lower bound effects can be attributed to the center and eccentric positions. Thus, these two positions were investigated relative to material degradation effects. For the material degradation investigation carried out within this study, a combination of moisture conditions, temperature and time intervals were looked at in order to produce the widest change in phenomena possible. The weight gain due to moisture concentration distribution and the moisture and temperature induced degradations in the E_z and G_{12} moduli are shown in Fig. 4.20 and 4.21, respectively [24]. For this analysis two temperatures were examined, 80 °F (300 °K) and 250 °F (394 °K). The 80 °F temperature represents room temperature conditions and the 250 °F temperature is roughly 100 degrees below the glass transition temperature. This 250 °F temperature does represent the point where the material properties really start to play an important role. Two moisture concentration conditions were chosen (Table 4.3). One was symmetric ($C_0=0.0$, $C_1=0.0105$, $C_2=0.0105$) and the other unsymmetric ($C_0=0.0$, $C_1=0.0$, $C_2=0.0105$). The moisture concentration is measured as a percentage of the original weight gained through moisture absorption. For the AS4/3501 graphite/epoxy, the saturation moisture concentration is assumed to be 1.05%. Finally, two different time events were chosen, a short 0.35 days ($t^*=0.001$) and a steady state 176.24 days ($t^*=0.5$) where t^* is a normalized time equal to Kt/h^2 . Shown in Table 4.4 are the relations between real and dimensionless time. With the combinations mentioned above, there will be

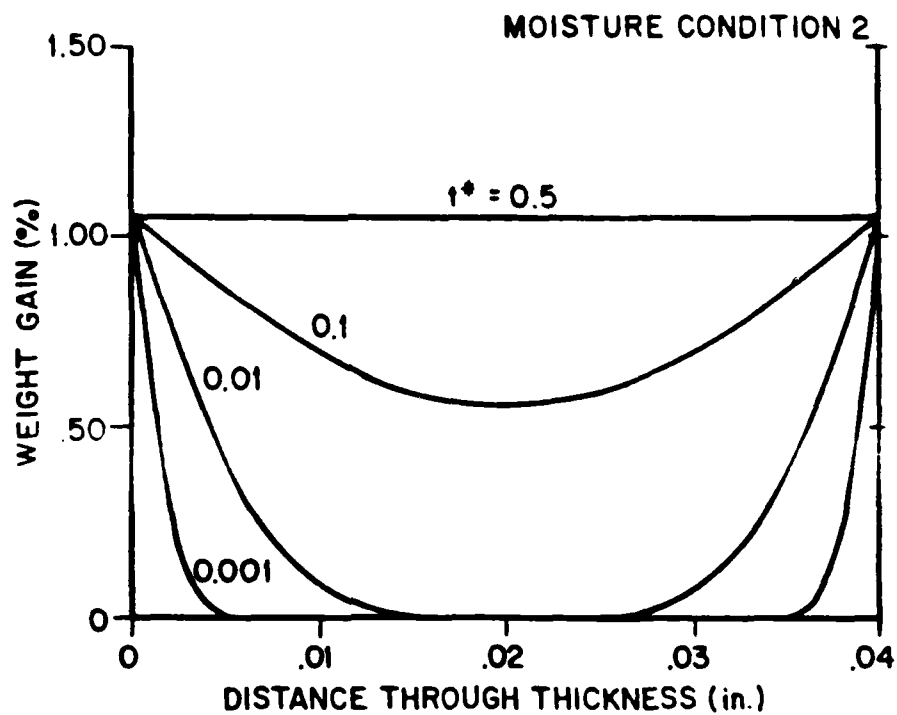
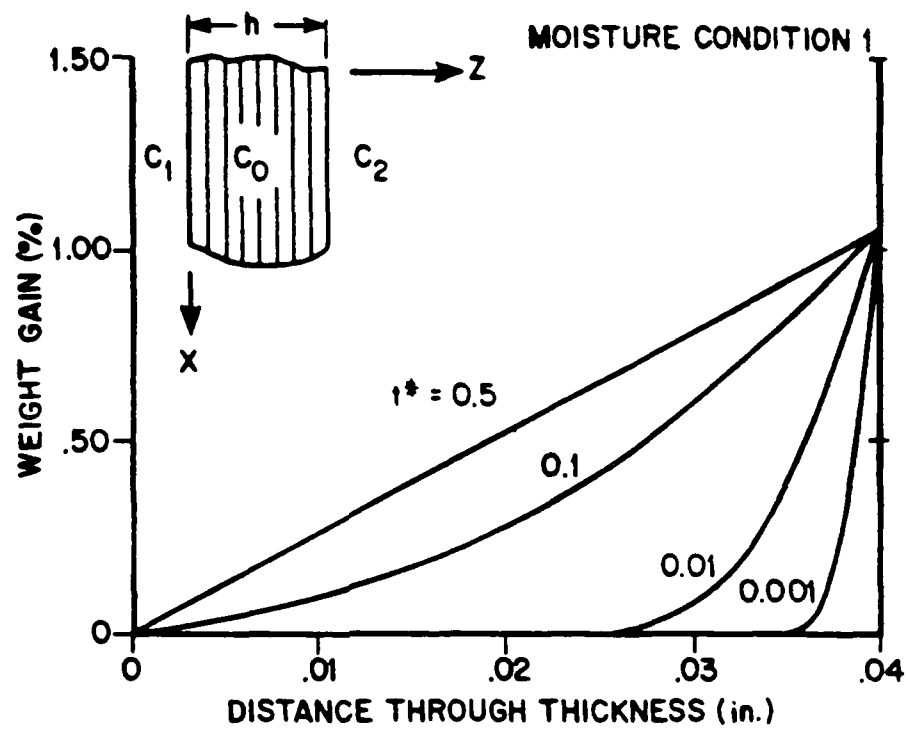


Fig. 4.20 Moisture Concentration Distribution for Unsymmetric and Symmetric Moisture Conditions

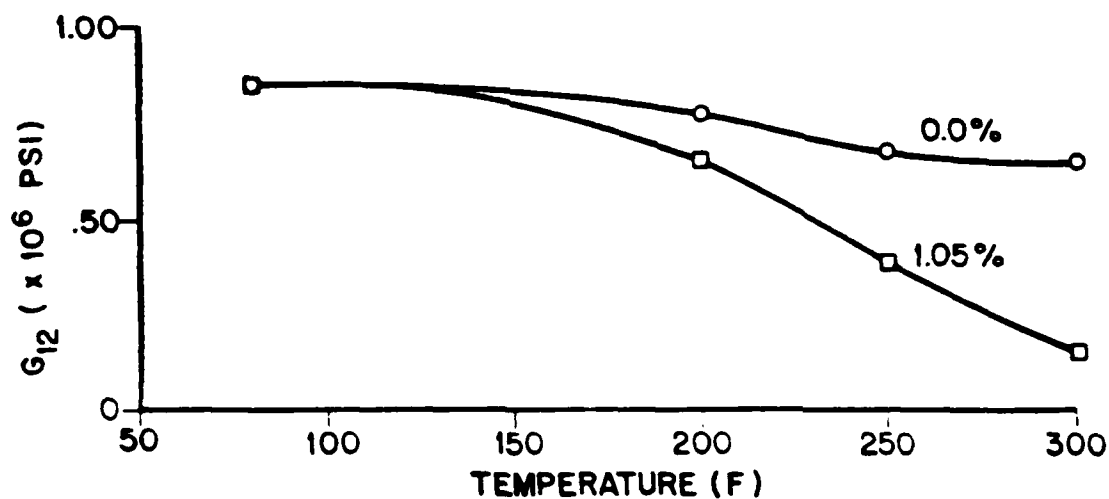
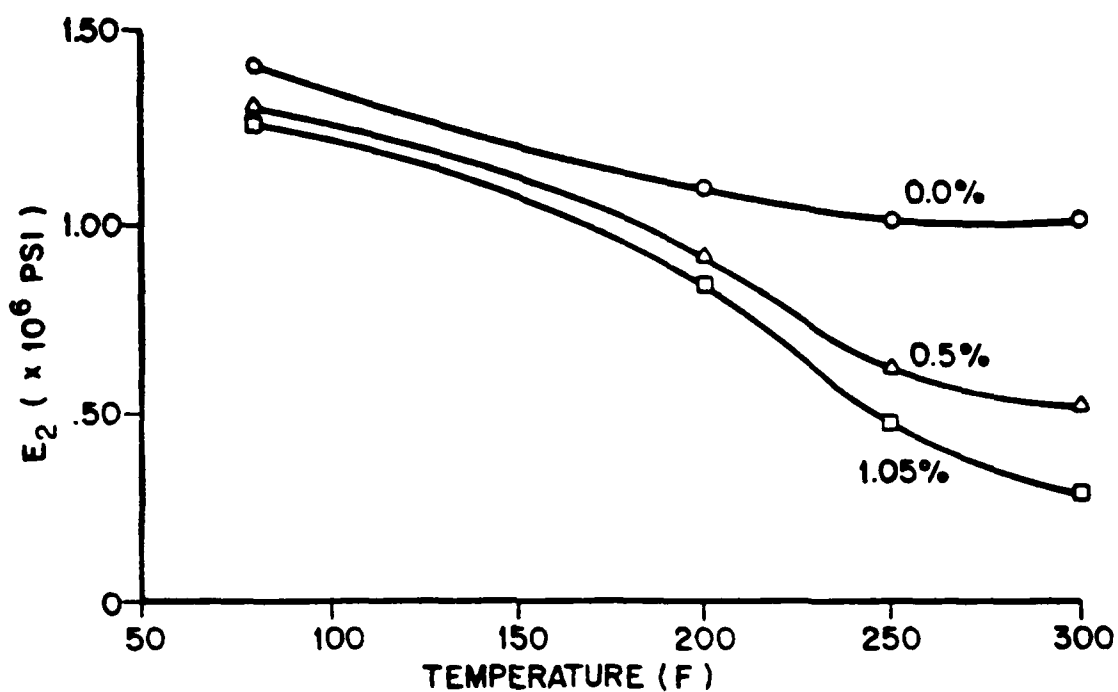


Fig. 4.21 E_2 and G_{12} Degradation vs Temperature at Constant Values of Moisture Concentration

Table 4.3 Moisture Conditions

Moisture Conditions			
Cond. No.	C ₀	C ₁	C ₂
1	0.00	0.00	0.0105
2	0.00	0.0105	0.0105

Table 4.4 Relation Between Real and Dimensionless Time

Relation Between Real and Dimensionless Time		
Real Time (sec)	Real Time (days)	Dimensionless Time t*
0.0	0.0	0.0
3.045E04	0.35	0.001
3.045E05	3.52	0.01
3.045E06	35.24	0.1
1.527E07	176.24	0.5

Note: These times were calculated using $K = 0.52537E-10$ (in²/sec) for an 8-ply, 0.04 thick, AS/3501-5 laminate.

a total of 8 runs for each case. Two cases were chosen for this study, a 2" x 2" cutout located in the middle of the panel (cutout location A) and a 2" x 2" cutout located on the side of the panel (cutout location C) which were found to represent the overall nature of cutout location.

The easiest way to analyze the material degradation effects is through the use of Figs. 4.22 and 4.23. In these plots $N_{x,orig}$ represents the bifurcation load for the room temperature condition at time equal to zero ($t^*=0.0$) for the various cutout conditions investigated. This condition is unaffected by either temperature or moisture degradations. As was expected, the panel bifurcation load decreased with increasing temperature and absorbed moisture. Fig. 4.22, the unsymmetric moisture condition plot, shows that as time increases there is little effect on the reduction in collapse load for the cutouts studied. Whereas, for the panel with no cutout, there is a significant reduction in the collapse load as the temperature is increased. Moreover, there is very little change in collapse for the two cutout locations considered as time progresses. In Fig. 4.23, the symmetric moisture condition plot, there is an effect on the reduction in the collapse load as temperature is increased for both the non-cutout and cutout panel. Again, there is very little effect due to different cutout locations on the change in the reduction of the collapse load due to the material degradation effects.

Looking once again at Figs. 4.22 and 4.23, involving buckling versus time for two different boundary conditions, one observes certain characteristics (previously mentioned), especially the fact that the symmetric boundary condition produces a greater reduction of the buckling load as temperature and time are increased. In order to explain these

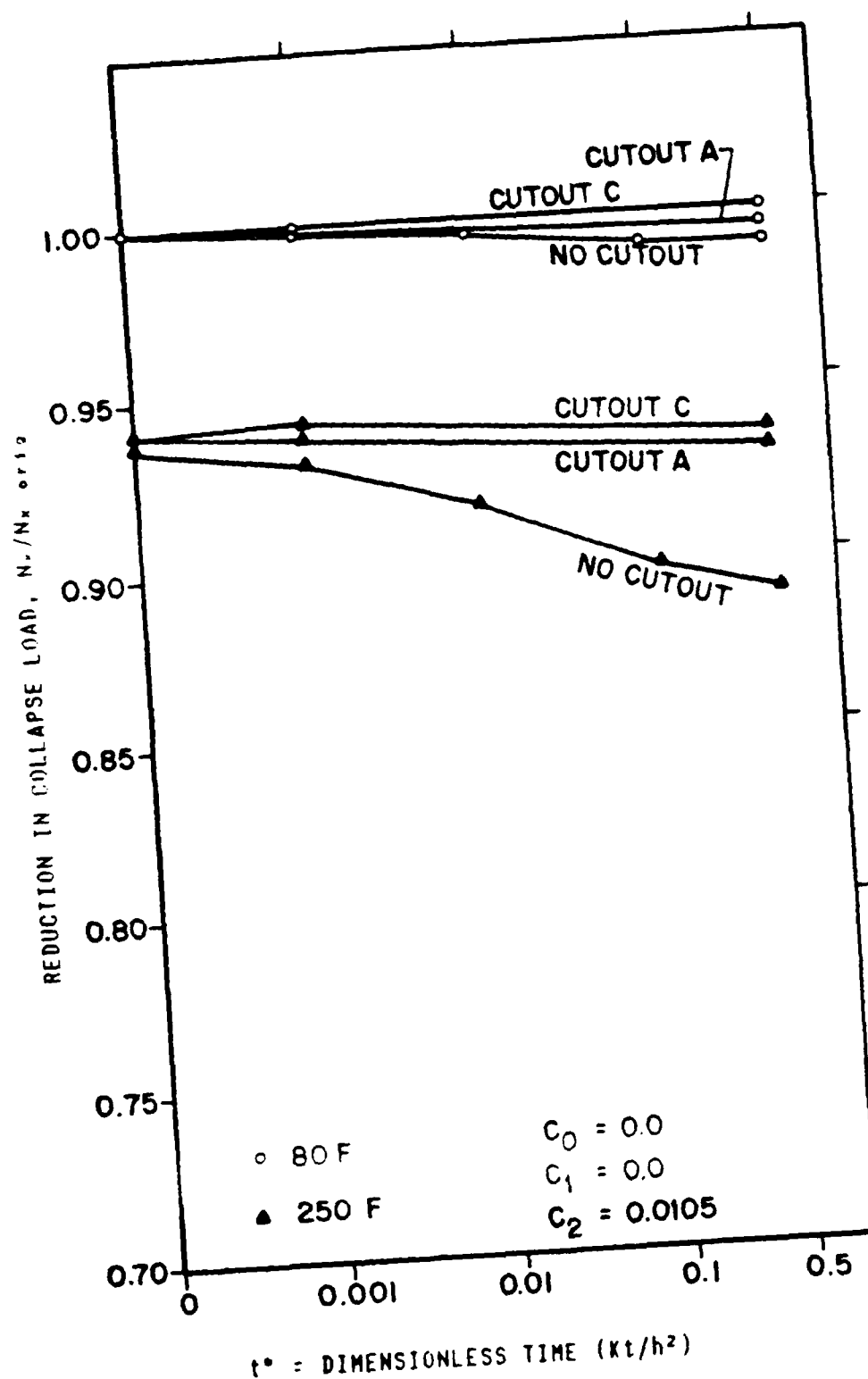


Fig. 4.22 Degradation in N_x for Unsymmetric Moisture Condition

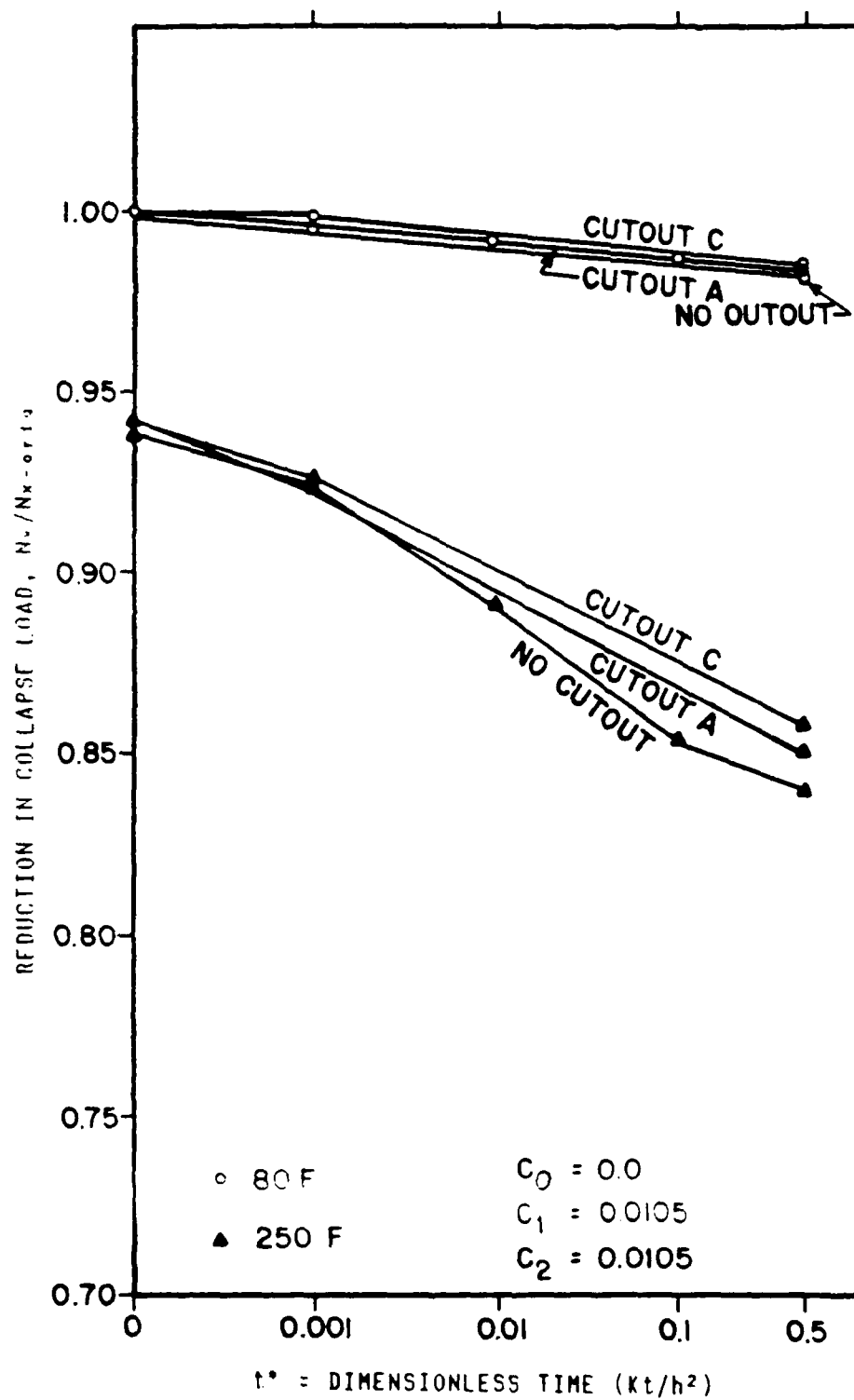
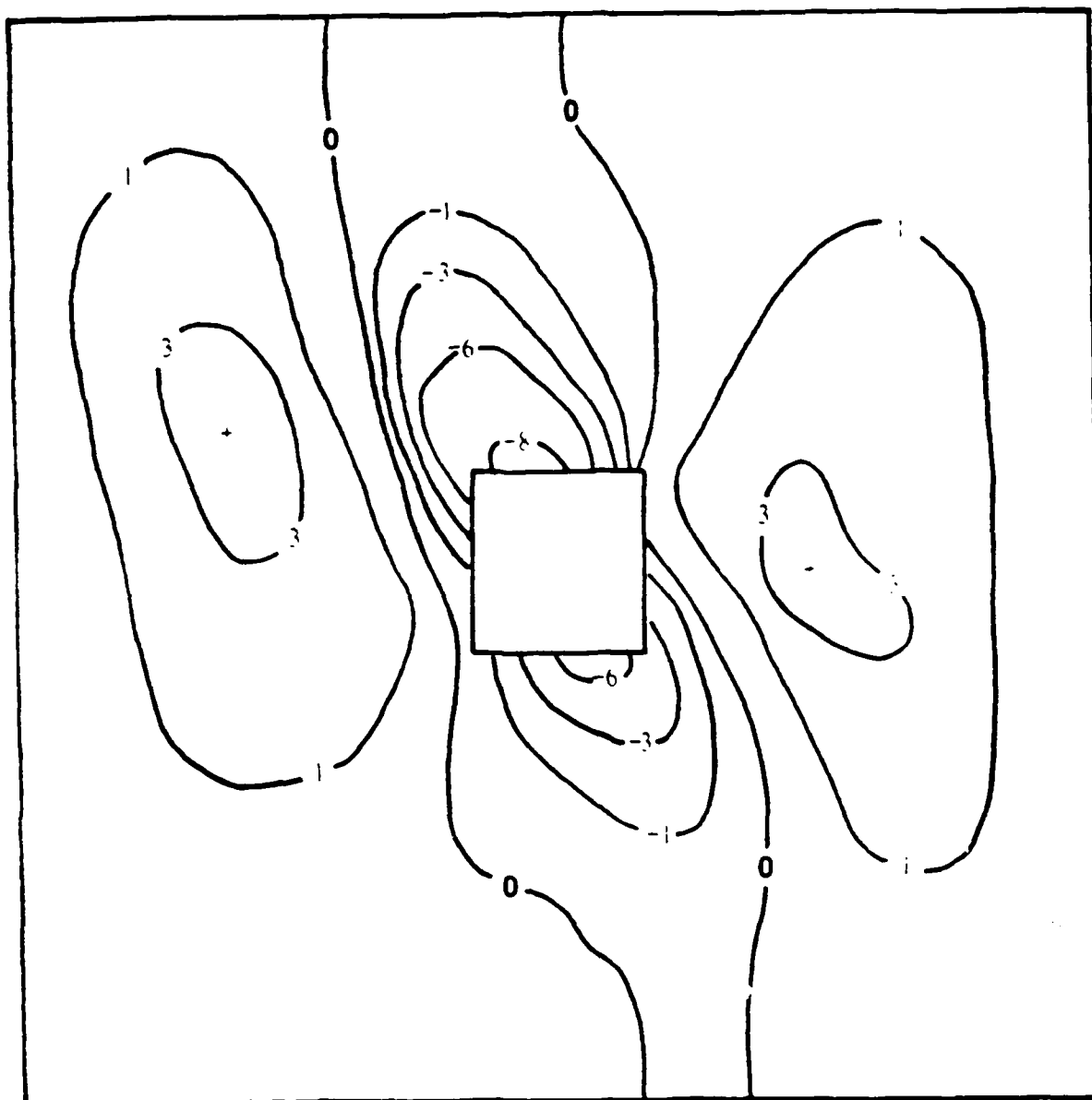


Fig. 4.23 Degradation in N_x for Symmetric Moisture Condition

characteristics, look at Figs. 4.20 and 4.21. For the unsymmetric case at $t^*=0.001$, the weight gain due to moisture (Fig. 4.20) conditions is concentrated on only one edge of the panel. In comparison, the symmetric moisture conditions produce twice as much weight gain. If one now looks at Fig. 4.21, it can be seen that the moisture concentration percentages follow a negative slope. The symmetric moisture condition, which is twice as concentrated as the unsymmetric case, would then produce greater changes in the material properties as temperature increases. If the same comparison is made for $t^*=0.5$, an even greater change can be seen. Therefore, the symmetric boundary condition, which is affected the most, produces a greater affect on the reduction of the buckling load as time and temperature are increased.

The radial displacement contour plots for the temperature and moisture affected panels produce the same results obtained for the non-material degraded panels. There is, however, a reduction in the collapse load as the moisture and temperature changes take effect. Shown in Figs. 4.24 and 4.25 are the radial displacement contour plots for the 2" x 2" cutout A at collapse load for room temperature (80 °F) and for the high temperature (250 °F) both at symmetric moisture conditions respectively. As can be seen by both Figs. 4.24 and 4.25 the conditions at collapse are almost identical for both cases as well as looking like the non-affected (no temperature or moisture degradation) panels. Fig. 4.26 represents the material degradation effect of the 4" x 4" cutout A which has nearly the same contour displacement plot as the normal non-affected 4" x 4" panel.

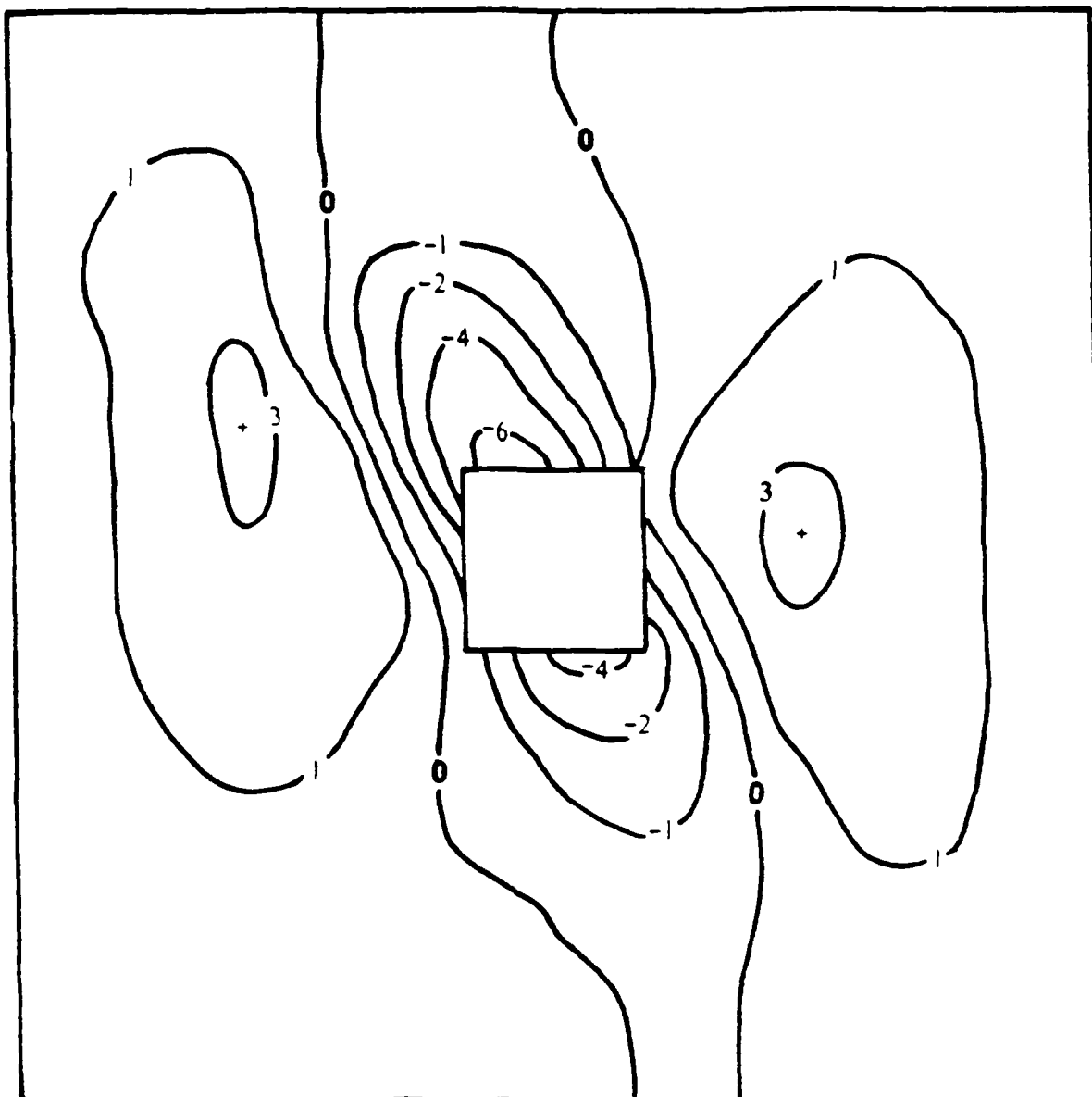
Now shown in Table 4.5 are the results of the material degradation study. This table clearly shows that the symmetric moisture condition produces a greater affect on the collapse load. Also, as temperature and moisture saturation are increased ($t^* = 0.5$ and 250°F) the value for the collapse load decreases. The overall affect of the material degradation can be seen more clearly in Figs. 4.27 and 4.28. These figures represent the reduction in collapse load as a panel with no cutout is altered by both a cutout and then temperature and moisture for both the symmetric and unsymmetric cases respectively. As Fig. 4.27 shows, material degraded panels could have their collapse load decreased by as much as 67% for a cutout located at position A and 75.5% for a cutout located at C. In other words, the effect of placing a 2" x 2" cutout in a panel and having this panel subjected to high temperature and symmetric saturated moisture conditions is to develop collapse at one-quarter of the uncut, room temperature panel's buckling load.



$W_{max} = -0.0467$ inches

CONTOUR LEVELS ARE IN 10ths OF MAXIMUM DISPLACEMENTS

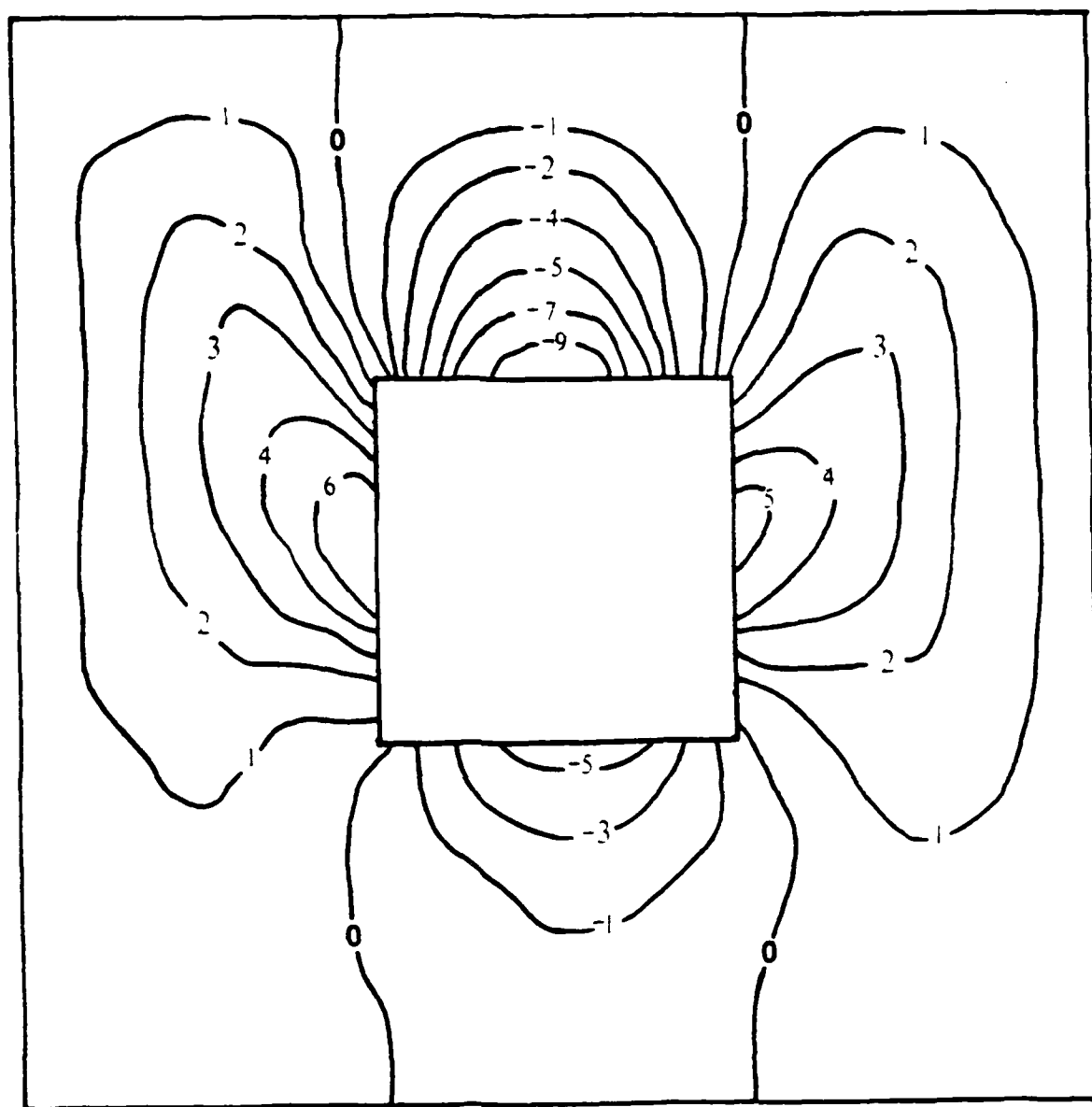
Fig. 4.24 Radial Displacement Contour Plot for 2" x 2" Cutout at Collapse Load of 198.5 lbs/in (0/+45/-45/90)s, Cutout A and Symmetric Moisture Distribution, $t^* = 0.001$, and Room Temperature (80 °F)



$$W_{max} = -0.0461 \text{ inches}$$

CONTOUR LEVELS ARE IN 10ths OF MAXIMUM DISPLACEMENTS

Fig. 4.25 Radial Displacement Contour Plot for 2" x 2" Cutout at Collapse Load of 169.8 lbs/in (0/+45/-45/90)_s, Cutout A and Symmetric Moisture Distribution, $t^* = 0.5$, and High Temperature (250 °F)



$W_{max} = -0.0650$ inches

CONTOUR LEVELS ARE IN 10ths OF MAXIMUM DISPLACEMENTS

Fig. 4.26 Radial Displacement Contour Plot for 4" x 4" Cutout at Collapse Load of 82.25 lbs/in (0/+45/-45/90)s, Cutout A and Symmetric Moisture Distribution, $t^* = 0.5$, and High Temperature (250 °F)

Table 4.5: Material Degradation Results

<u>2" x 2" Cutout</u>						
Temperature (°F)	Nondimensional Time (t*)	Cutout Location	Unsymmetric		Symmetric	
			<u>Moisture</u>		<u>Moisture</u>	
			Collapse Load	% Change	Collapse Load	% Change
30	0.001	A	199.4	0.00	198.5	0.45
		C	147.2	0.00	146.8	0.26
		NON	514.4	0.08	513.8	0.19
80	0.5	A	198.8	0.30	196.0	1.71
		C	147.0	0.12	145.3	1.28
		NON	510.7	0.80	506.8	1.55
250	0.001	A	187.3	6.09	183.8	7.82
		C	138.9	5.63	136.3	7.39
		NON	479.2	6.92	476.6	7.42
250	0.5	A	186.3	6.57	169.8	14.84
		C	137.9	6.31	126.3	14.19
		NON	452.6	12.08	432.6	15.97

$$t^* = kt/h^2$$

collapse load in lbs/in

Room temp./no moisture

Cutout A = 199.4

Cutout C = 147.2

No Cutout = 514.8

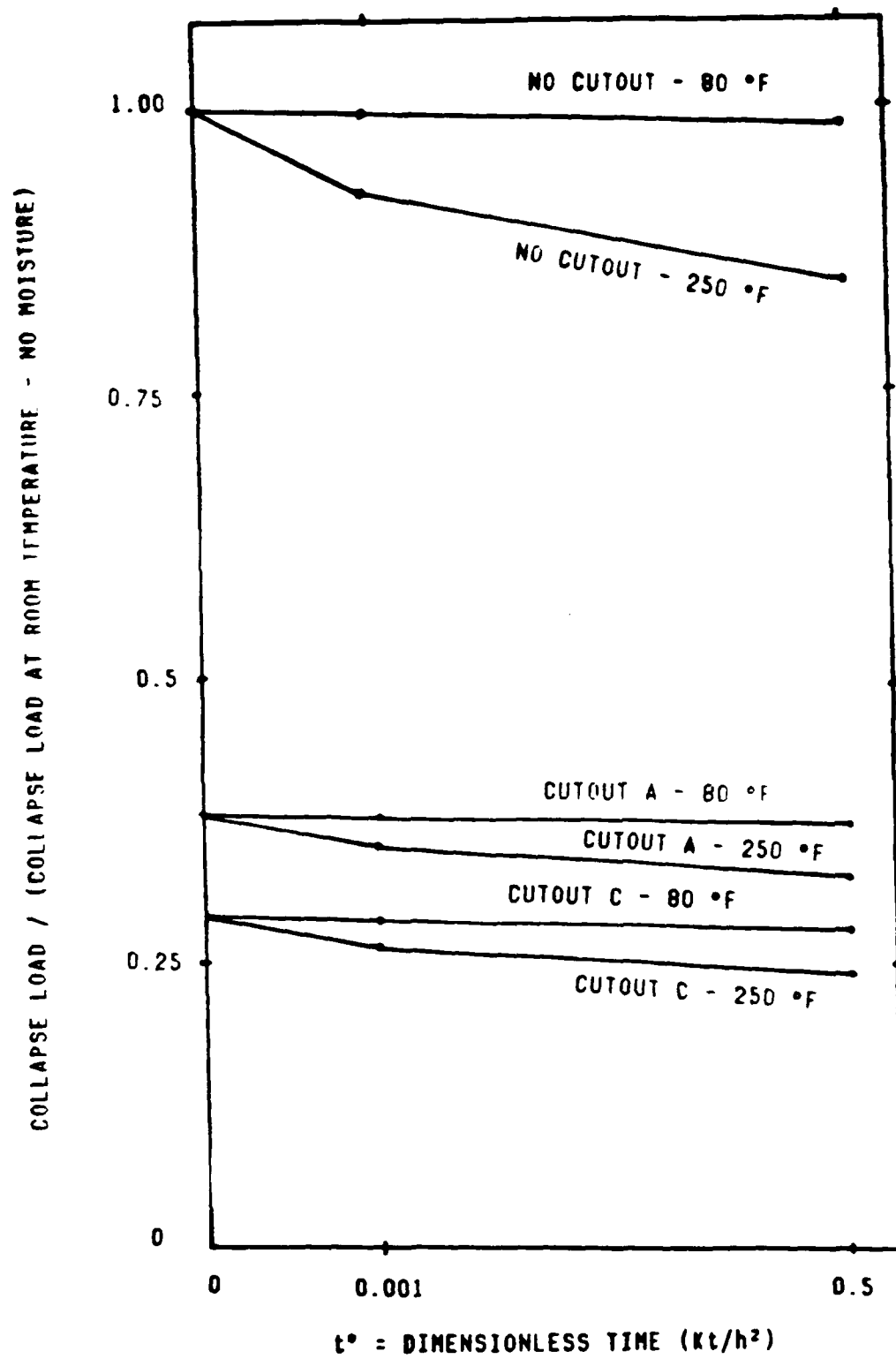


Fig. 4.27 Reduction in Collapse Load - Symmetric Moisture Condition

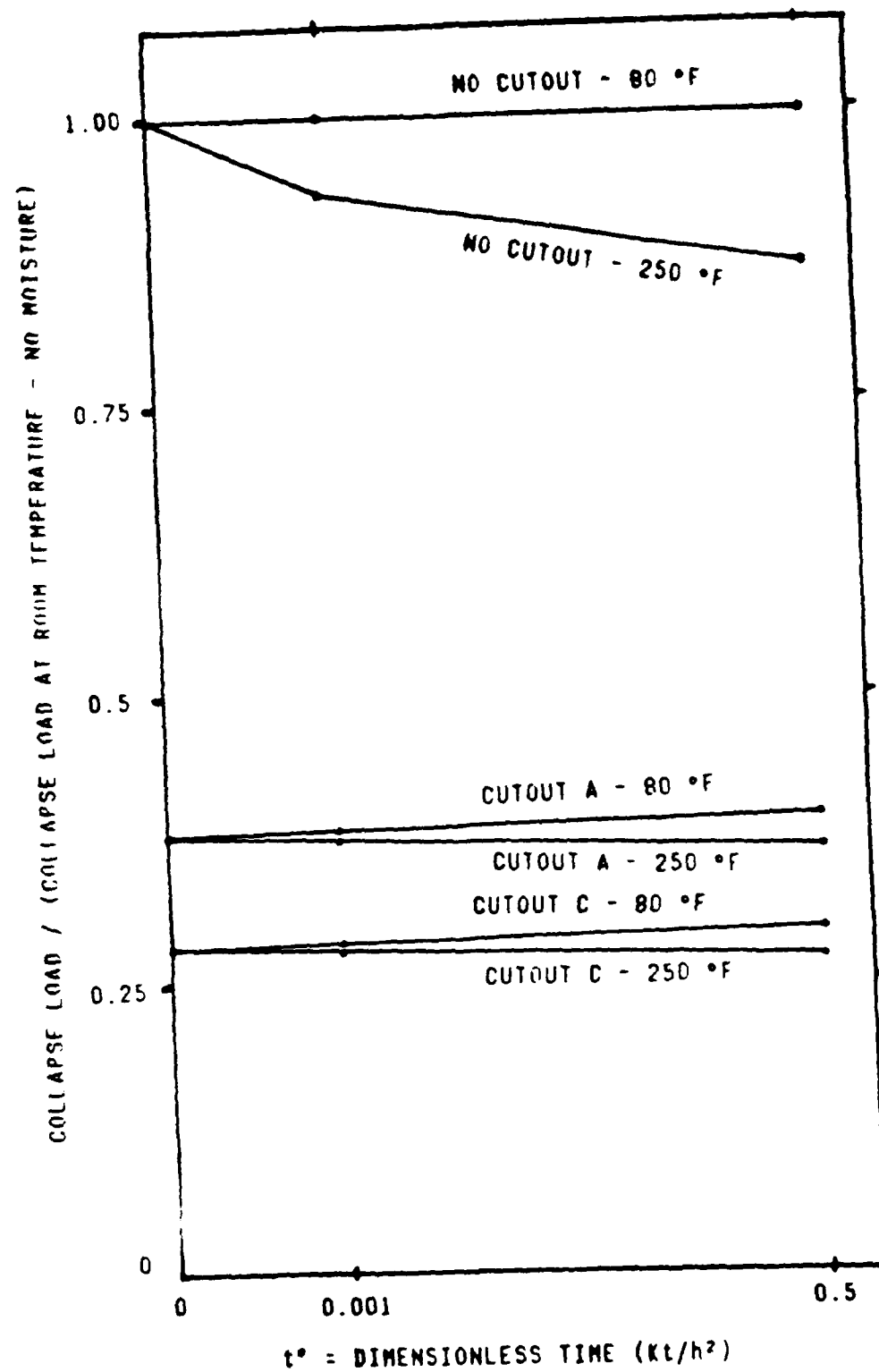


Fig. 4.28 Reduction in Collapse Load - Unsymmetric Moisture Condition

V. CONCLUSIONS

The following conclusions can be stated based on the results developed from this study.

1. Collapse characteristics of composite panels are dependent on the ply layup and the size of the cutout.
2. Two ply orientations $(0/+45/-45/90)_s$ and $(0/-45/+45/90)_s$ were studied, and for cutouts located along the vertical axis of symmetry there was no affect on the collapse load due to the two ply orientations (cutouts A and B).
3. For the same two ply orientations stated in (2), there was a reduction in the collapse load of 17.6% for a 2" x 2" cutout located near the side support (eccentric location).
4. Cutouts moved from the middle to the side can produce as much as a 26.7% reduction in the collapse load.
5. A panel with a small cutout (2" x 2") behaves almost linearly throughout the loading and at collapse produces a trough like that of the secondary loading path (the eigenvector).

6. A panel with the larger cutout (4" x 4"), due to the larger amount of bending, behaves nonlinearly throughout the entire loading range.
7. Material degradation effects (high temperature and saturated moisture conditions) can result in as much as a 15% reduction in collapse load for a panel with a cutout.
8. Material degradation effects on collapse load have nearly the same percentage change no matter where the cutout is located.
9. The unsymmetric moisture condition produces up to a 6.57% reduction in the collapse load of a panel with cutouts.
10. The symmetric moisture condition produces up to a 14.84% reduction in the collapse load of a panel with cutouts.
11. A panel with a cutout located along one edge subjected to saturated moisture conditions and high temperature will have the collapse load reduced by as much as 75.5% when compared to a room temperature, no moisture, uncut panel.

VI. RECOMMENDATIONS AND SUGGESTIONS

- (1) Panels subjected to damage (a satellite panel striking a small object in space) result in a cutout that is not square in nature but more closely resembles a circle. Therefore, work could be done in the area of an axially loaded composite panel with a circular cutout.
- (2) Experimental work to verify the results of this thesis would be very helpful and an area for further study.
- (3) More work should be done with the STAGS user-written subroutines. STAGS has the option for the user to enter his own subroutines and this would allow for a wider range of problems to be investigated.

APPENDIX A

Appendix A consists of a collection of plots that were used in the analysis of the information presented in this thesis. These plots are not formally discussed but are included as additional information for the reader.

Appendix A1

CUTOUT LOCATION A:

Radial displacement as a function of location, taken 3, 6, and 9 inches from the loading edge, as load is increased.

Moment profiles as a function of location, taken 3, 6, and 9 inches from the loading edge, as load is increased.

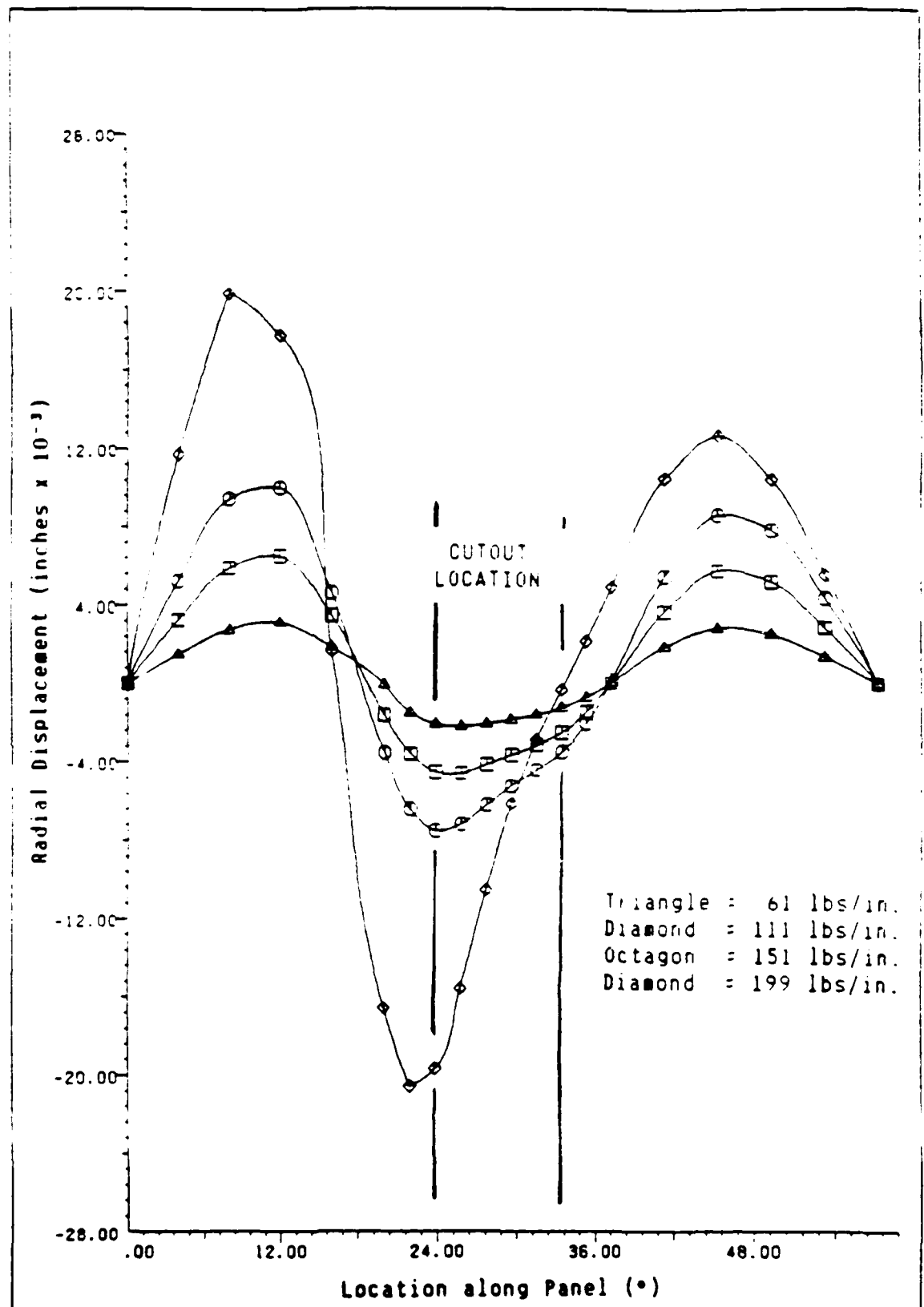


Fig. A1.1 Radial Displacement as a Function of Location taken 3 inches from the Loading Edge

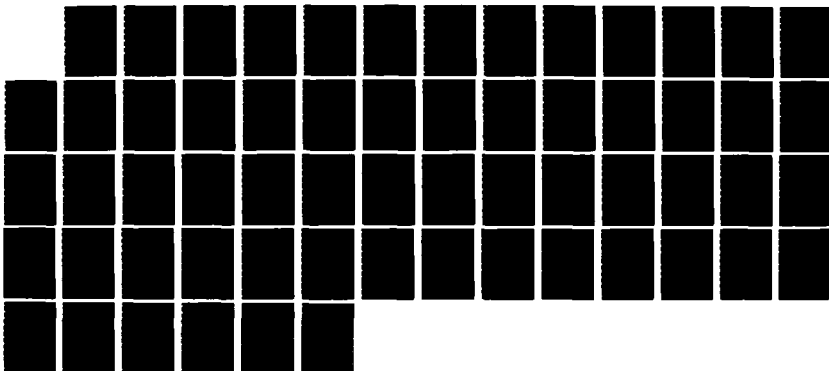
AD-A172 448

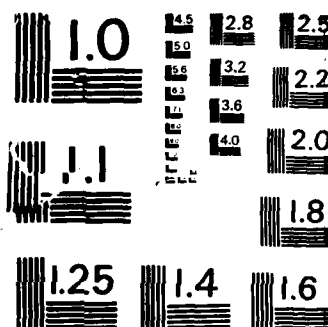
THE COLLAPSE OF COMPOSITE CYLINDRICAL PANELS WITH
VARIOUS CUTOUT LOCATION (U) AIR FORCE INST OF TECH
WRIGHT-PATTERSON AFB OH SCHOOL OF ENGI M F HERNSEN
MAR 86 AFIT/GAE-86M-2 F/G 11/4

2/2

UNCLASSIFIED

NL





MICROCOPY RESOLUTION TEST CHART
NATIONAL BUREAU OF STANDARDS-1963-A

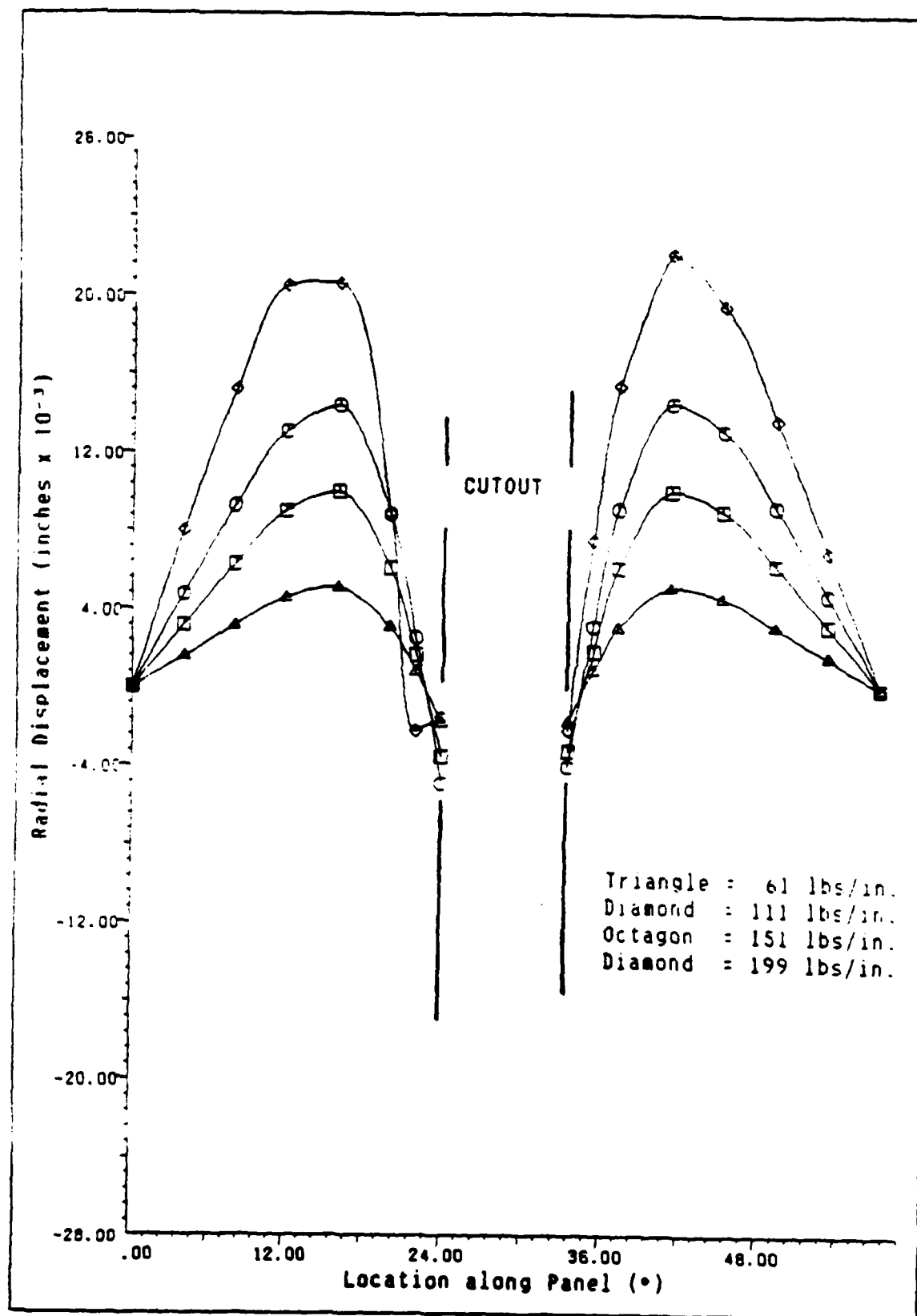


Fig. A1.2 Radial Displacement as a Function of Location taken 6 inches from the Loading Edge

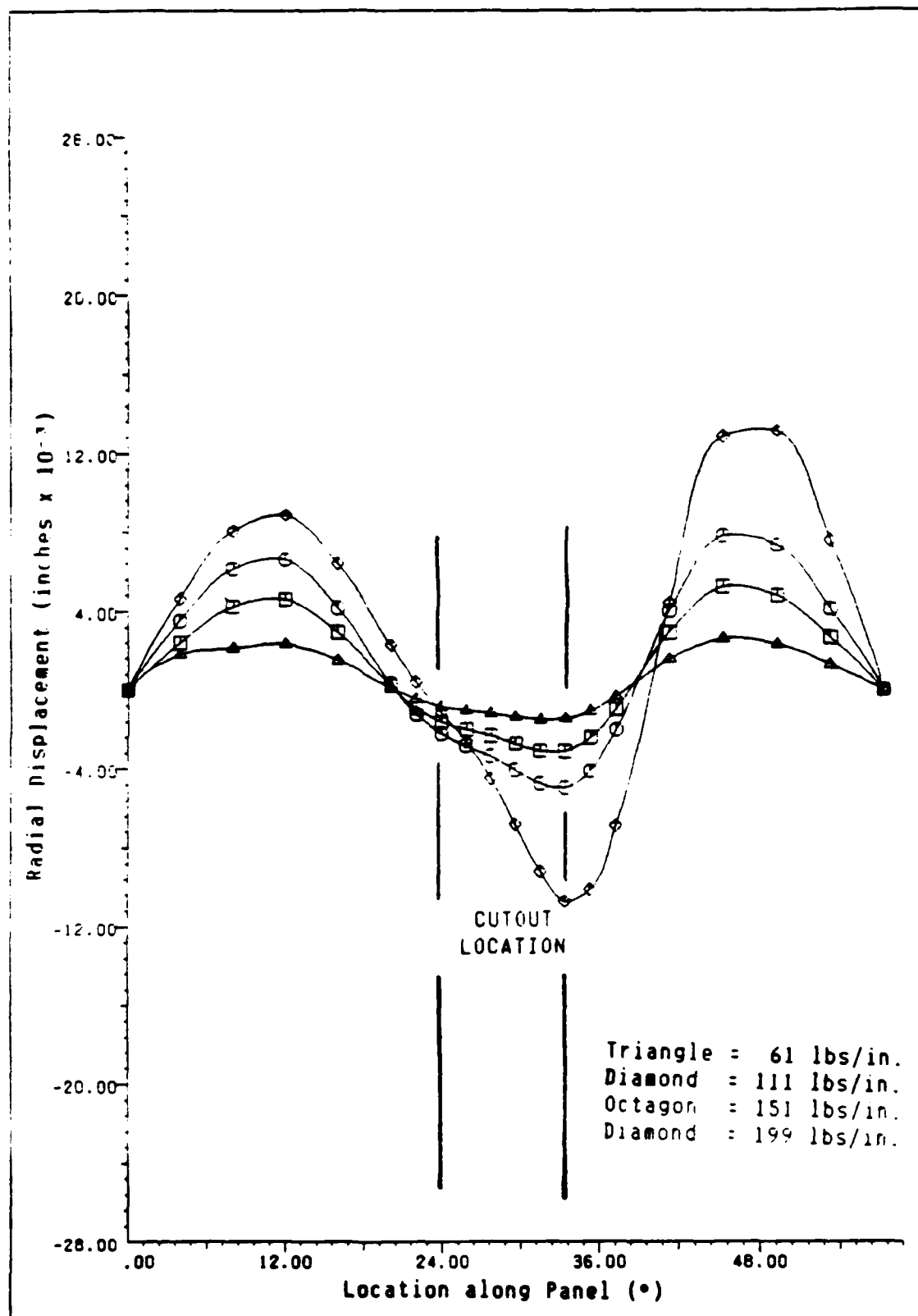


Fig. A1.3 Radial Displacement as a Function of Location taken 9 inches from the Loading Edge

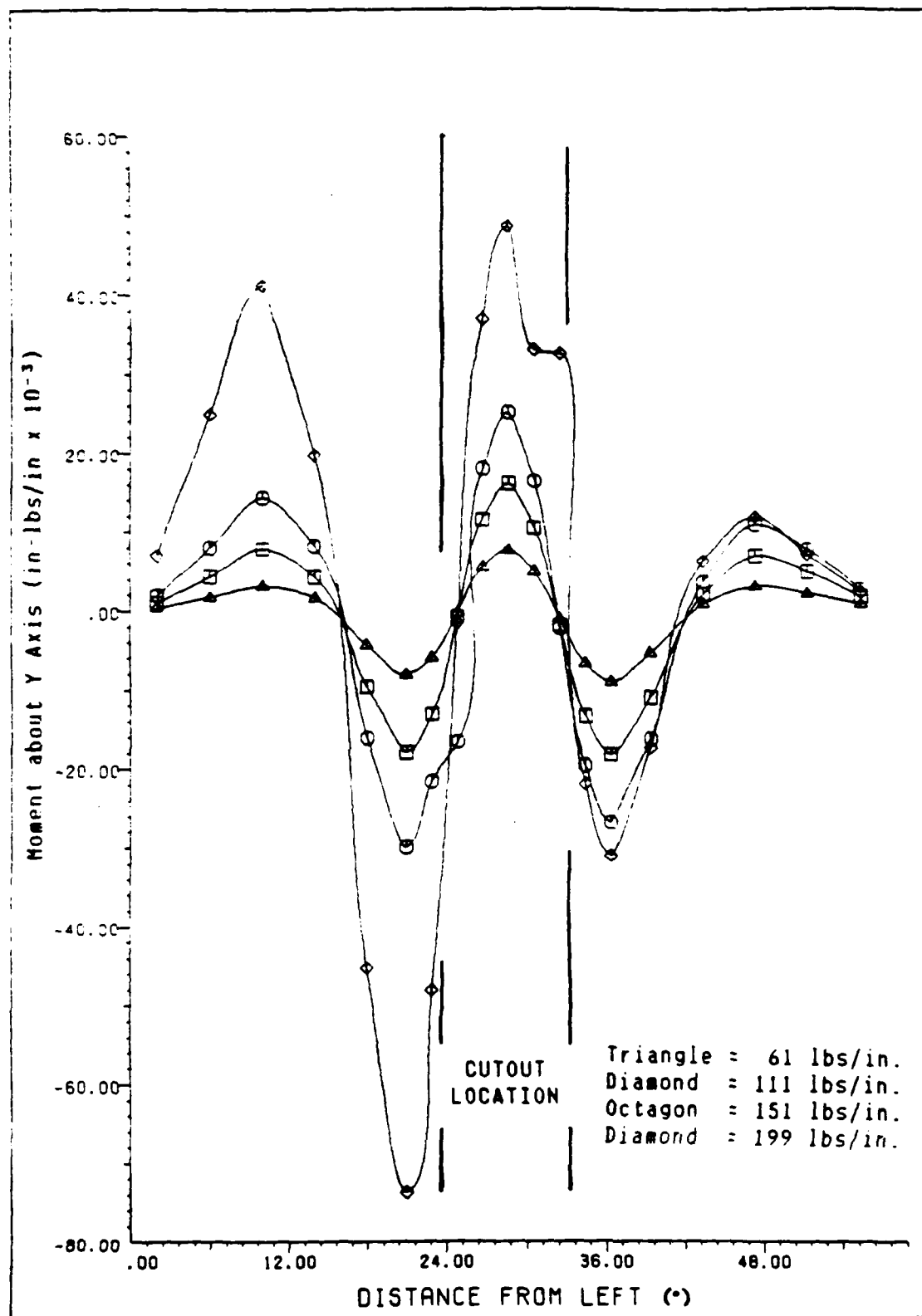


Fig. A1.4 Moment Profiles as a Function of Panel Location taken 3 inches from the Loading Edge

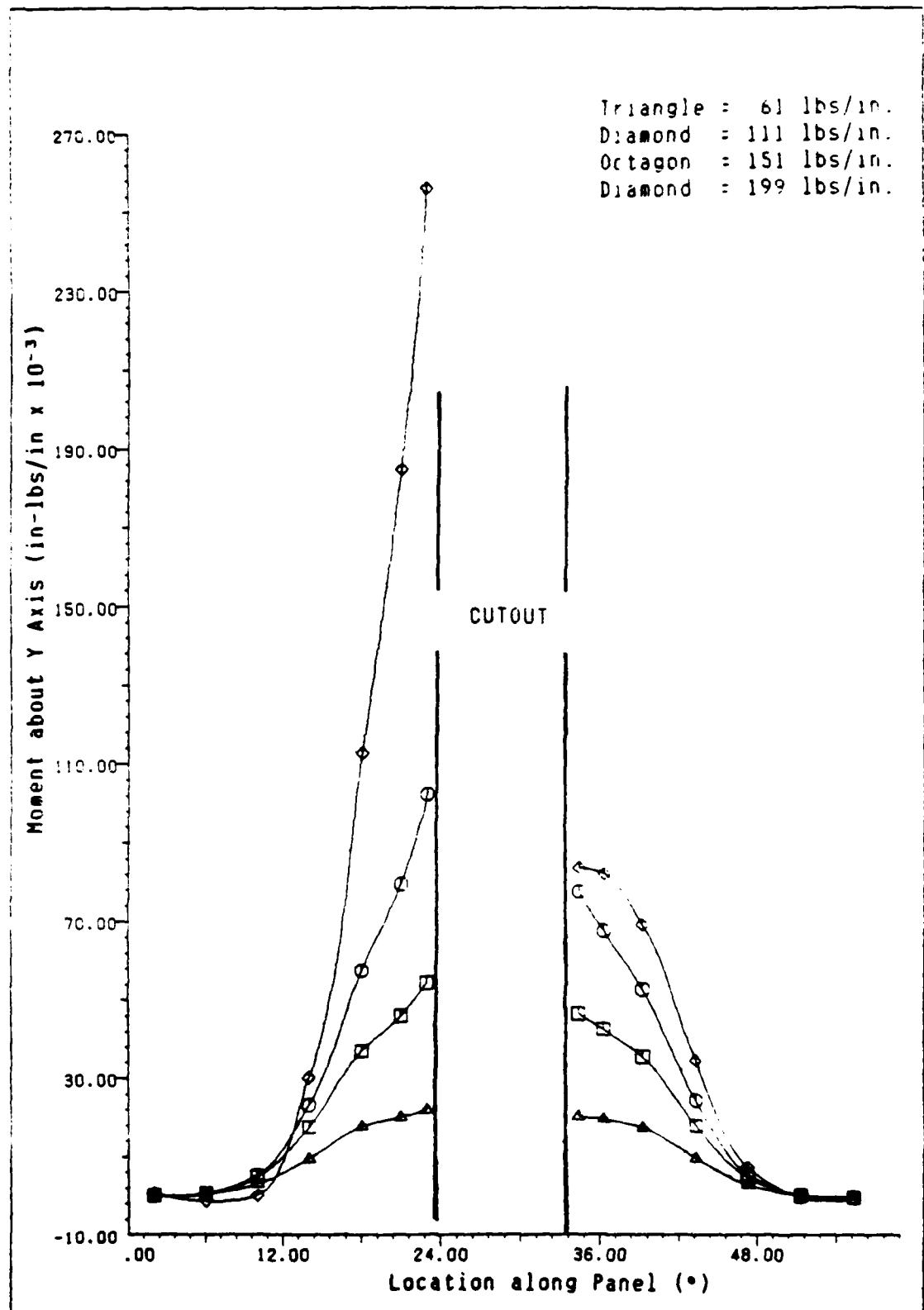


Fig. A1.5 Moment Profiles as a Function of Panel Location taken 6 inches from the Loading Edge

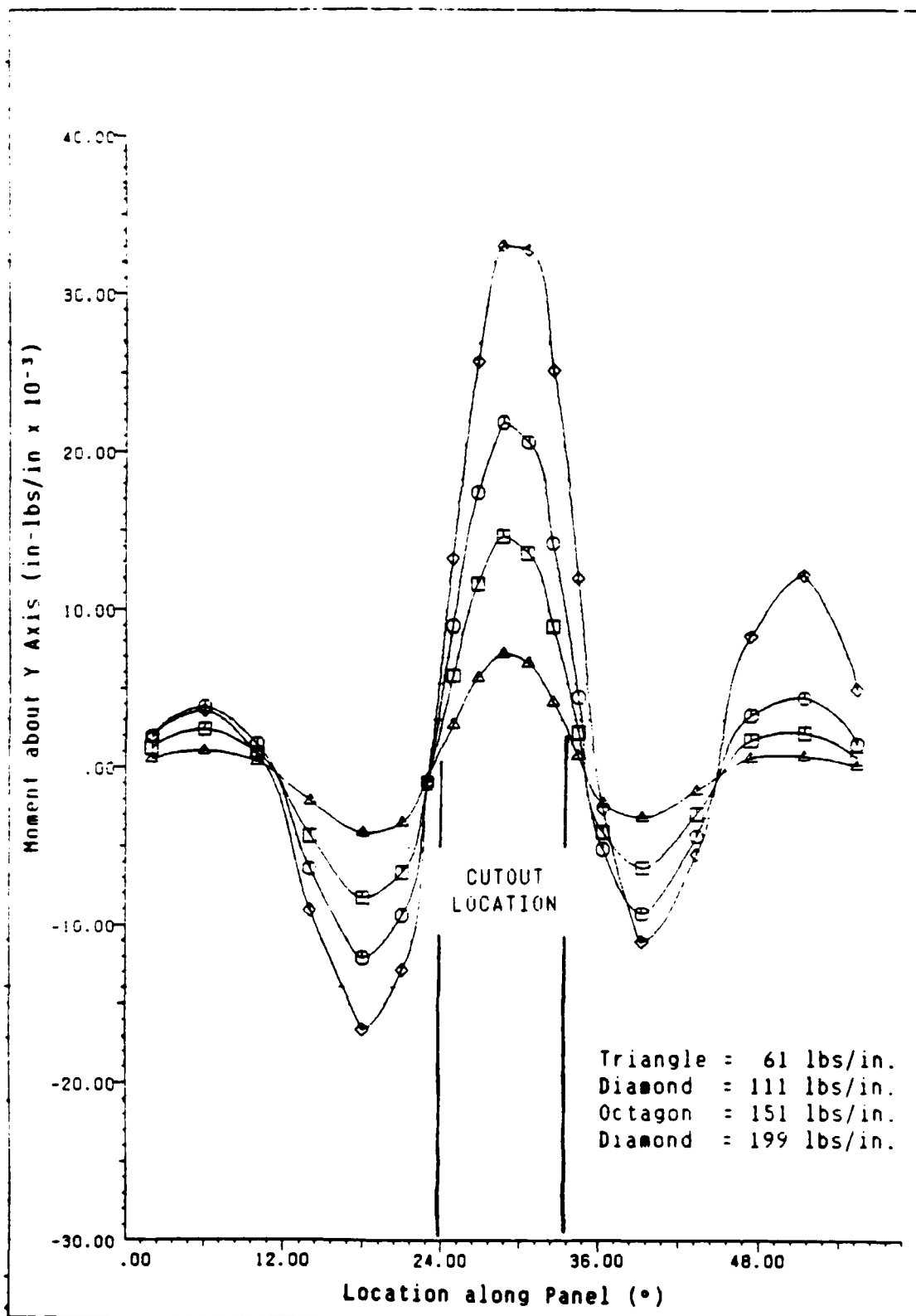


Fig. A1.6 Moment Profiles as a Function of Panel Location taken 9 inches from the Loading Edge

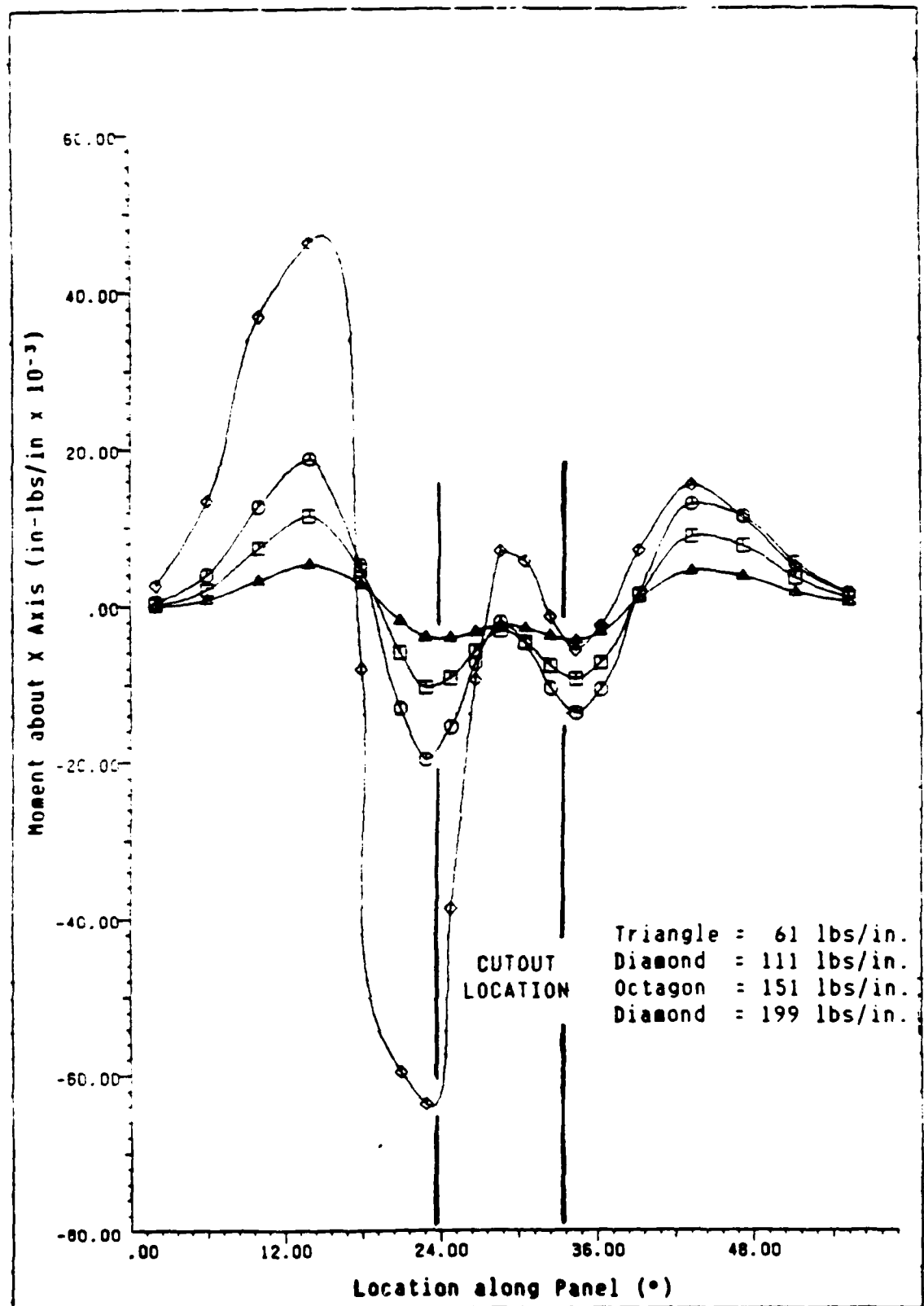


Fig. A1.7 Moment Profiles as a Function of Panel Location taken 3 inches from the Loading Edge

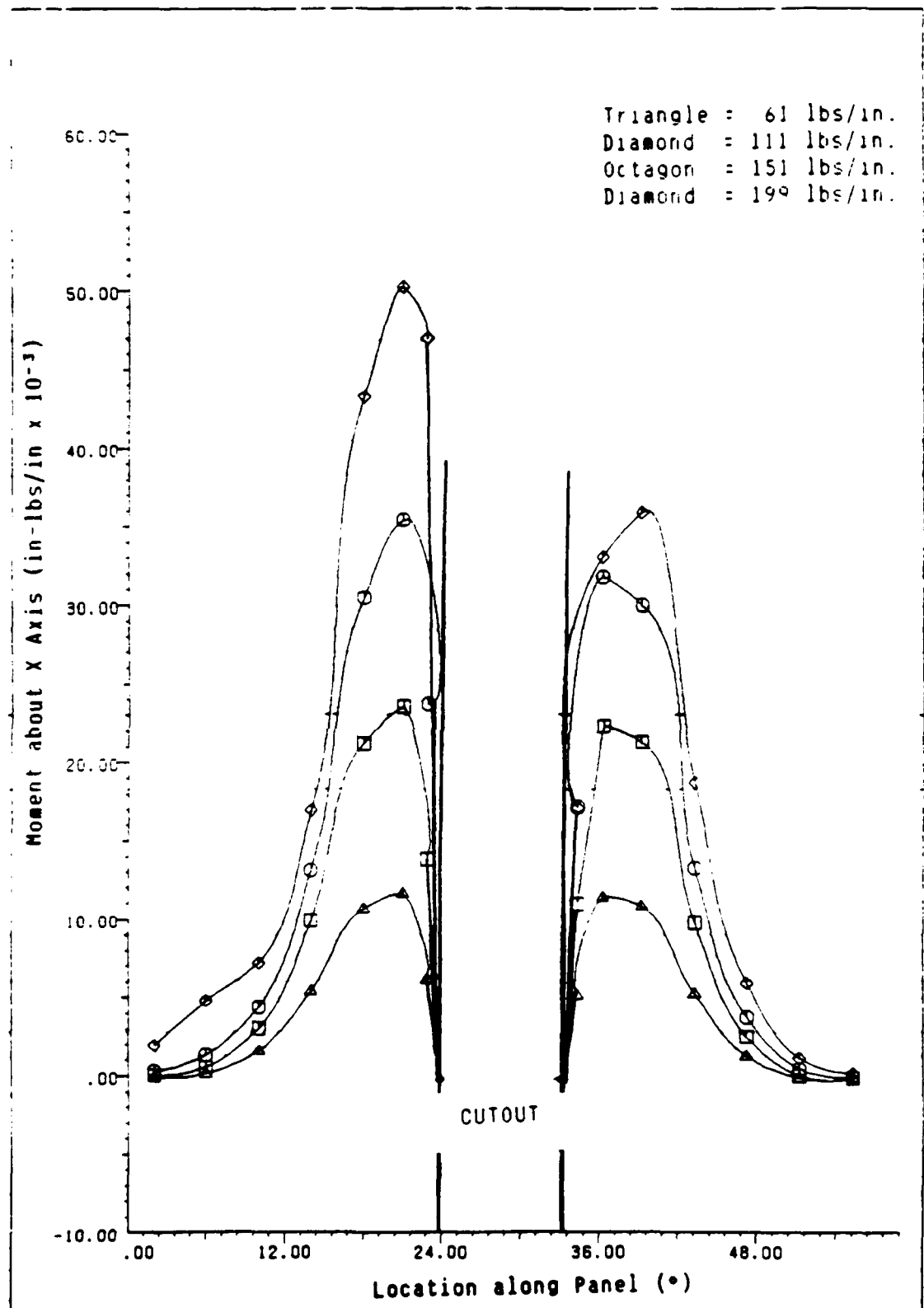


Fig. A1.8 Moment Profiles as a Function of Panel Location taken 6 inches from the Loading Edge

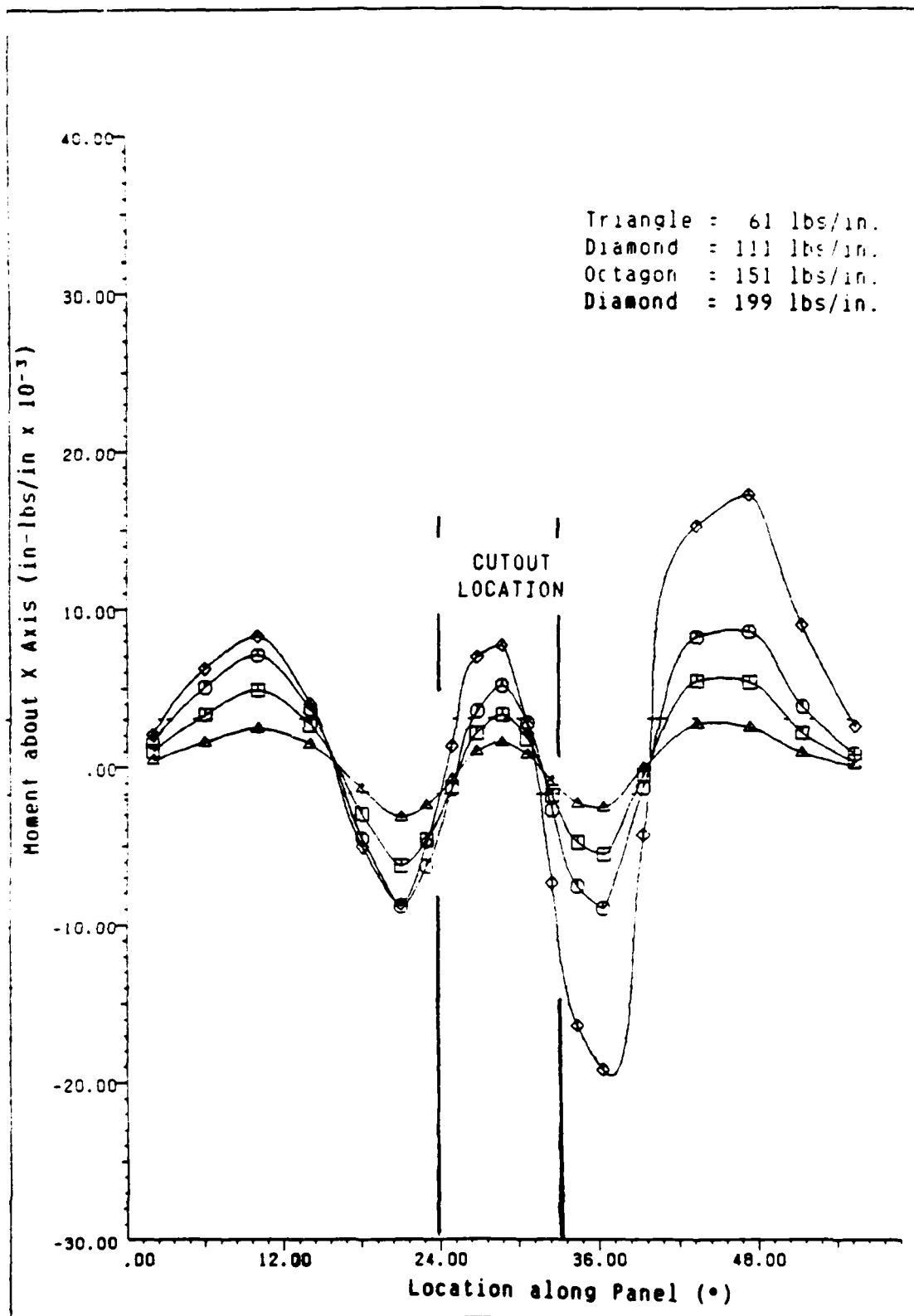


Fig. A1.9 Moment Profiles as a Function of Panel Location taken 9 inches from the Loading Edge

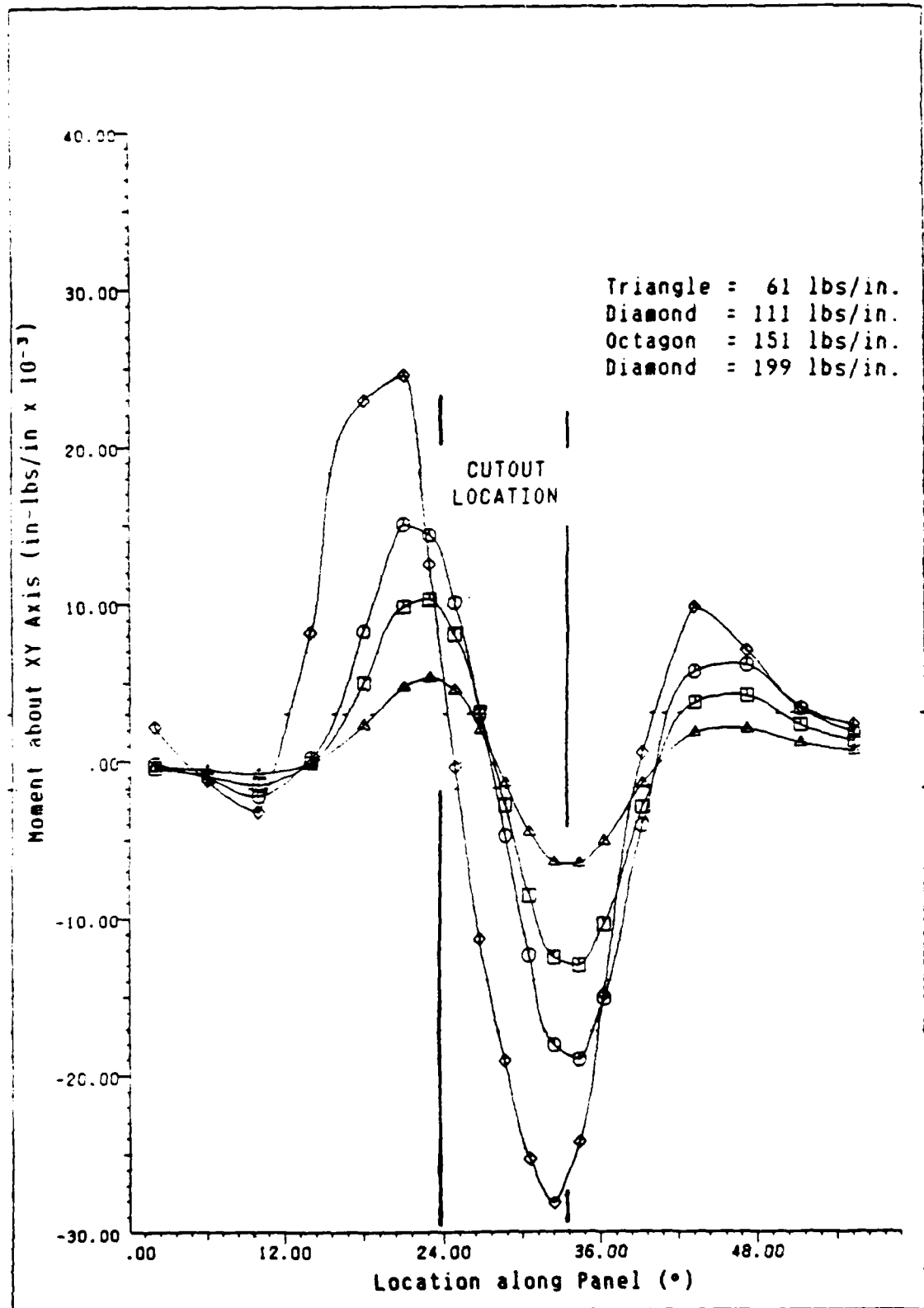


Fig. A1.10 Moment Profiles as a Function of Panel Location taken 3 inches from the Loading Edge

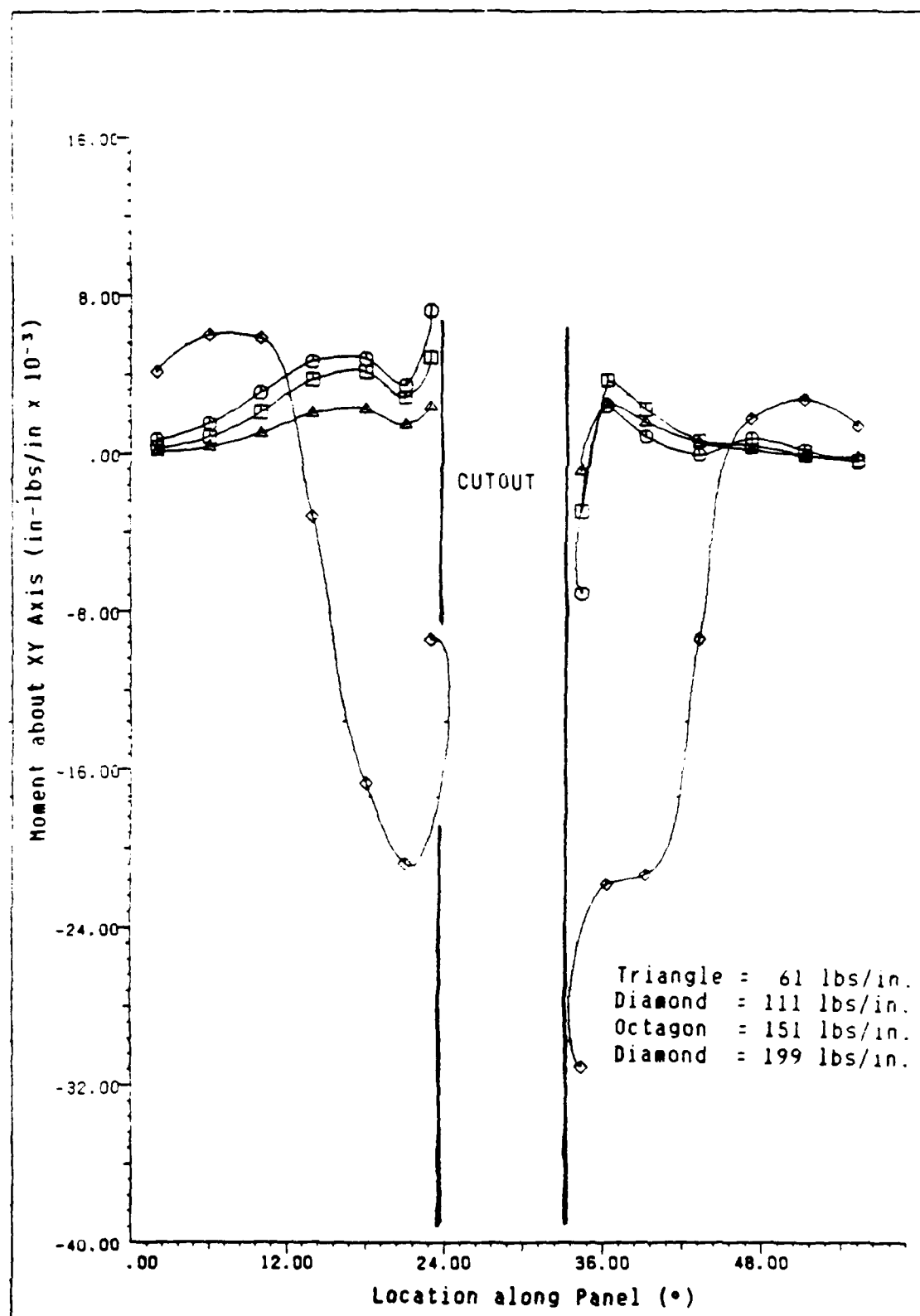


Fig. A1.11 Moment Profiles as a Function of Panel Location taken 6 inches from the Loading Edge

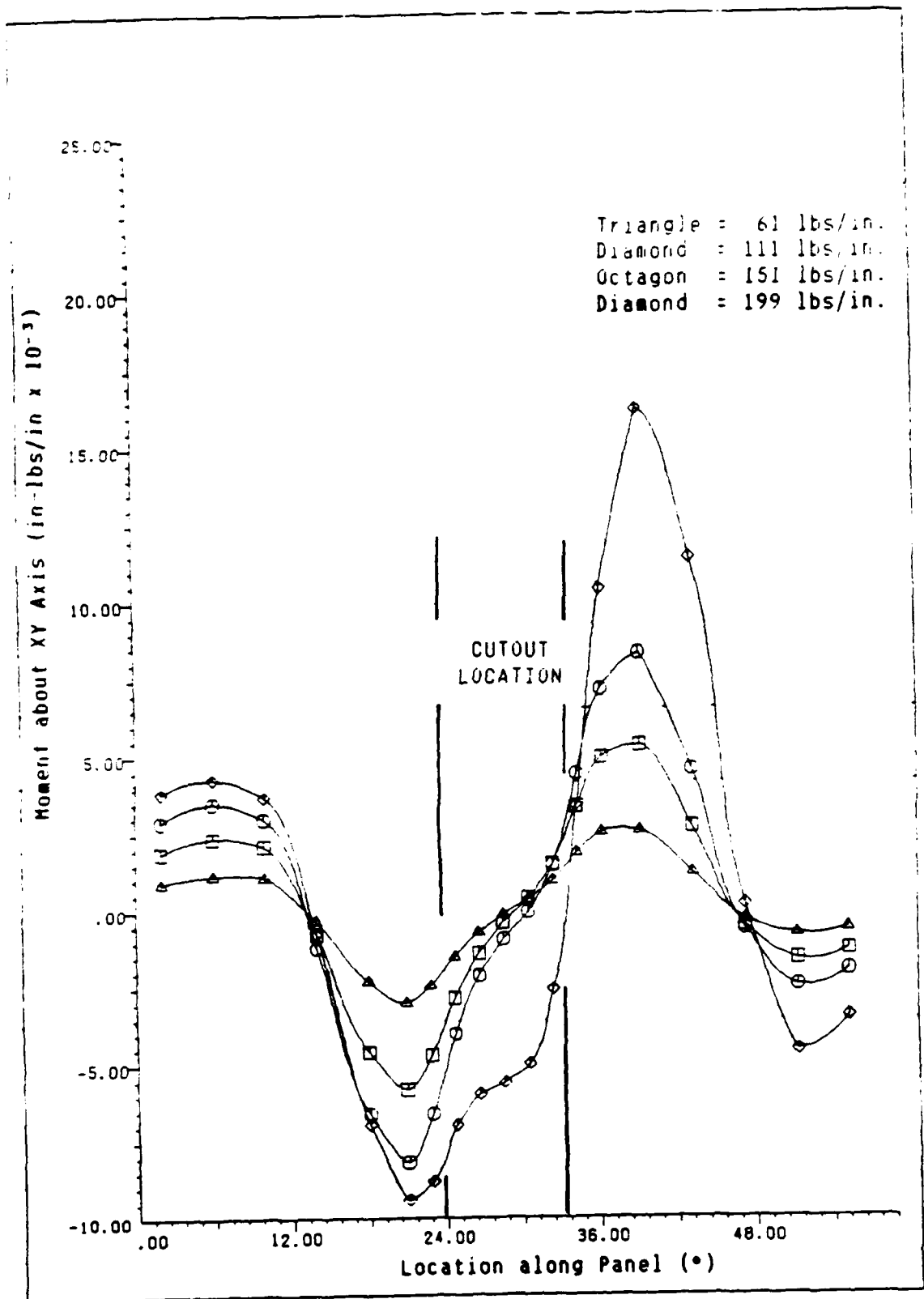


Fig. A1.12 Moment Profiles as a Function of Panel Location taken 9 inches from the Loading Edge

Appendix A2

LOADING EDGE DISPLACEMENT STUDY

Cutout location A	-	A2.1 - A2.3
Cutout location C	-	A2.4 - A2.6
Cutout location D	-	A2.7 - A2.9

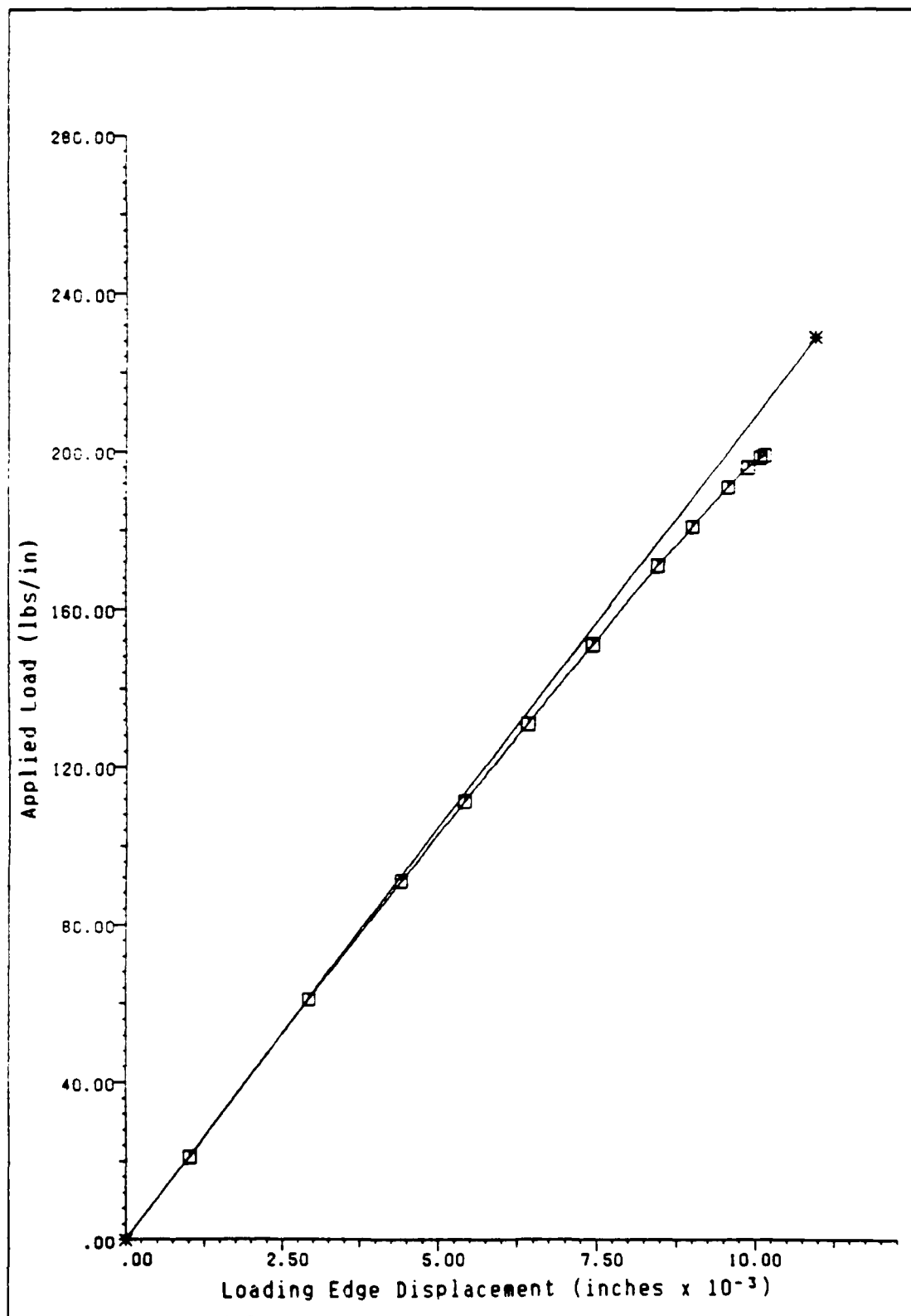


Fig. A2.1 Loading Edge Displacement vs Applied Load, Cutout A for +45 Second Ply

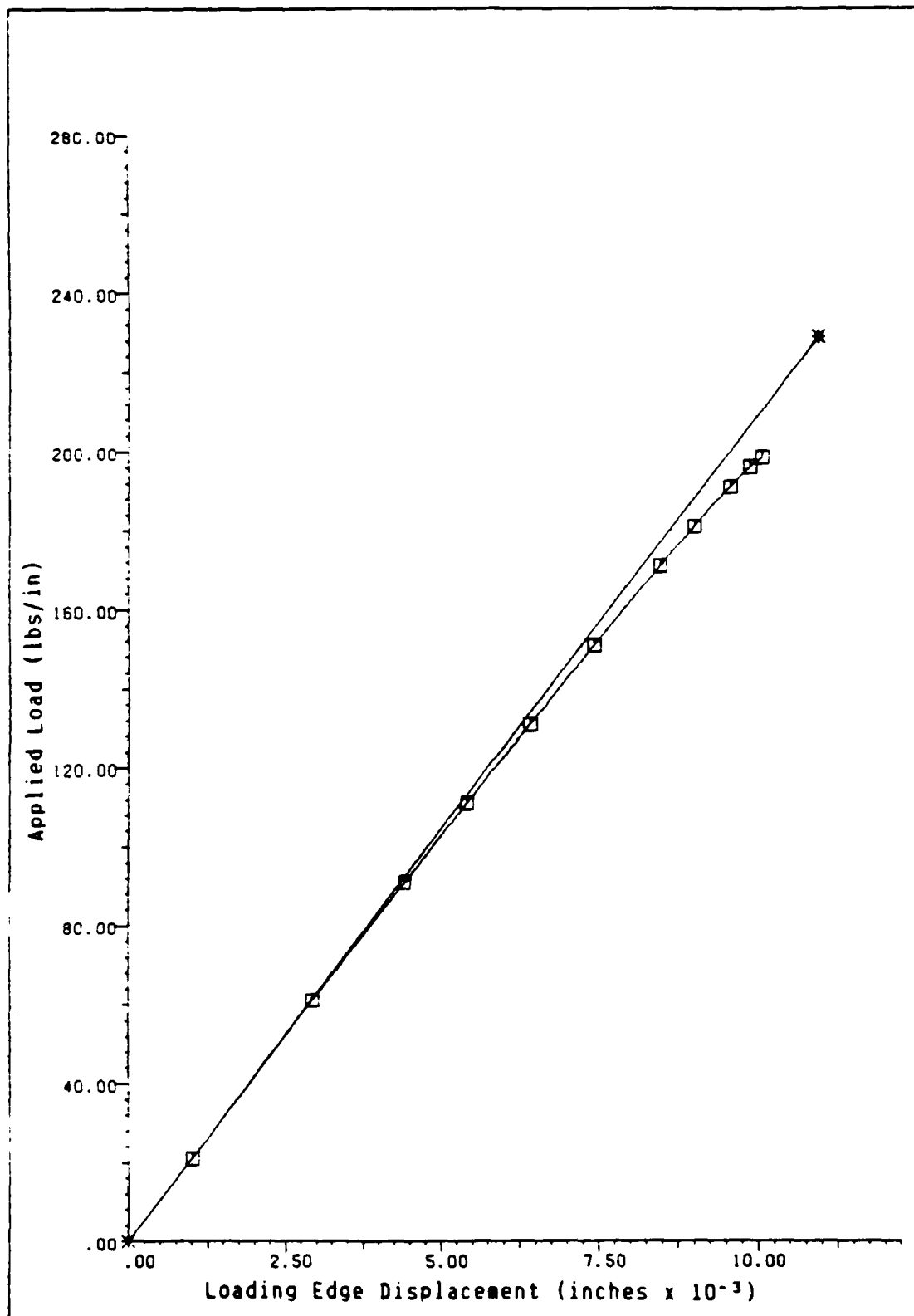


Fig. A2.2 Loading Edge Displacement vs Applied Load, Cutout A for -45 Second Ply

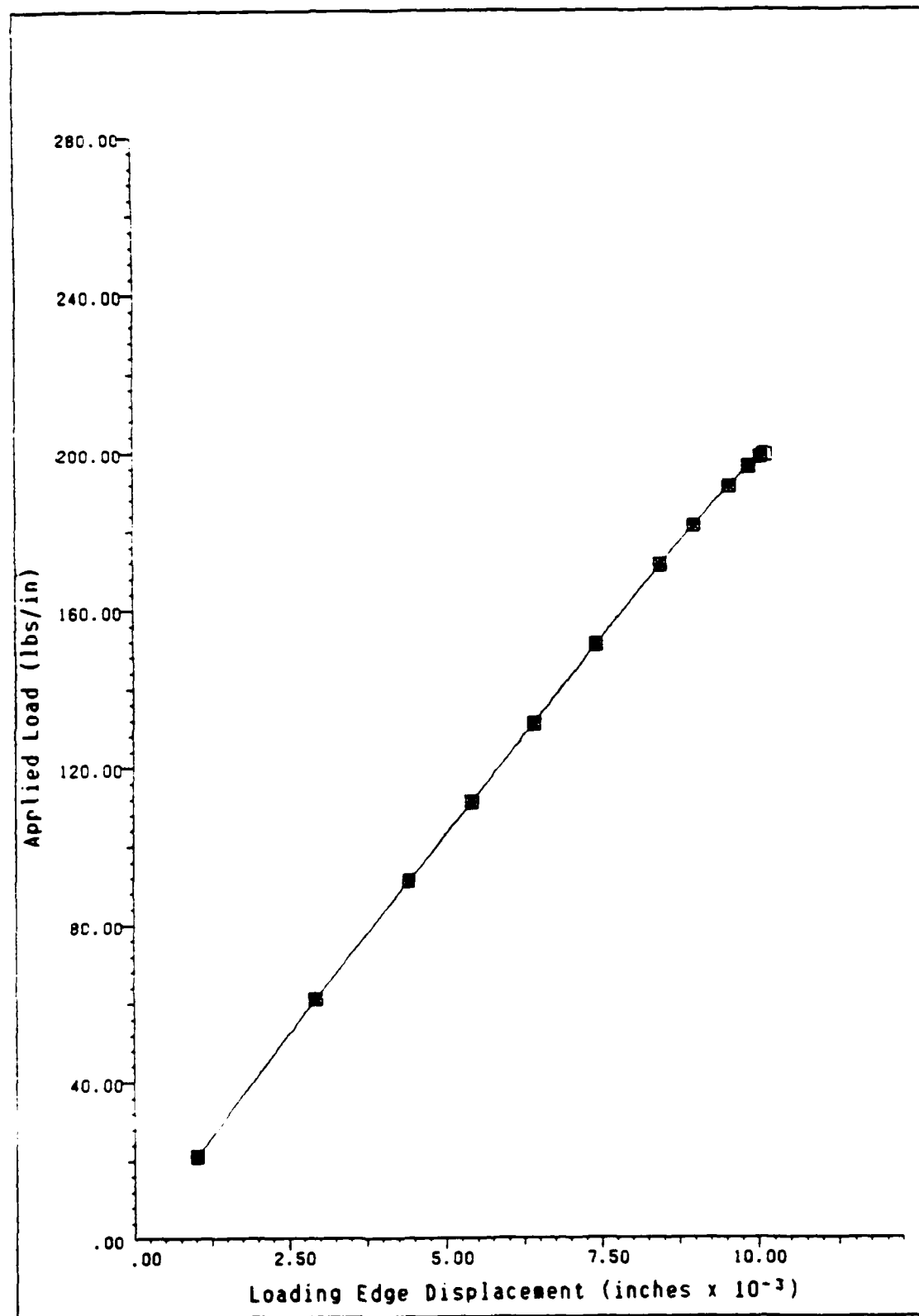


Fig. A2.3 Loading Edge Displacement vs Applied Load, Cutout A for both +45 and -45 Second Ply

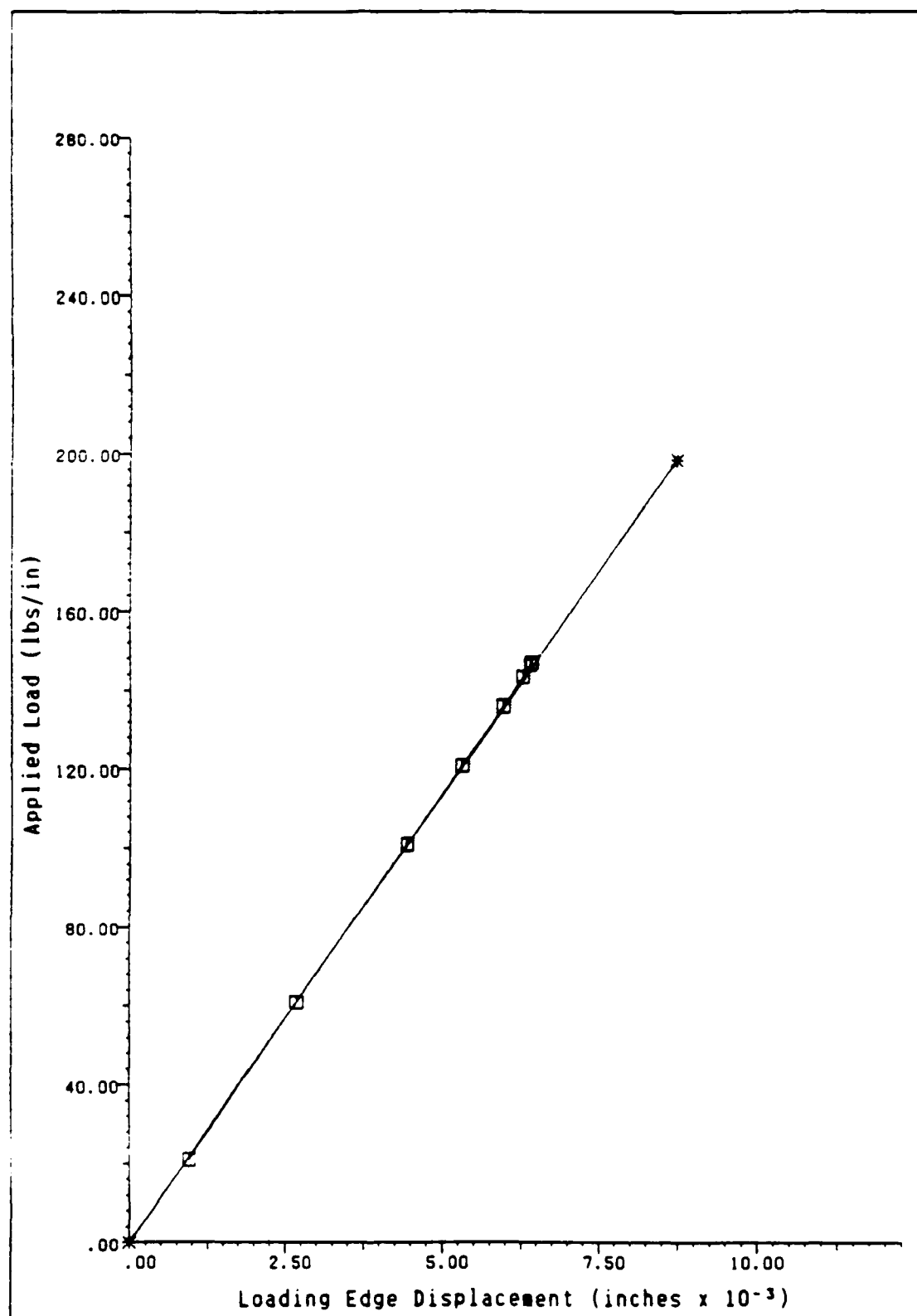


Fig. A2.4 Loading Edge Displacement vs Applied Load, Cutout C for +45 Second Ply

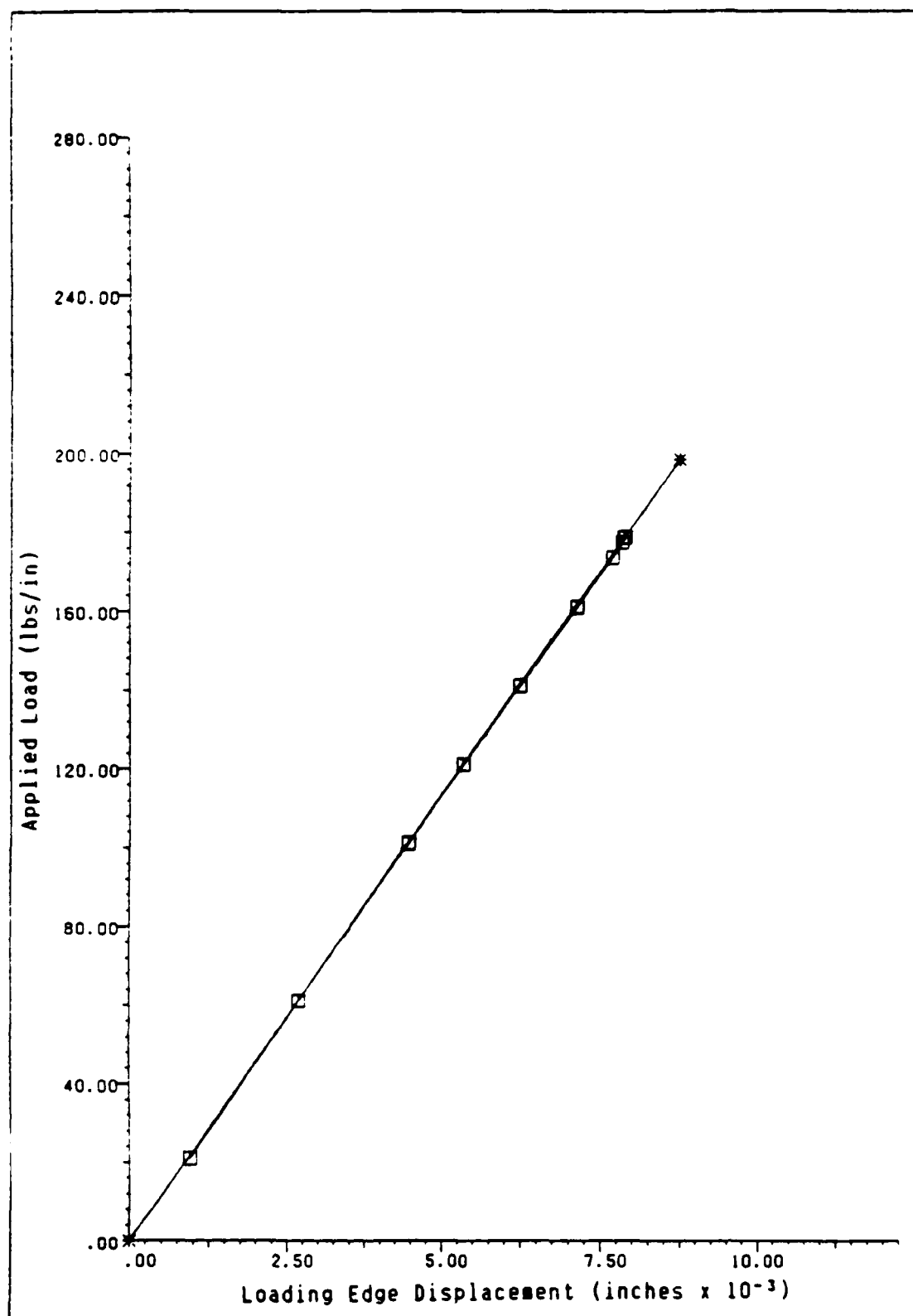


Fig. A2.5 Loading Edge Displacement vs Applied Load, Cutout C for -45 Second Ply

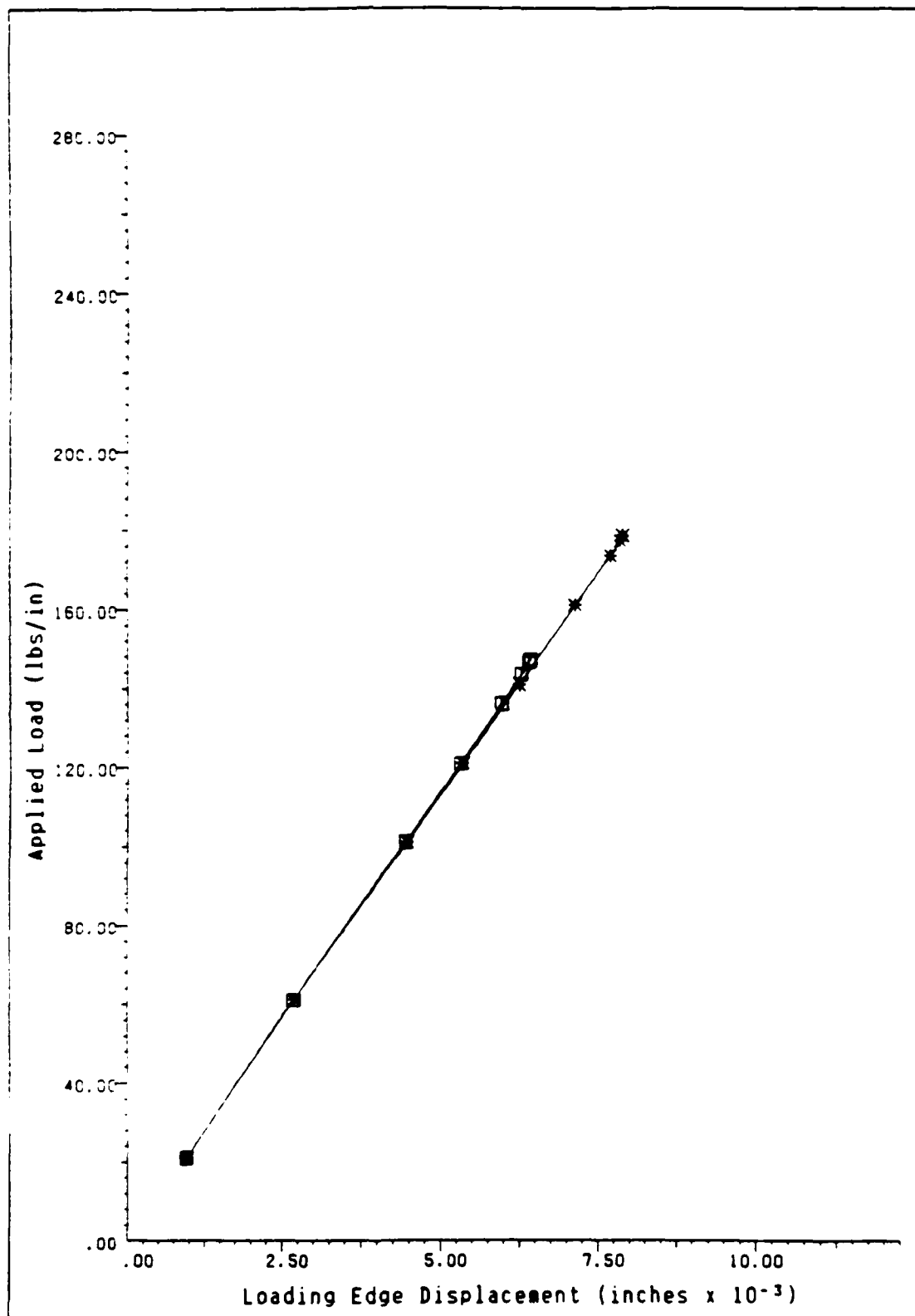


Fig. A2.6 Loading Edge Displacement vs Applied Load, Cutout C for both +45 and -45 Second Ply

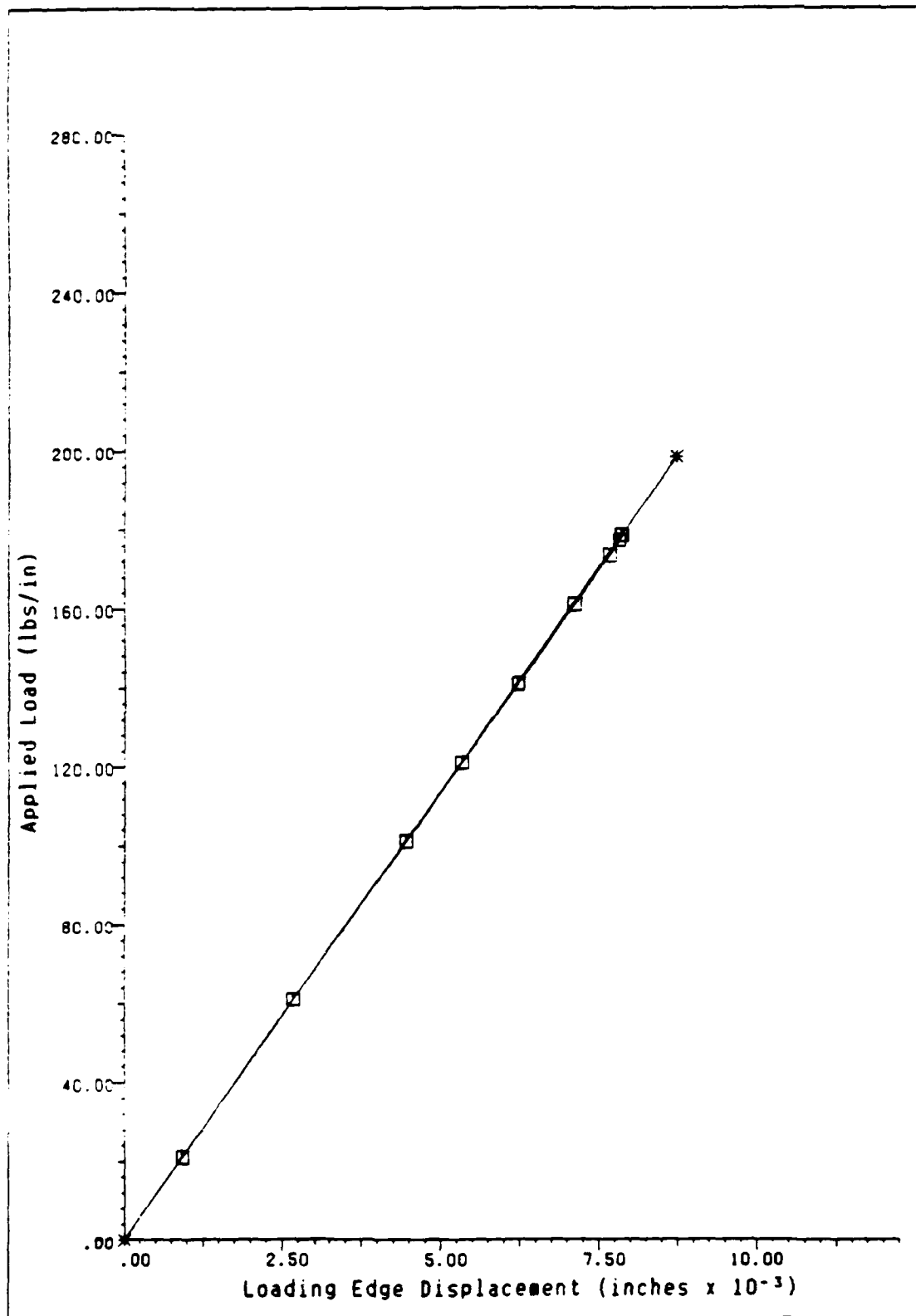


Fig. A2.7 Loading Edge Displacement vs Applied Load, Cutout D for +45 Second Ply

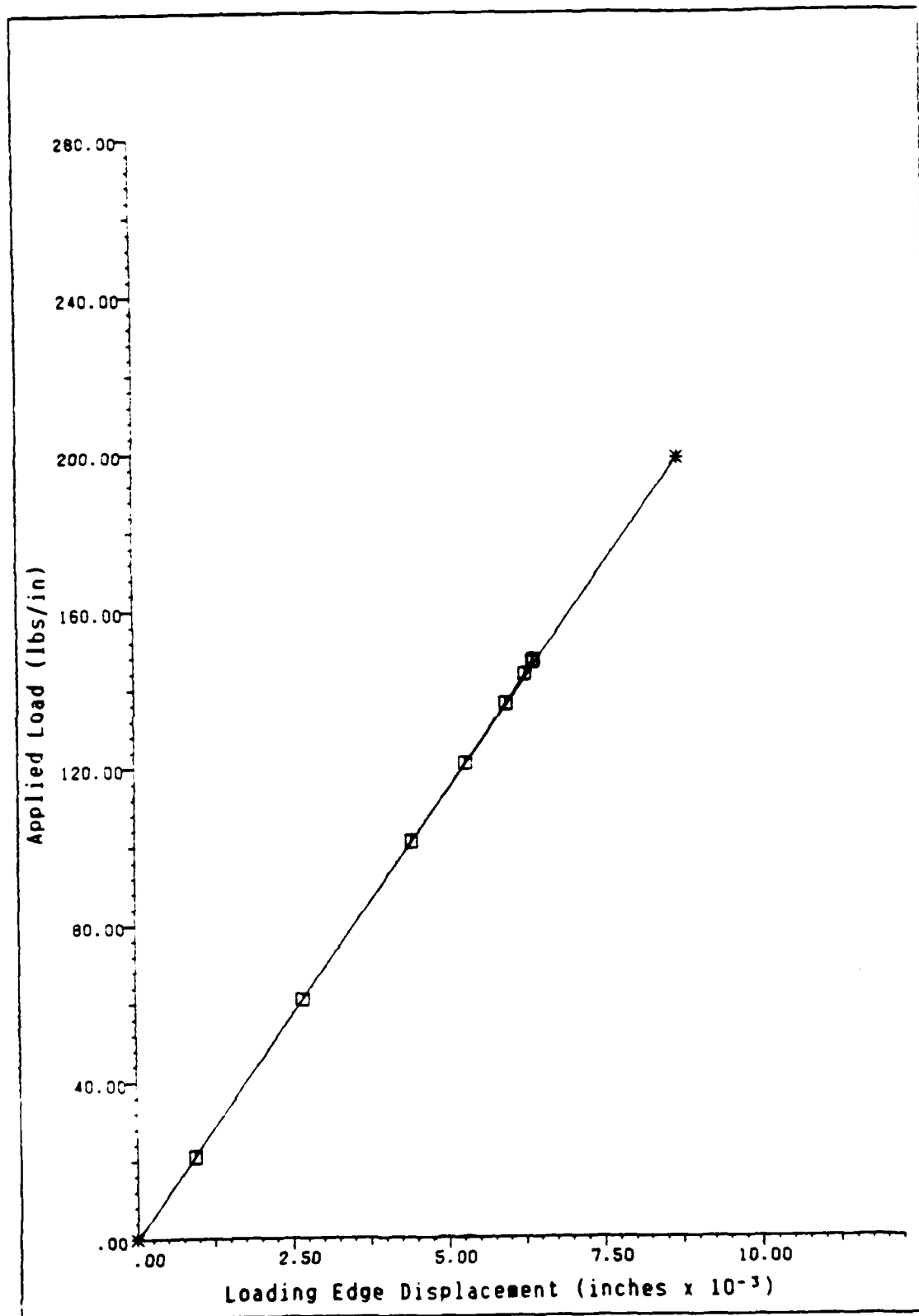


Fig. A2.8 Loading Edge Displacement vs Applied Load, Cutout D for -45 Second Ply

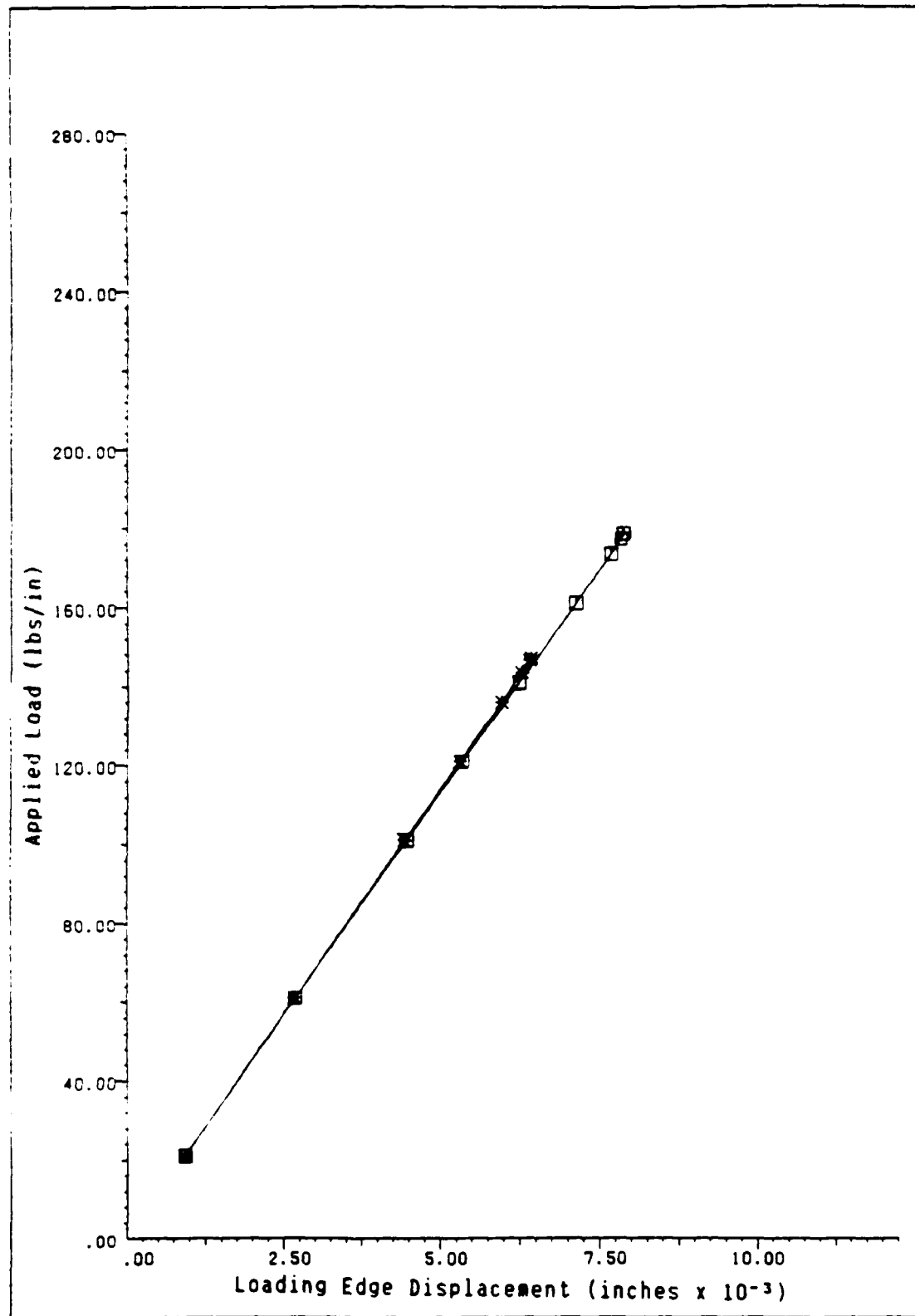


Fig. A2.9 Loading Edge Displacement vs Applied Load, Cutout D for both +45 and -45 Second Ply

Appendix A3

W DISPLACEMENT PROFILES AT 4.5 AND 5.0 INCHES FROM THE LOADING EDGE

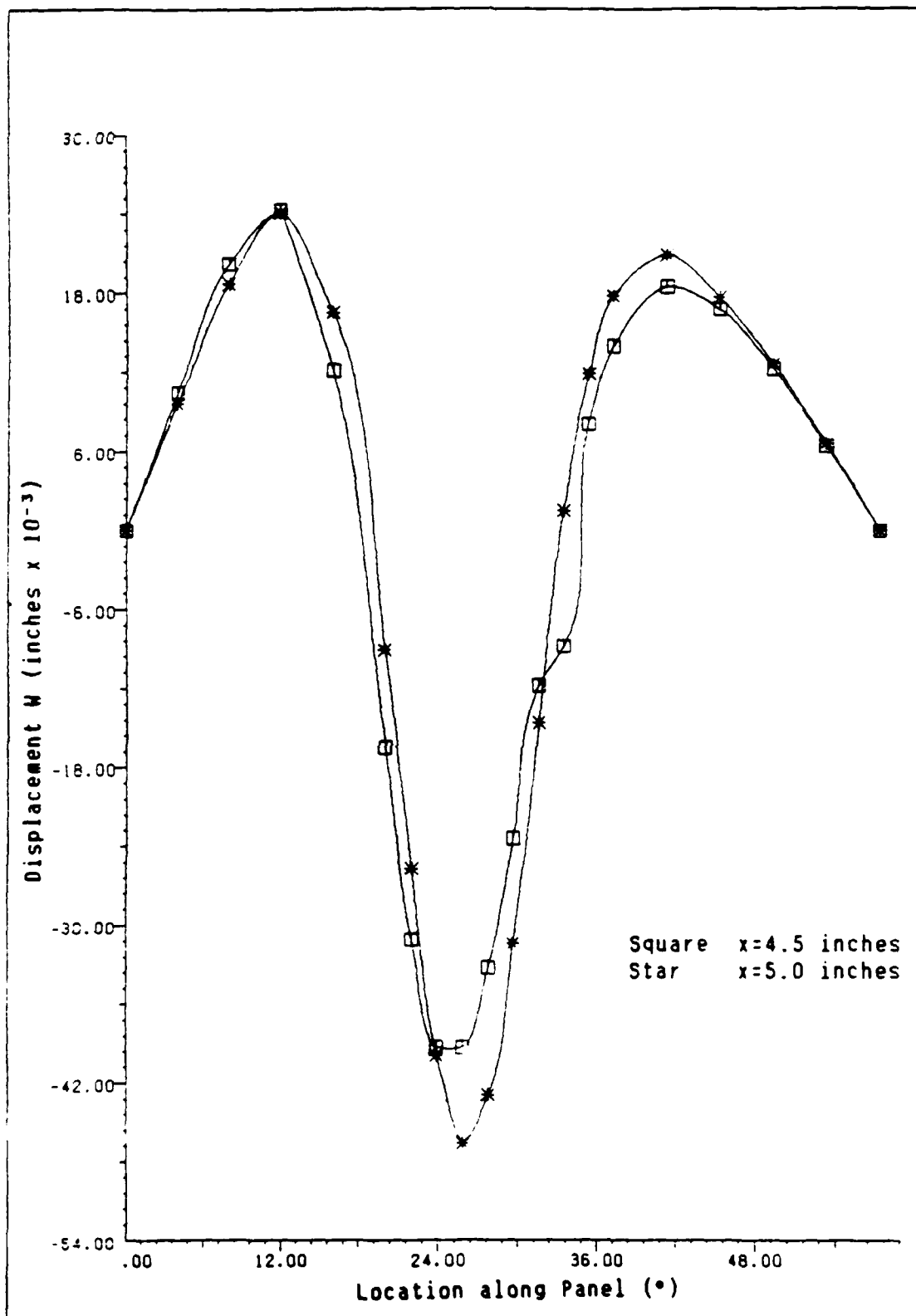


Fig. A3.1 W Profiles at 4.5 and 5.0 inches from the Loading Edge as a function of Location, for Cutouts A and +45 Second Ply

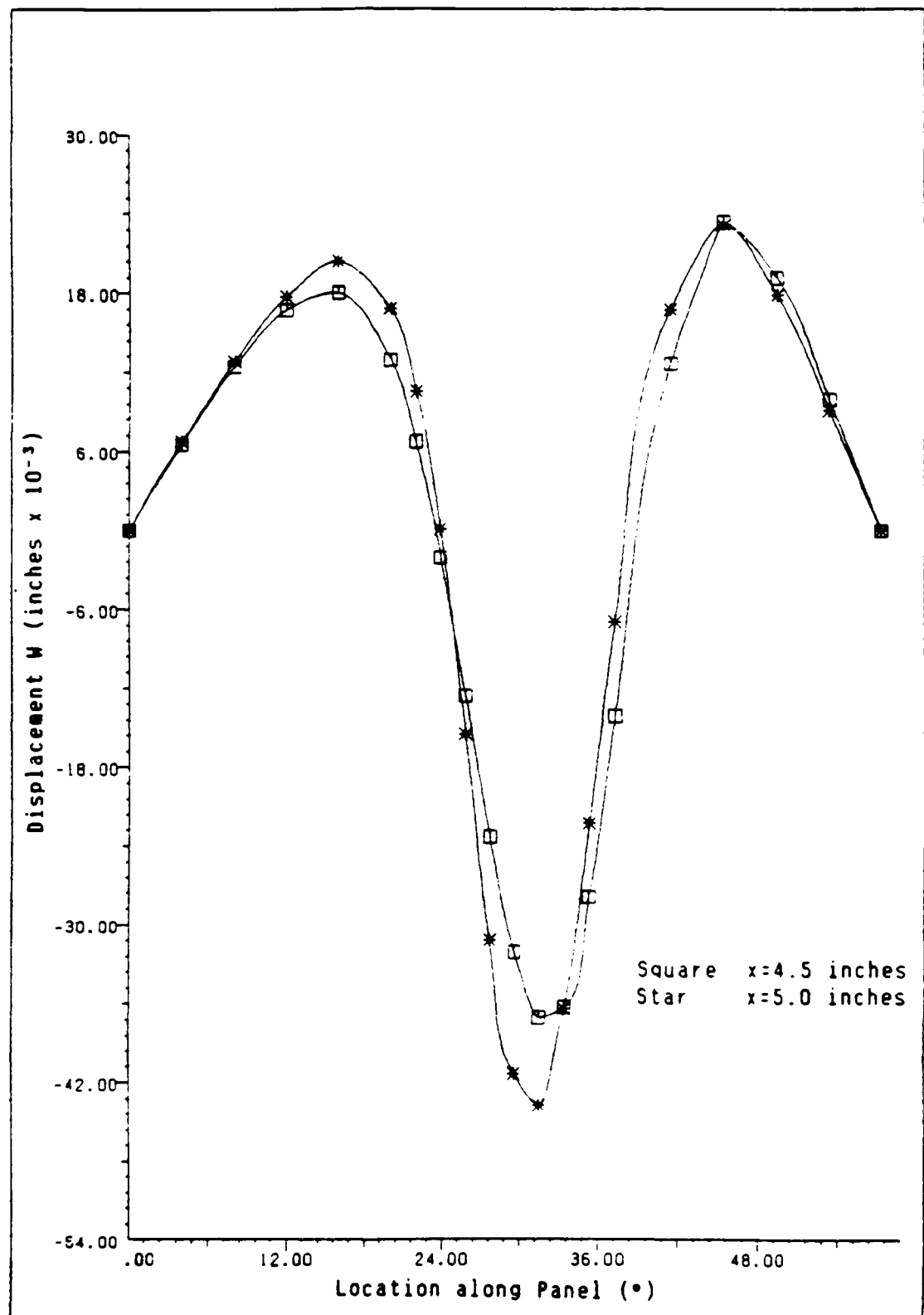


Fig. A3.2 W Profiles at 4.5 and 5.0 inches from the Loading Edge as a function of Location, for Cutouts A and -45 Second Ply

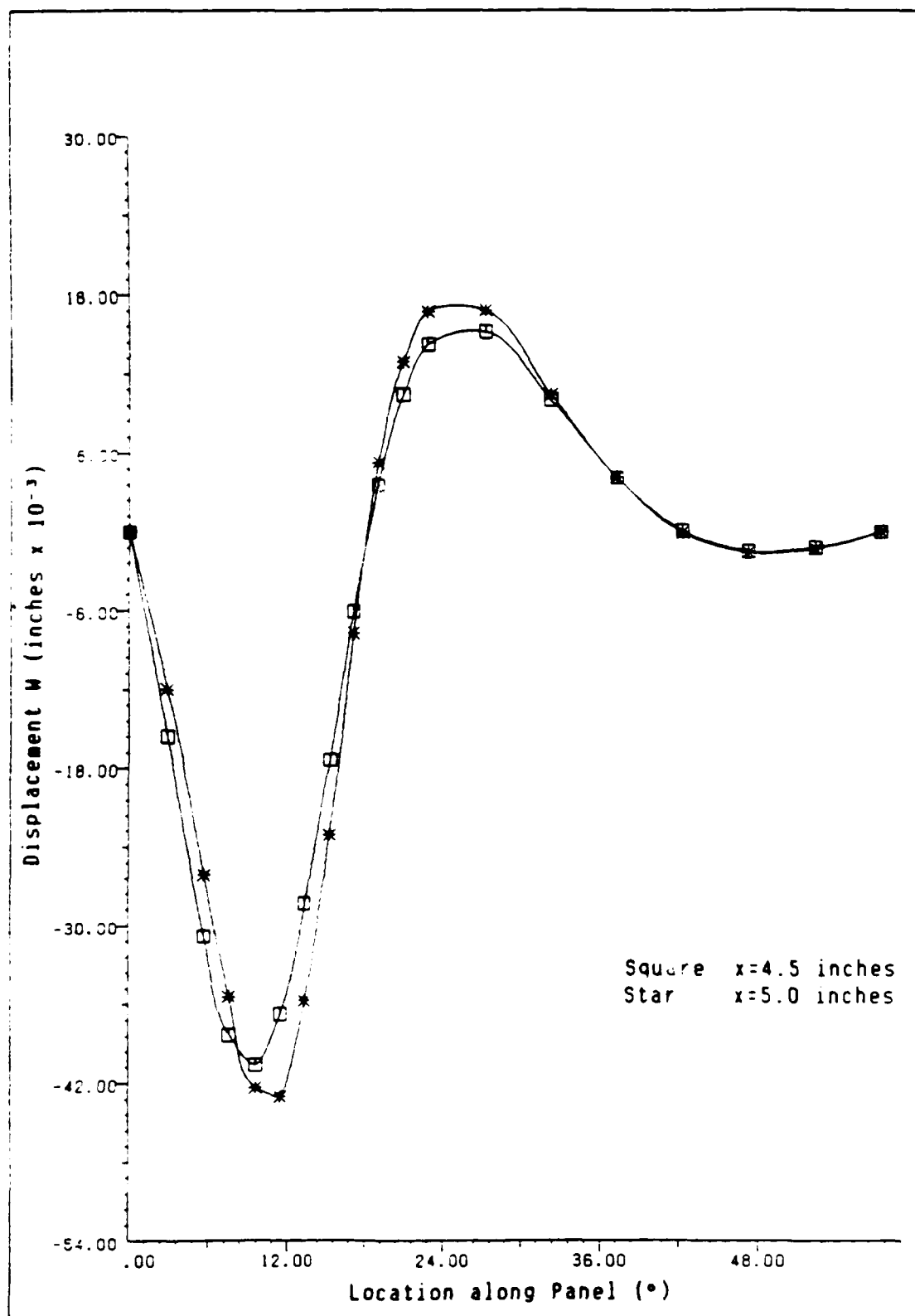


Fig. A3.3 W Profiles at 4.5 and 5.0 inches from the Loading Edge as a function of Location, for Cutouts C and +45 Second Ply

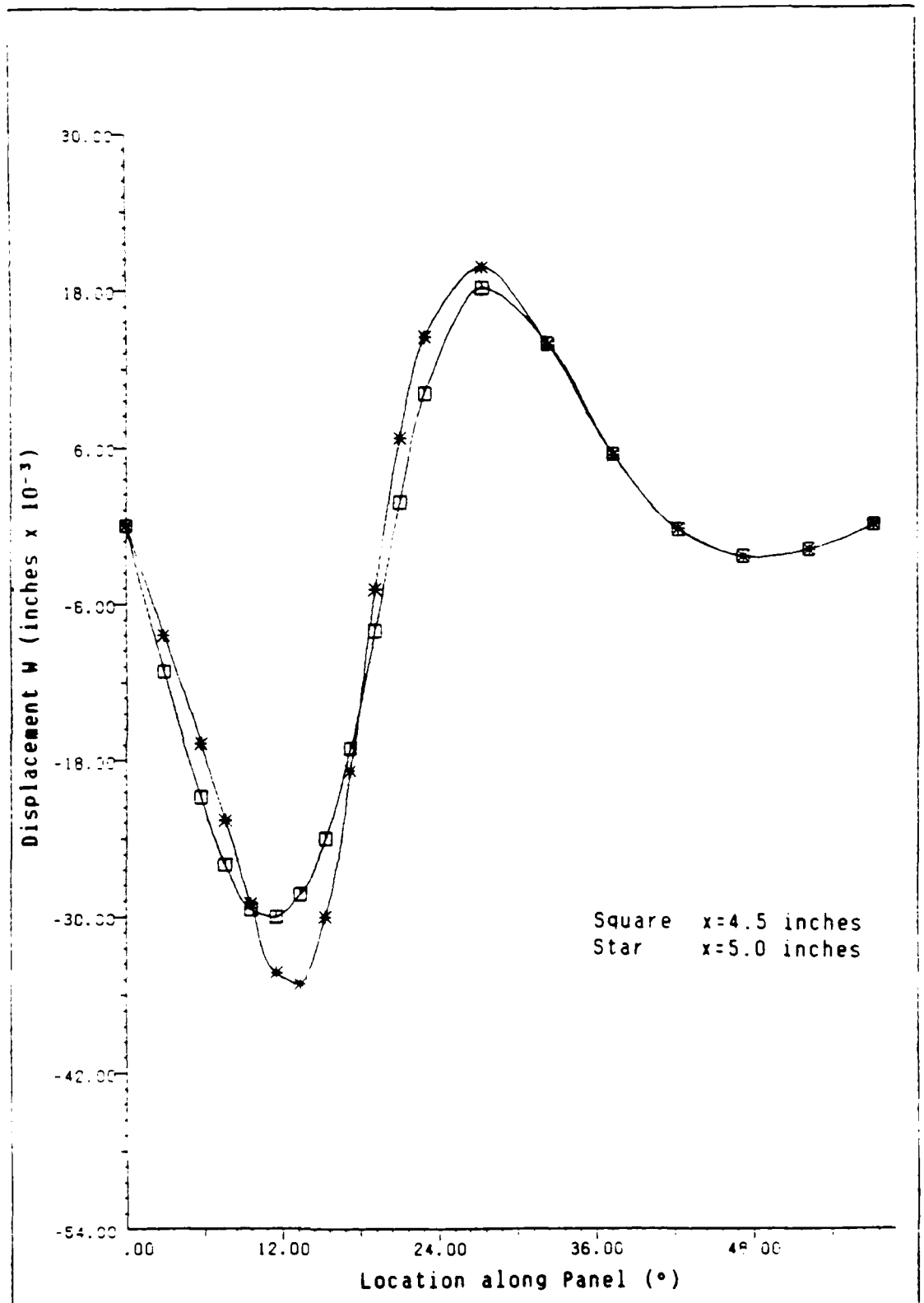


Fig. A3.4 W Profiles at 4.5 and 5.0 inches from the Loading Edge as a function of Location, for Cutouts C and -45 Second Ply

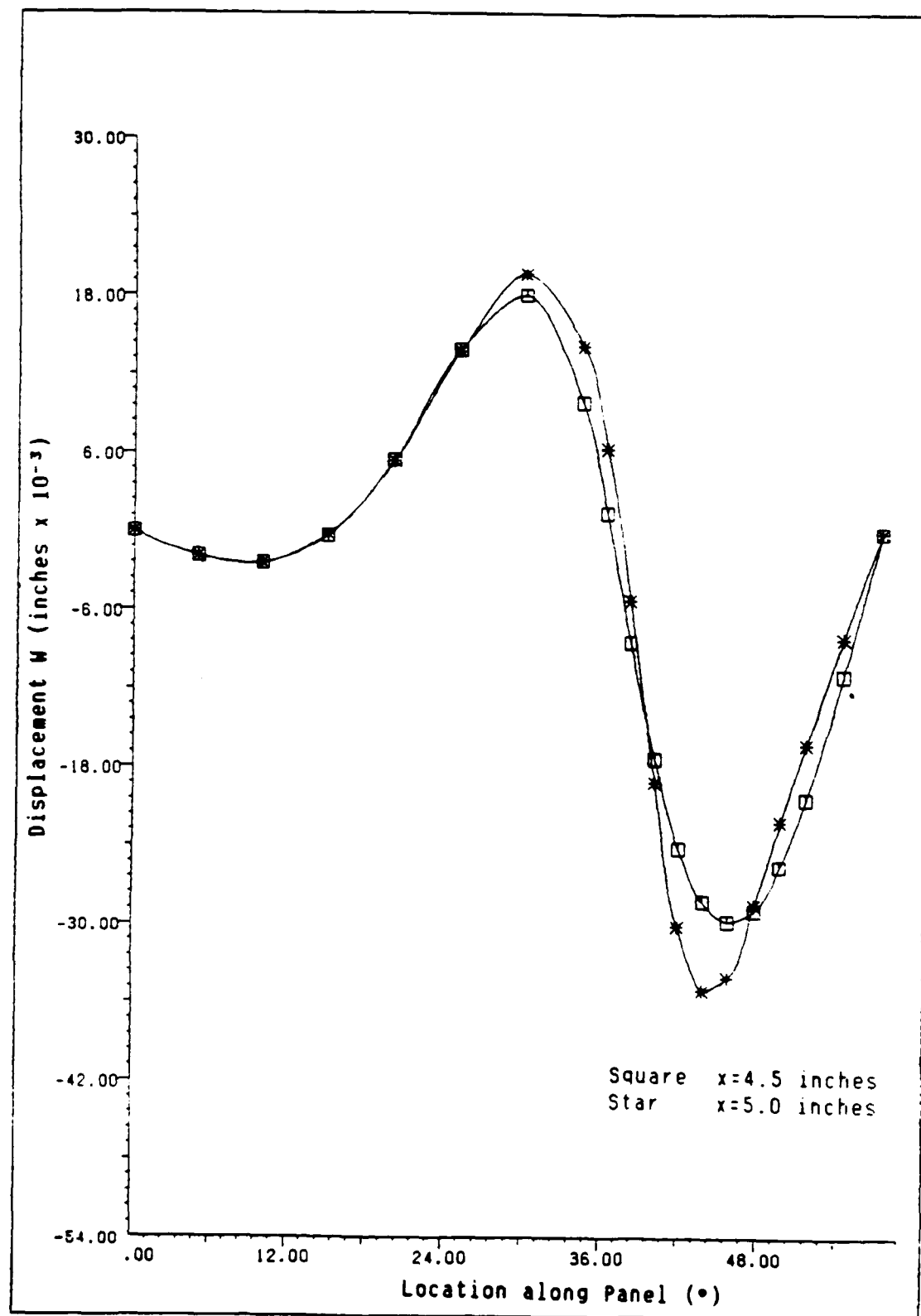


Fig. A3.5 W Profiles at 4.5 and 5.0 inches from the Loading Edge as a function of Location, for Cutouts D and +45 Second Ply

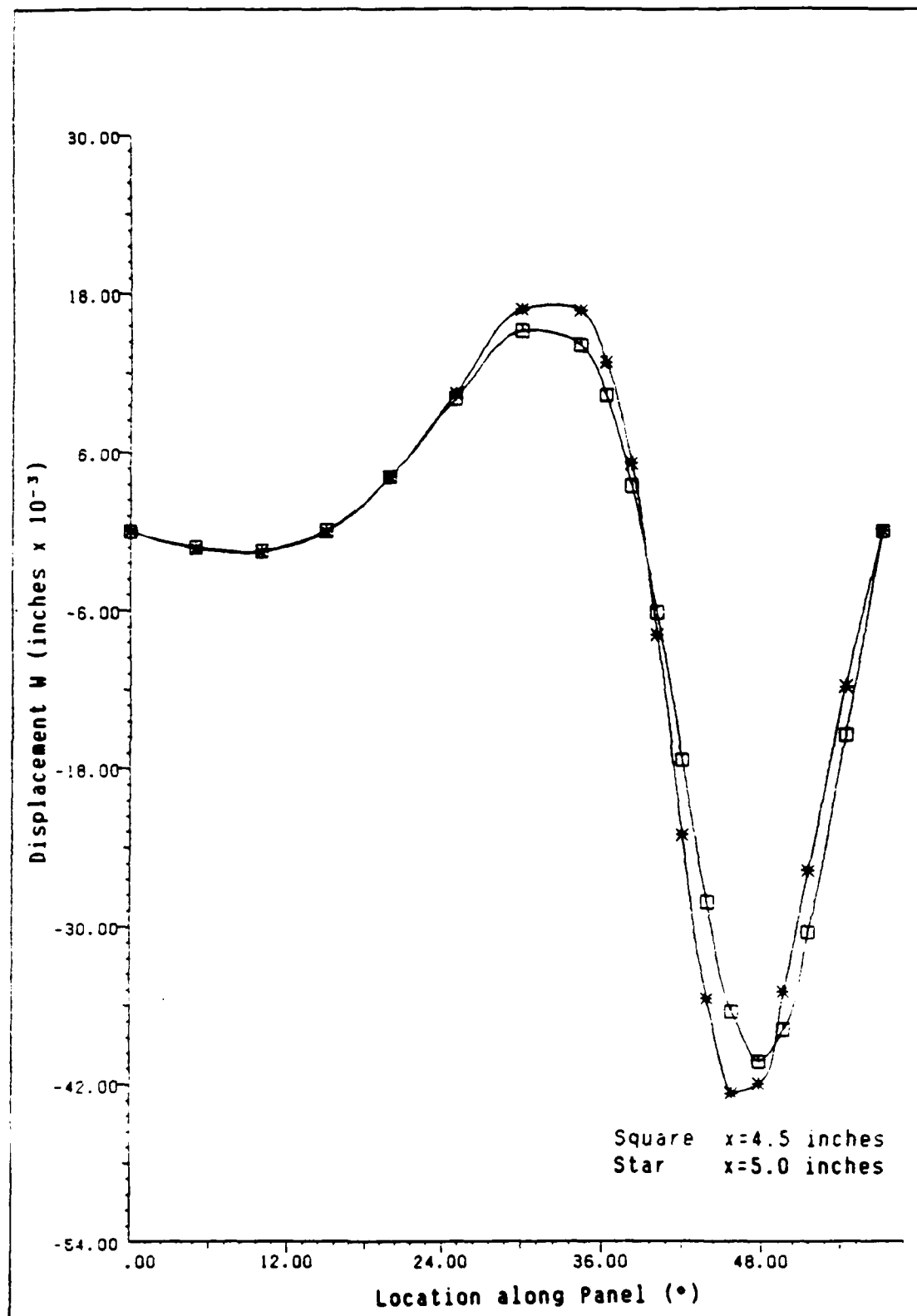


Fig. A3.6 W Profiles at 4.5 and 5.0 inches from the Loading Edge as a function of Location, for Cutouts D and -45 Second Ply

Appendix A4

MOMENT PROFILE STUDY

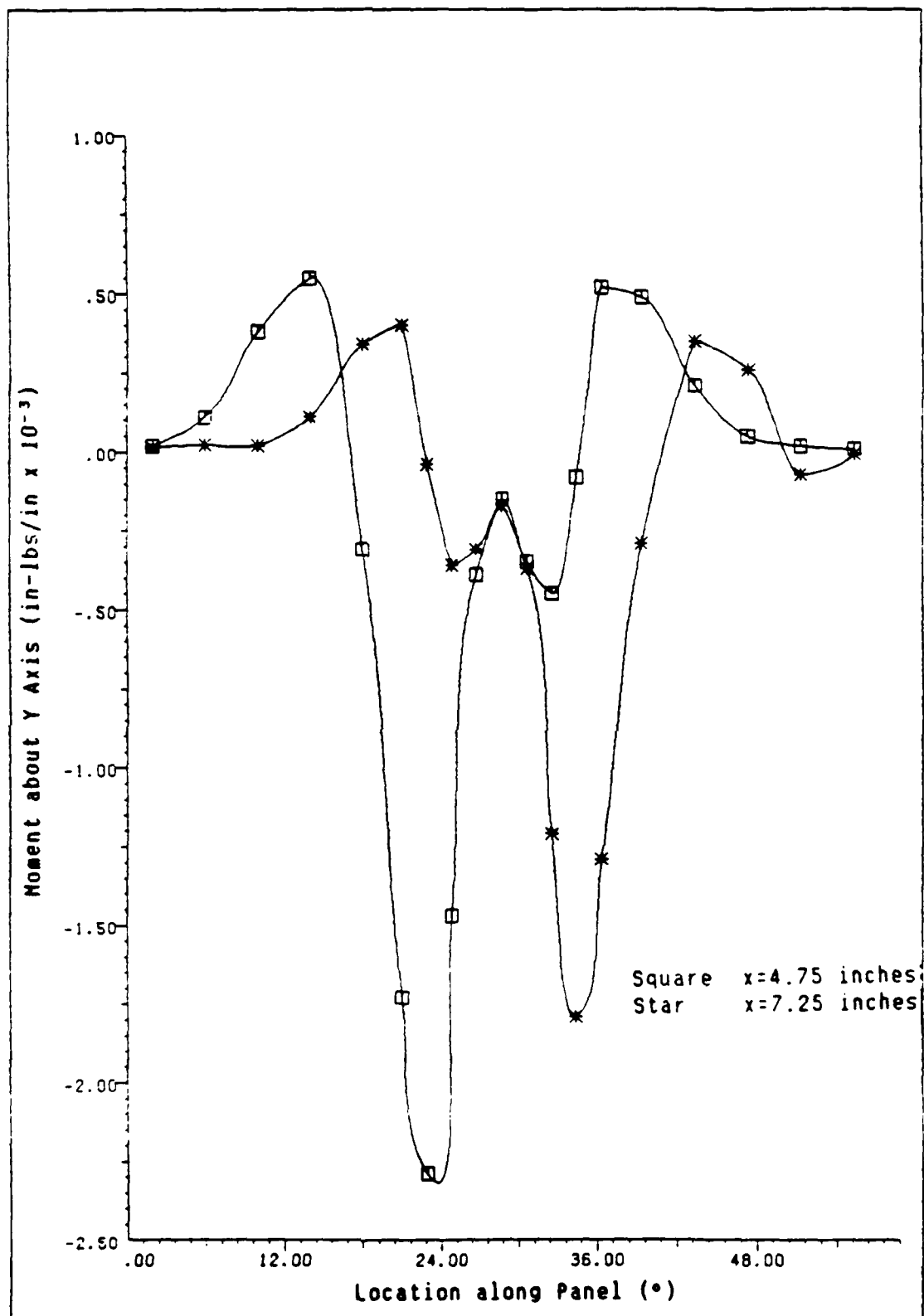


Fig. A4.1 Moment Profiles at $x=4.750$ and $x=7.250$ inches from the Loading Edge for Cutout A, +45 Second Ply, at Collapse Load of 199.4 lbs/in.

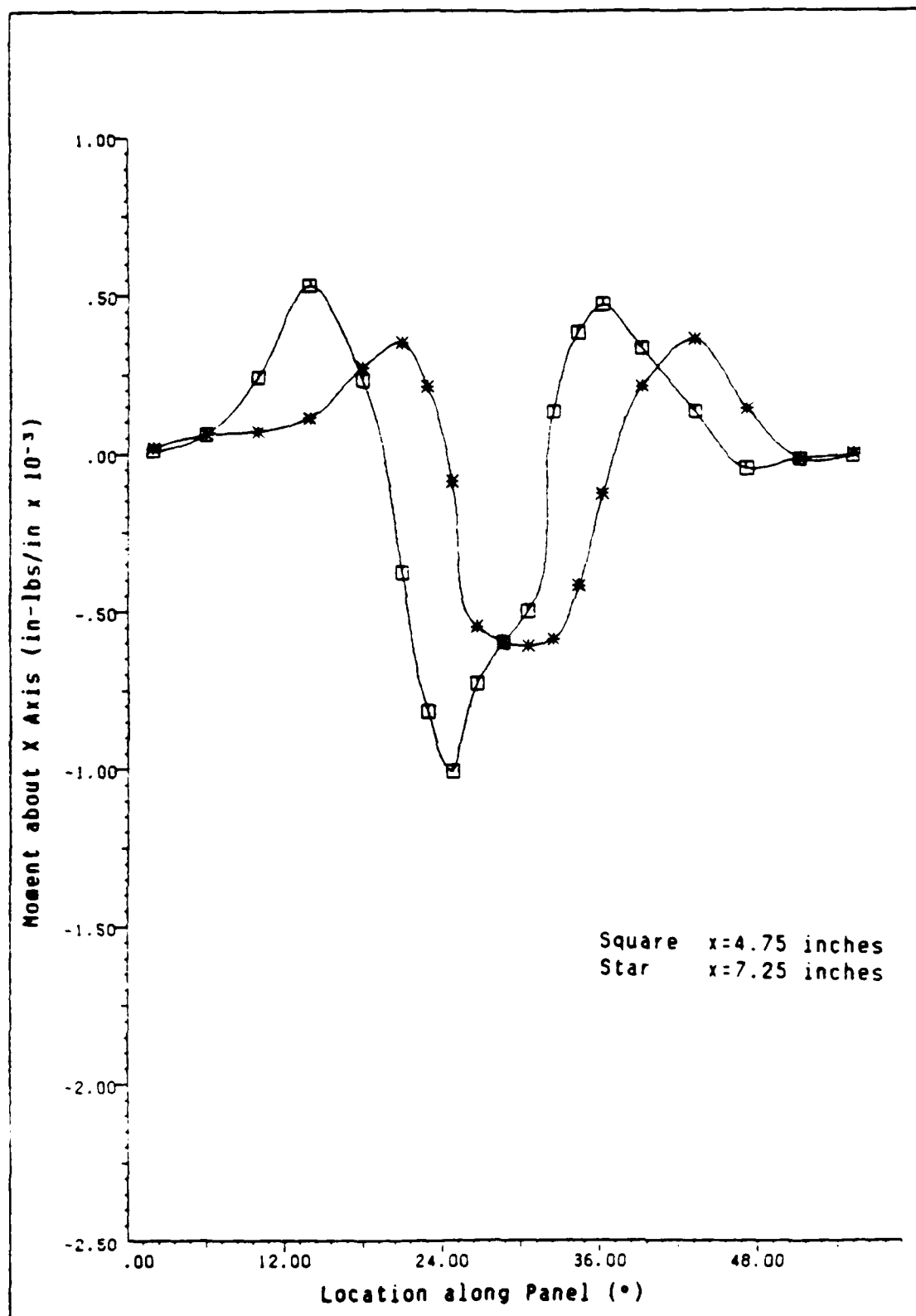


Fig. A4.2 Moment Profiles at $x=4.750$ and $x=7.250$ inches from the Loading Edge for Cutout A, +45 Second Ply, at Collapse Load of 199.4 lbs/in.

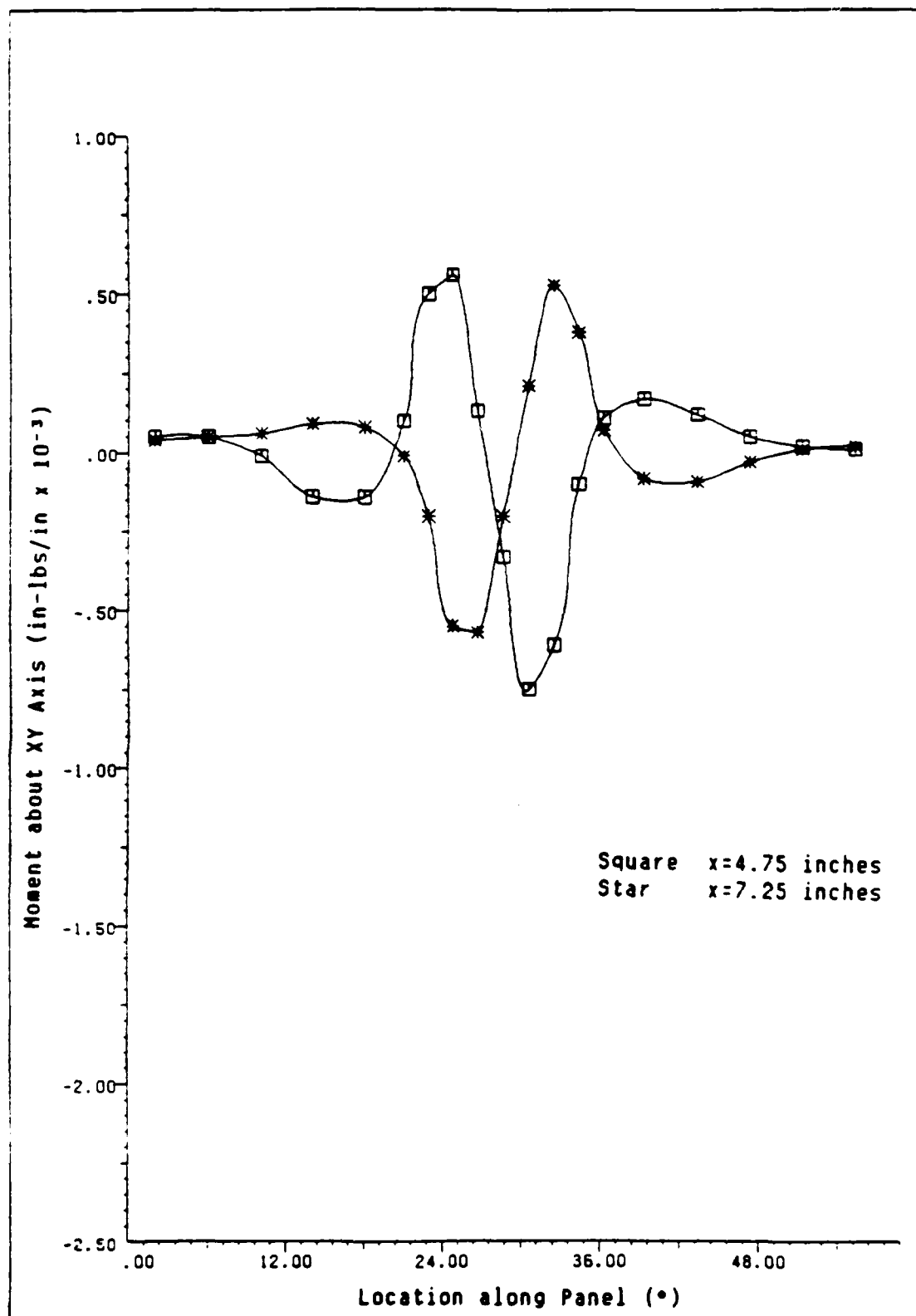


Fig. A4.3 Moment Profiles at $x=4.750$ and $x=7.250$ inches from the Loading Edge for Cutout A, +45 Second Ply, at Collapse Load of 199.4 lbs/in.

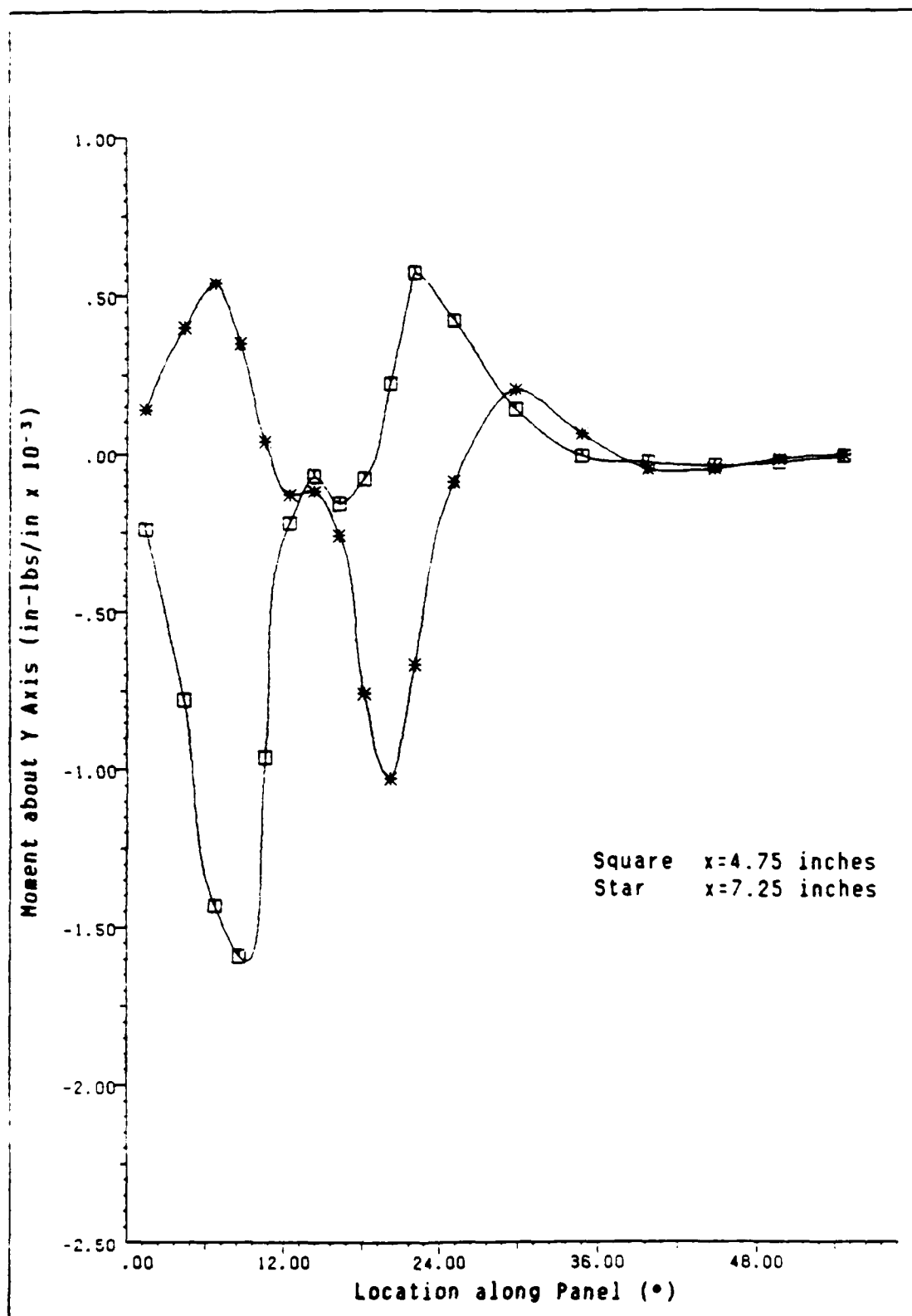


Fig. A4.4 Moment Profiles at $x=4.750$ and $x=7.250$ inches from the Loading Edge for Cutout C, +45 Second Ply, at Collapse Load of 147.2 lbs/in.

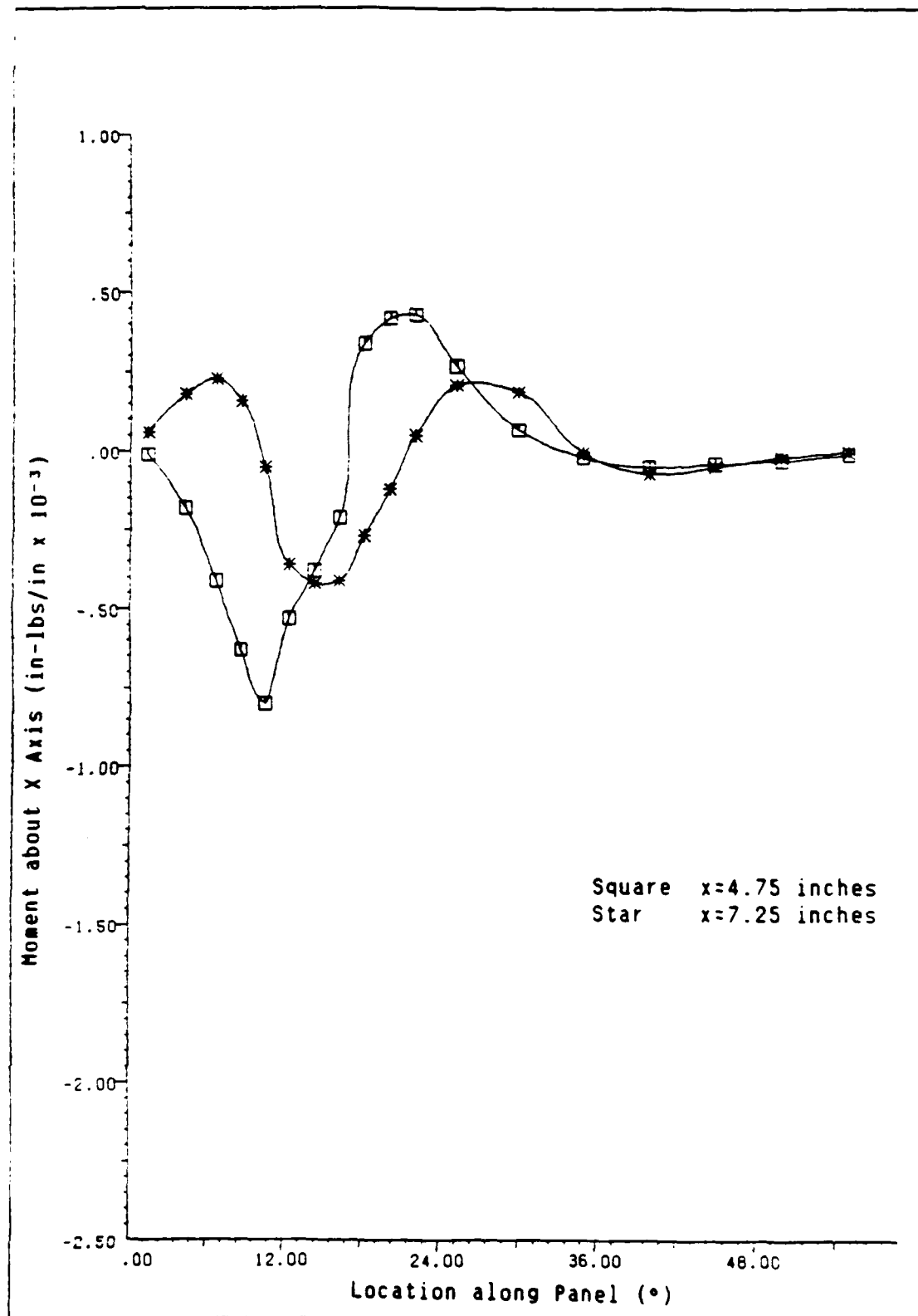


Fig. A4.5 Moment Profiles at $x=4.750$ and $x=7.250$ inches from the Loading Edge for Cutout C, +45 Second Ply, at Collapse Load of 147.2 lbs/in.

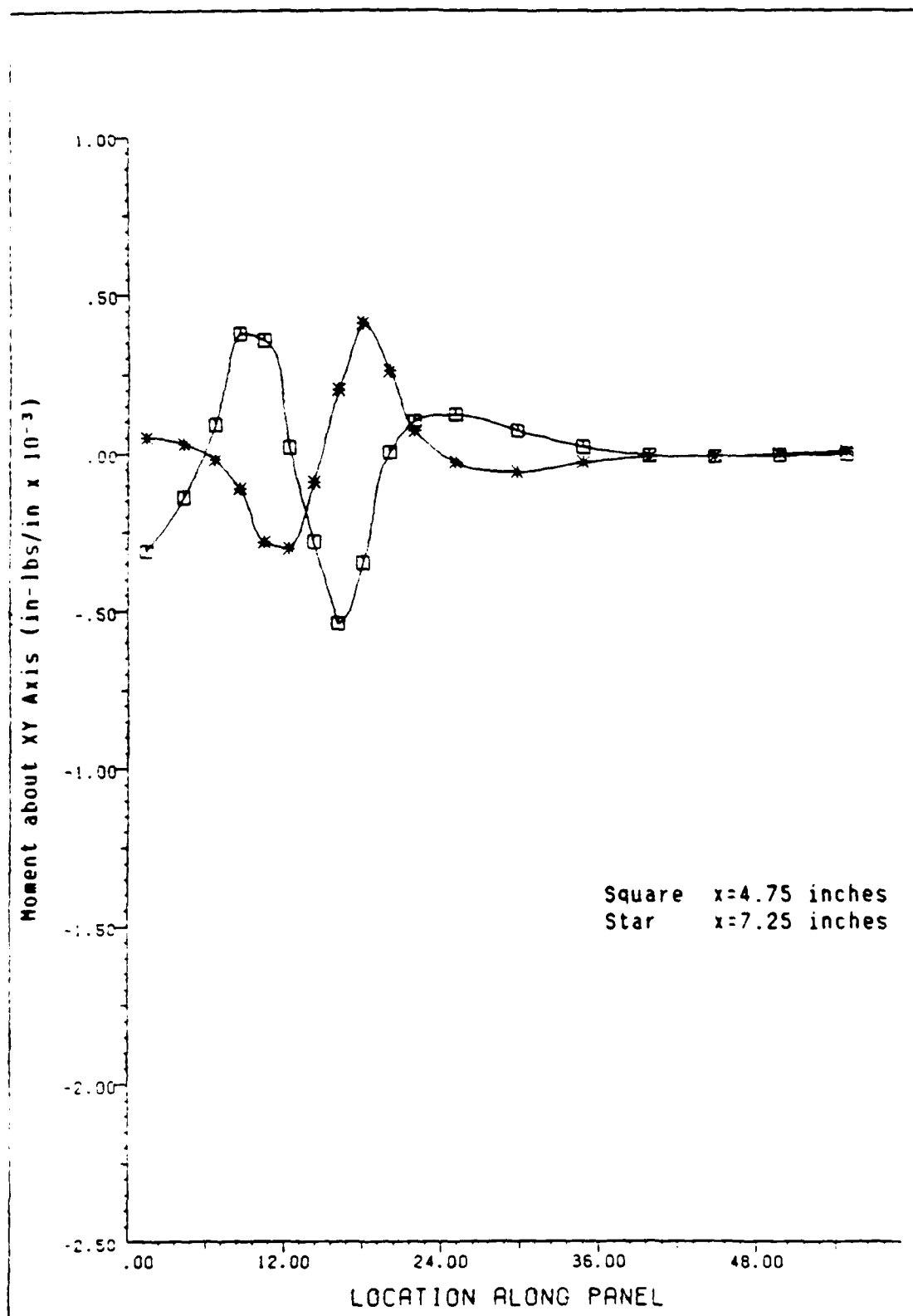


Fig. A4.6 Moment Profiles at $x=4.750$ and $x=7.250$ inches from the Loading Edge for Cutout C, +45 Second Ply, at Collapse Load of 147.2 lbs/in.

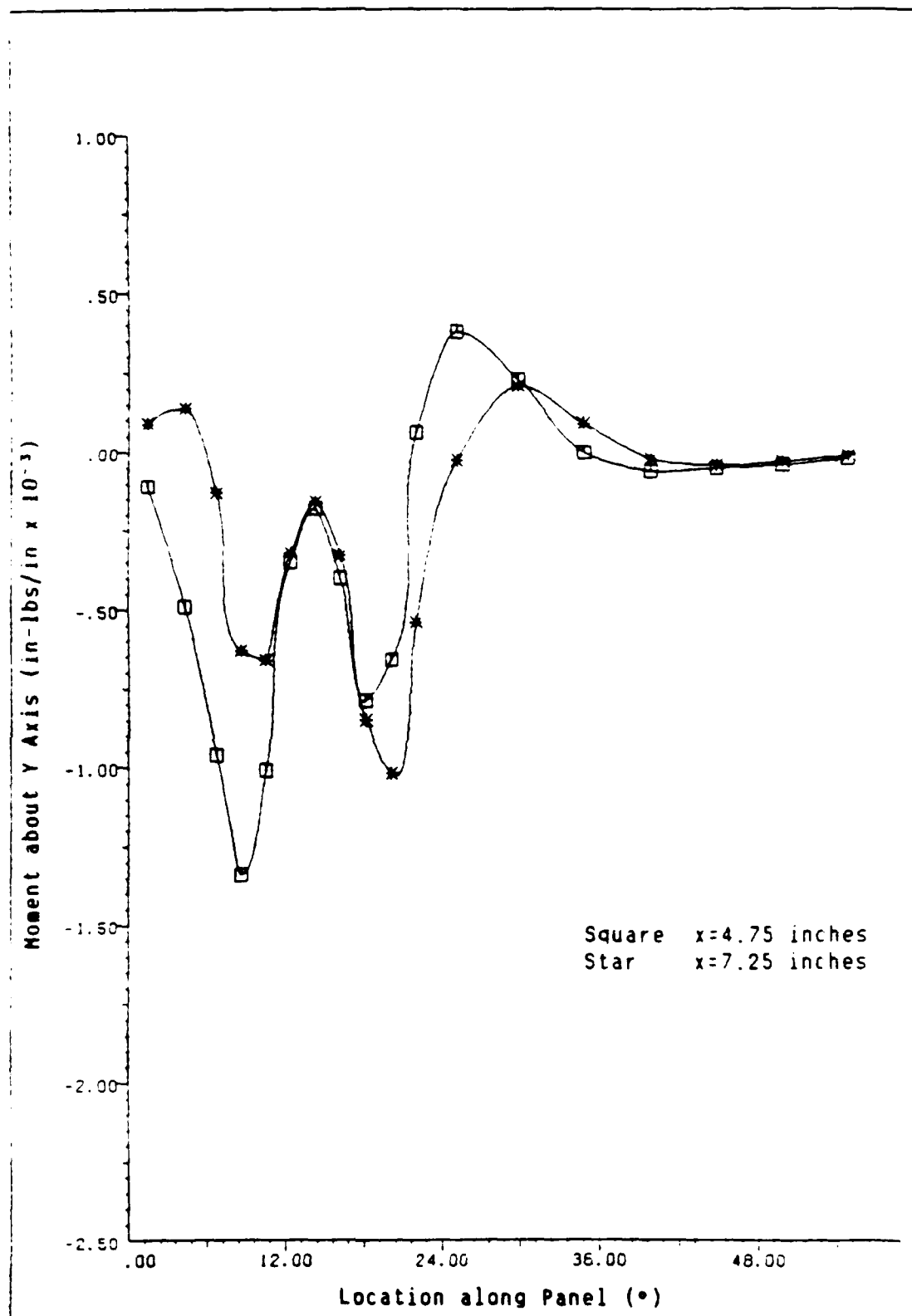


Fig. A4.7 Moment Profiles at $x=4.750$ and $x=7.250$ inches from the Loading Edge for Cutout C, -45 Second Ply, at Collapse Load of 178.6 lbs/in.

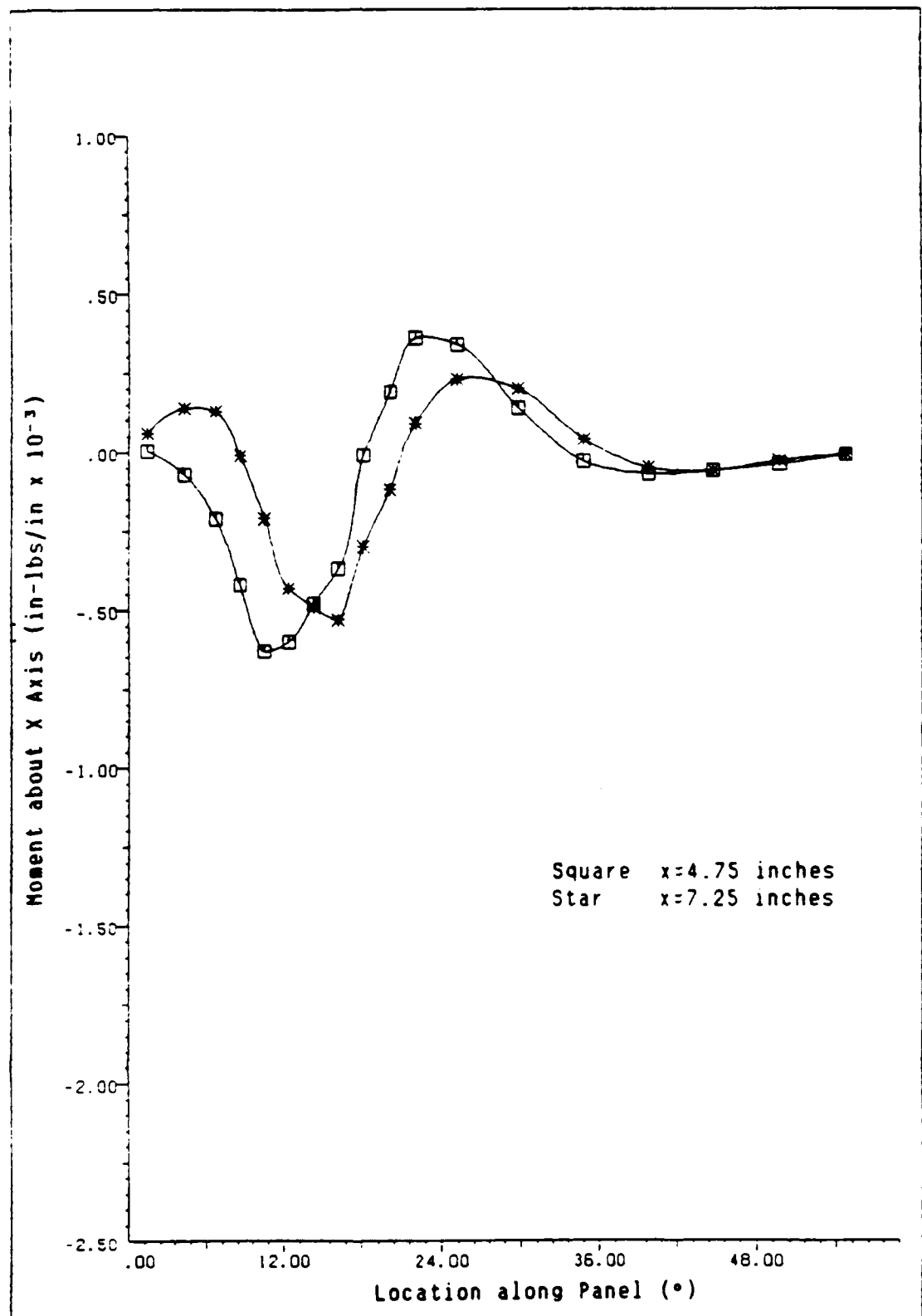


Fig. A4.8 Moment Profiles at x=4.750 and x=7.250 inches from the Loading Edge for Cutout C, -45 Second Ply, at Collapse Load of 178.6 lbs/in.

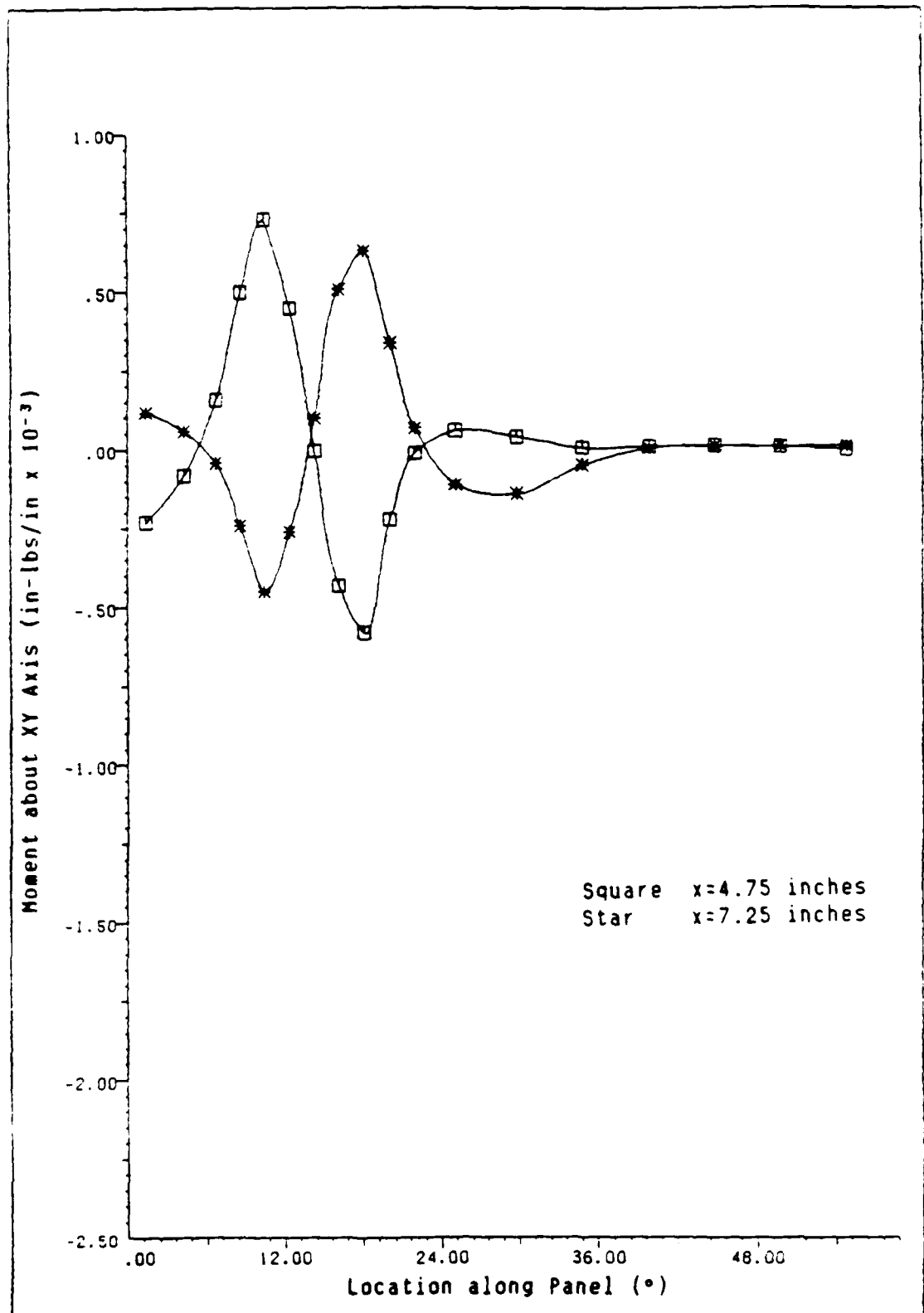


Fig. A4.9 Moment Profiles at $x=4.750$ and $x=7.250$ inches from the Loading Edge for Cutout C, -45 Second Ply, at Collapse Load of 178.6 lbs/in.

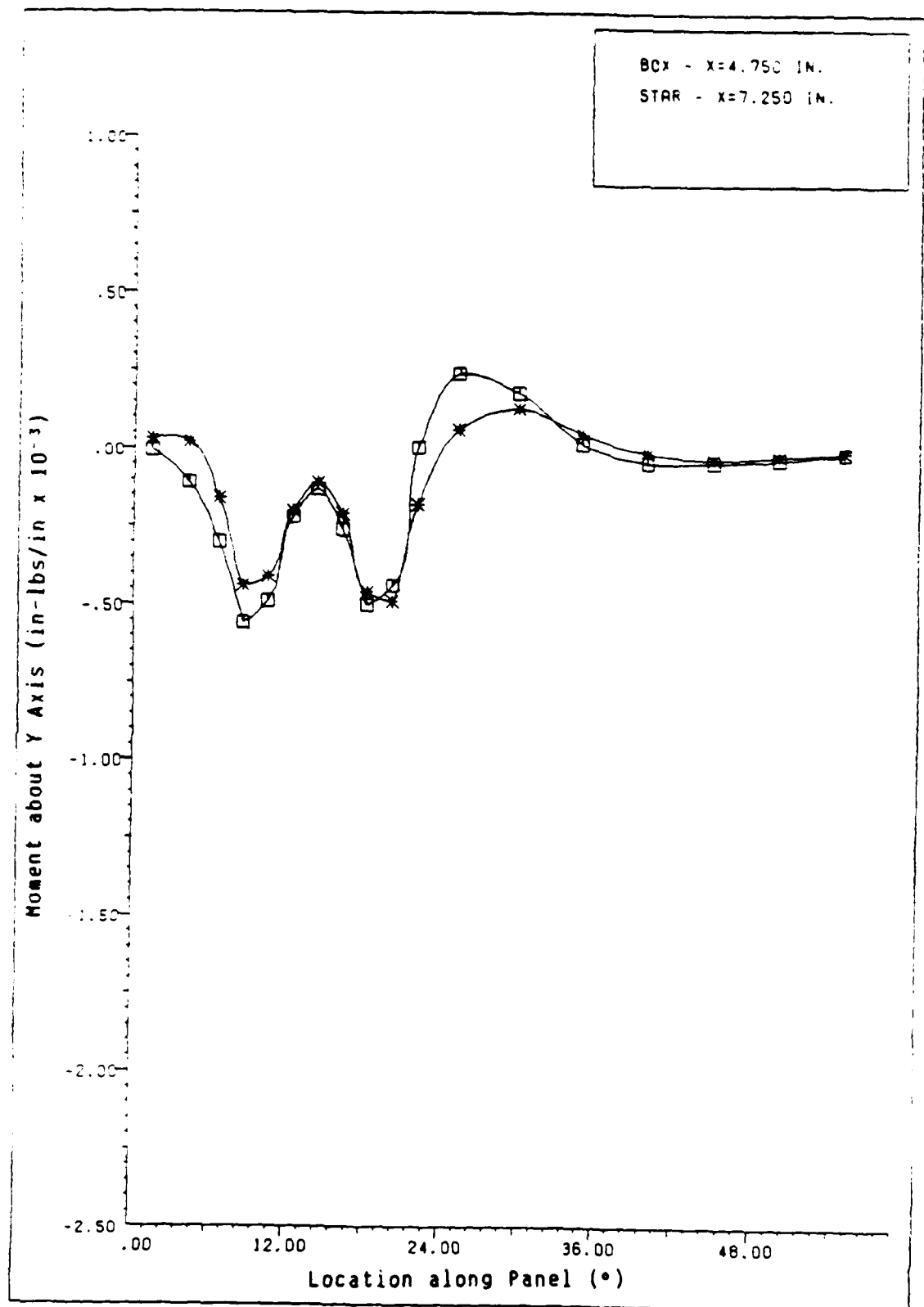


Fig. A4.10 Moment Profiles at $x=4.750$ and $x=7.250$ inches from the Loading Edge for Cutout C, +45 Second Ply, at a Load of 141 lbs/in.

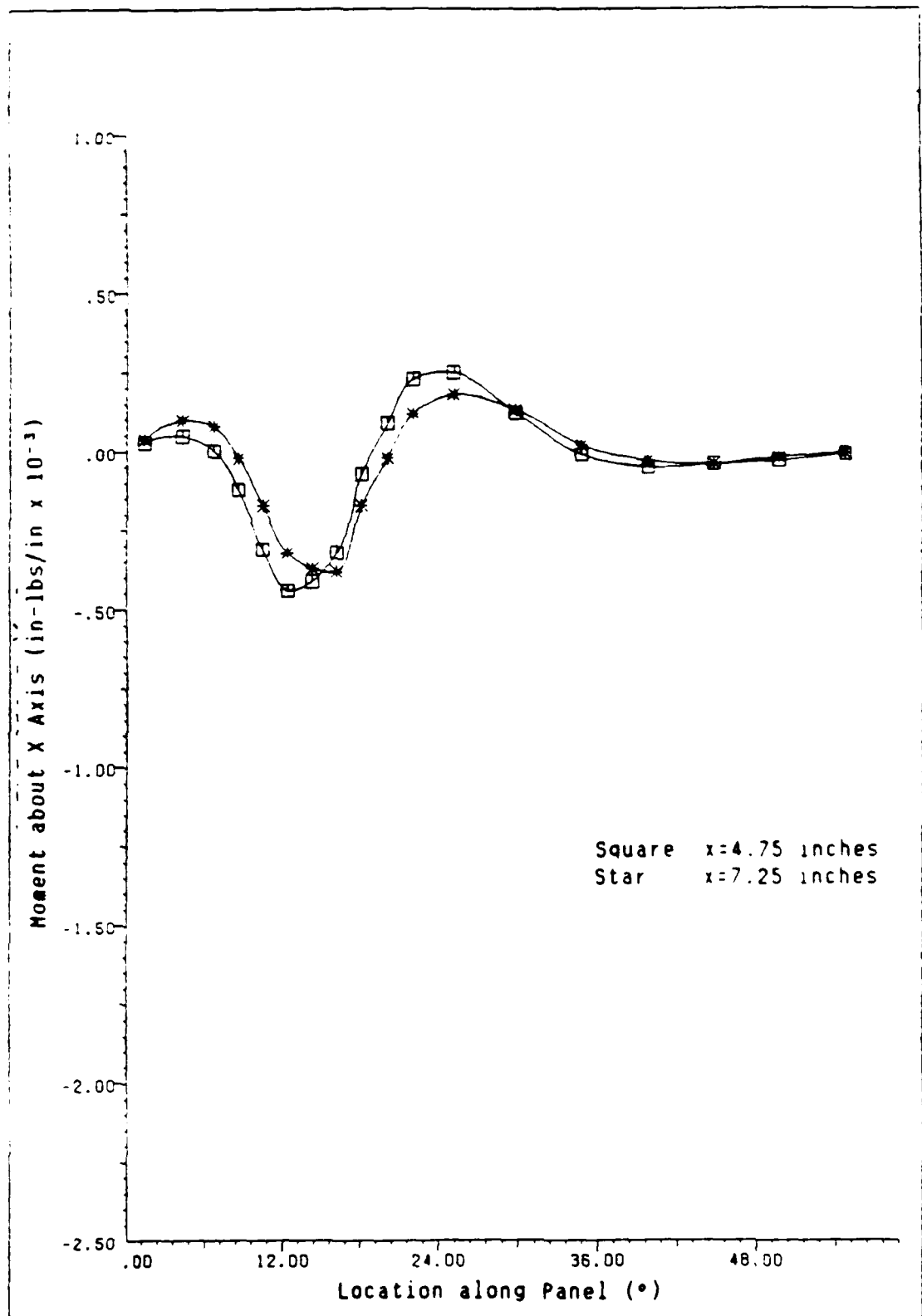


Fig. A4.11 Moment Profiles at $x=4.750$ and $x=7.250$ inches from the Loading Edge for Cutout C, +45 Second Ply, at a Load of 141 lbs/in.

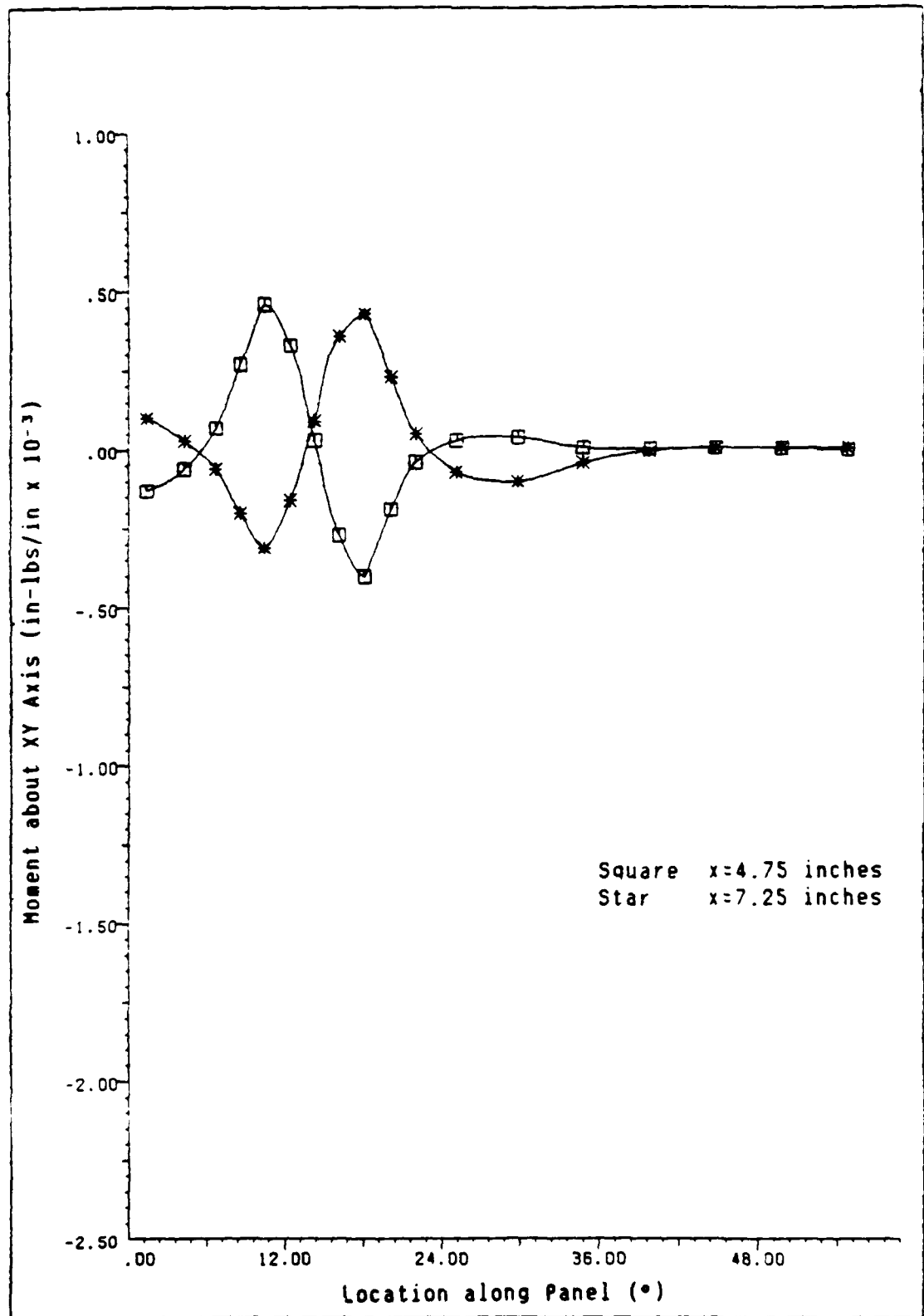


Fig. A4.12 Moment Profiles at x=4.750 and x=7.250 inches from the Loading Edge for Cutout C, +45 Second Ply, at a Load of 141 lbs/in.

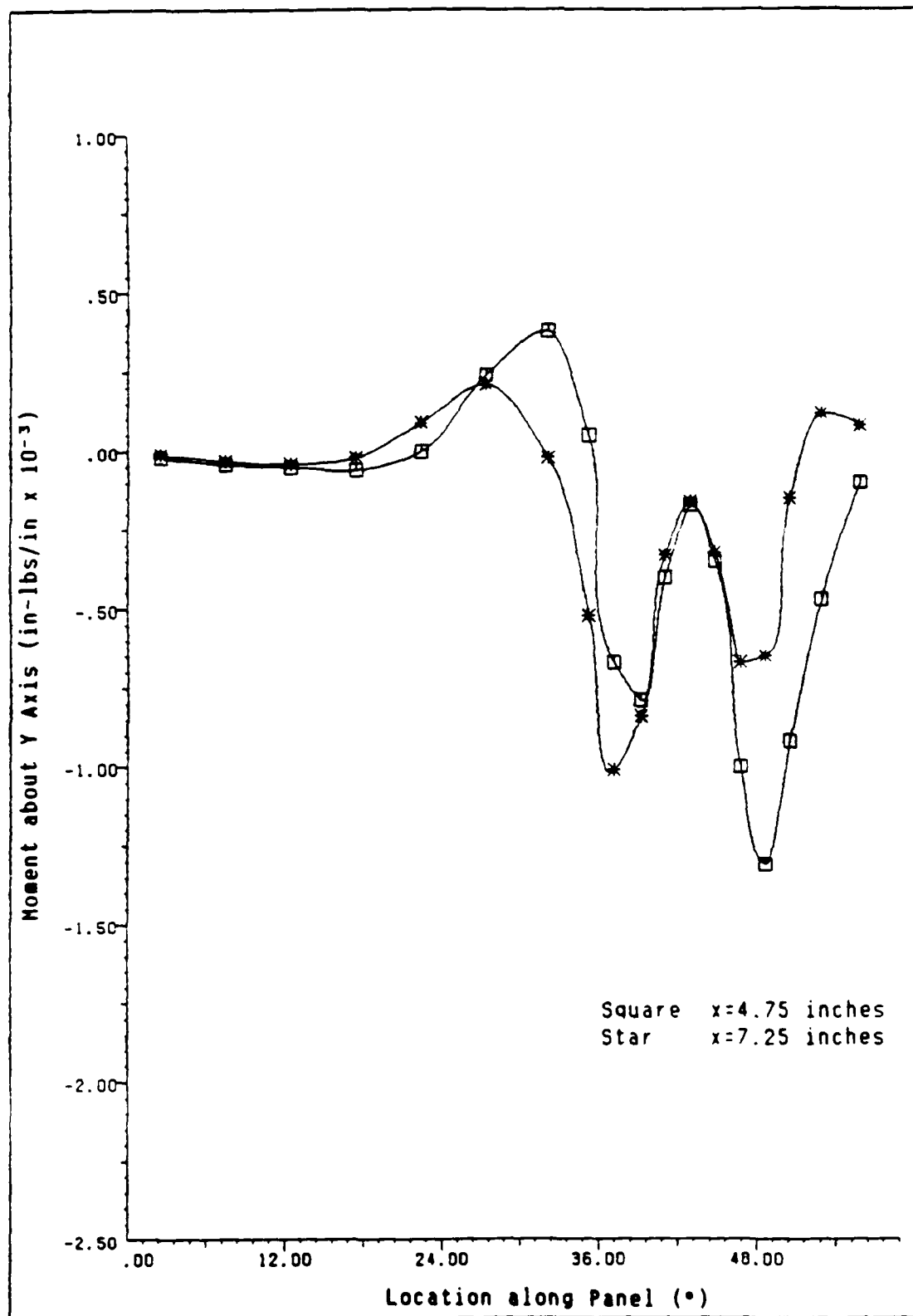


Fig. A4.13 Moment Profiles at $x=4.750$ and $x=7.250$ inches from the Loading Edge for Cutout D, +45 Second Ply, at Collapse Load of 178.5 lbs/in.

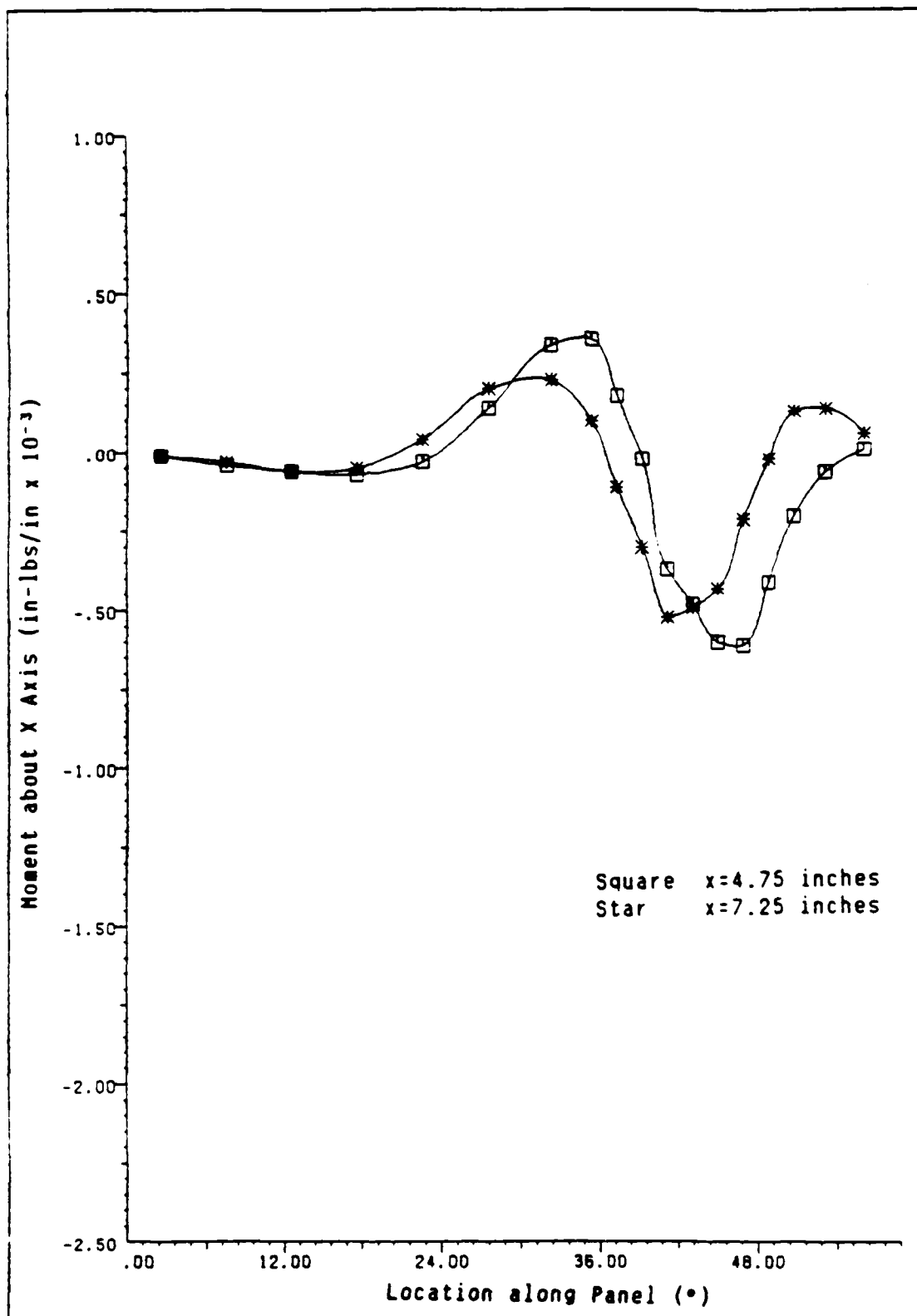


Fig. A4.14 Moment Profiles at $x=4.750$ and $x=7.250$ inches from the Loading Edge for Cutout D, +45 Second Ply, at Collapse Load of 178.5 lbs/in.

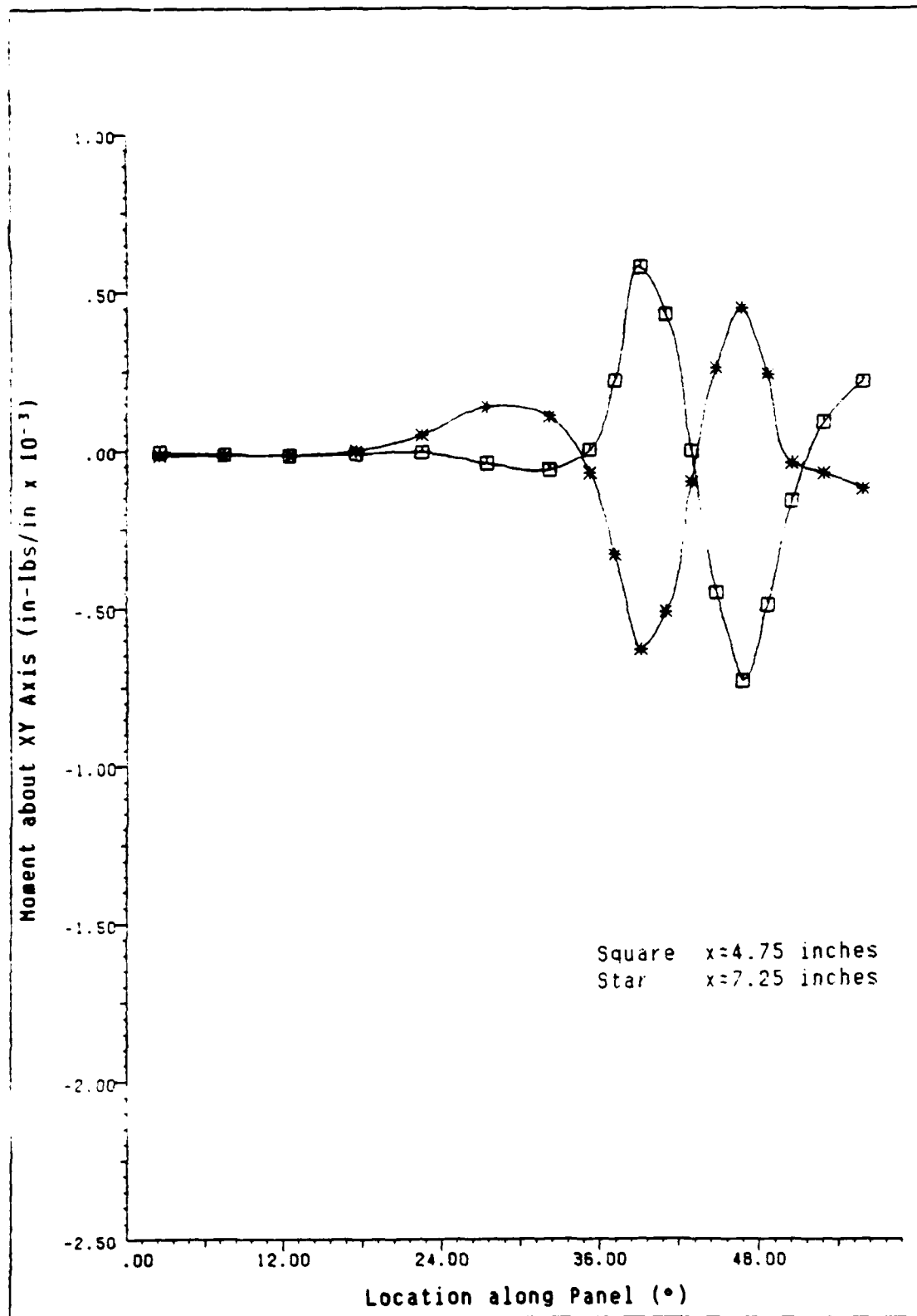


Fig. A4.15 Moment Profiles at $x=4.750$ and $x=7.250$ inches from the Loading Edge for Cutout D, +45 Second Ply, at Collapse Load of 178.5 lbs/in.

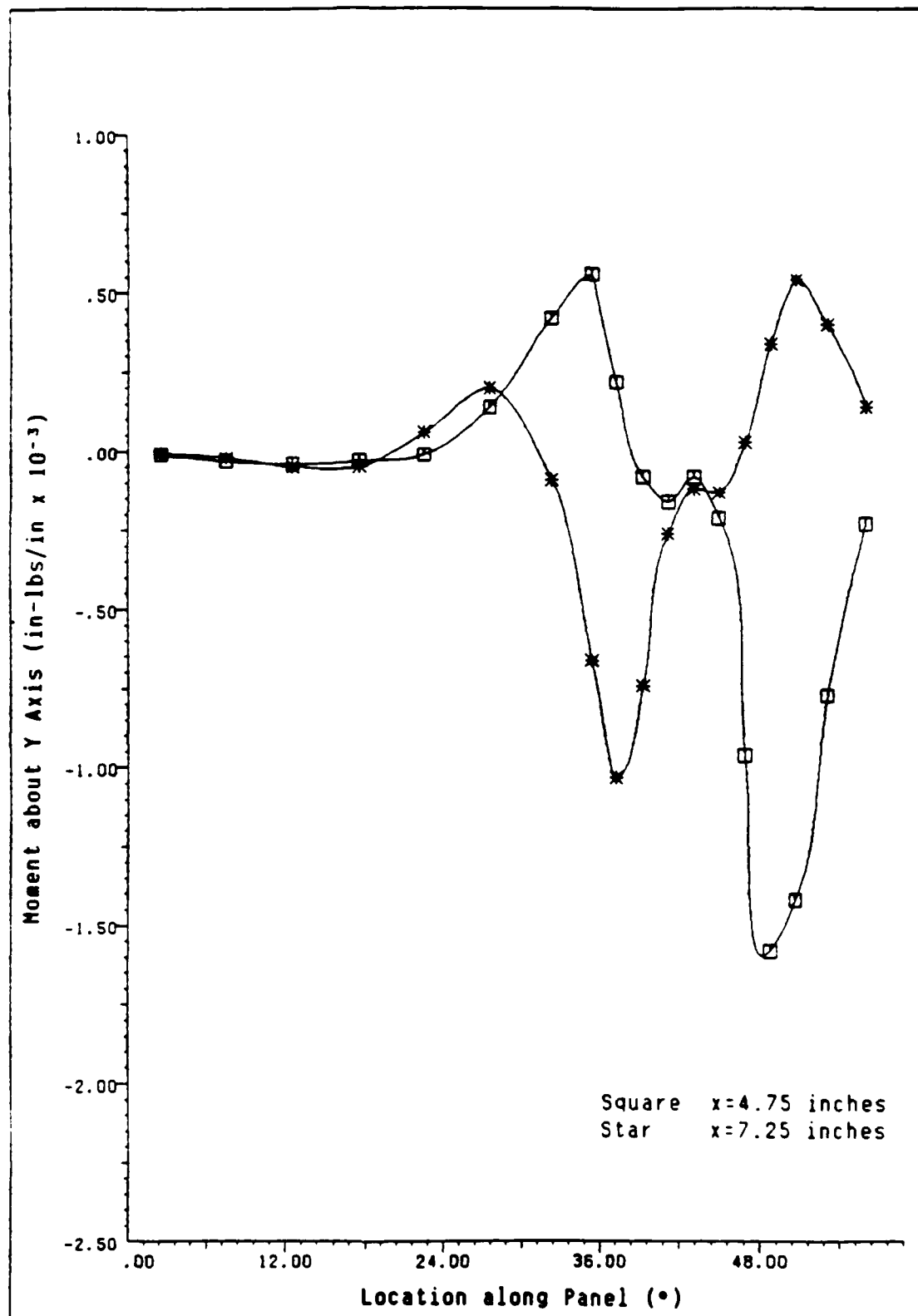


Fig. A4.16 Moment Profiles at $x=4.750$ and $x=7.250$ inches from the Loading Edge for Cutout D, -45 Second Ply, at Collapse Load of 147.2 lbs/in.

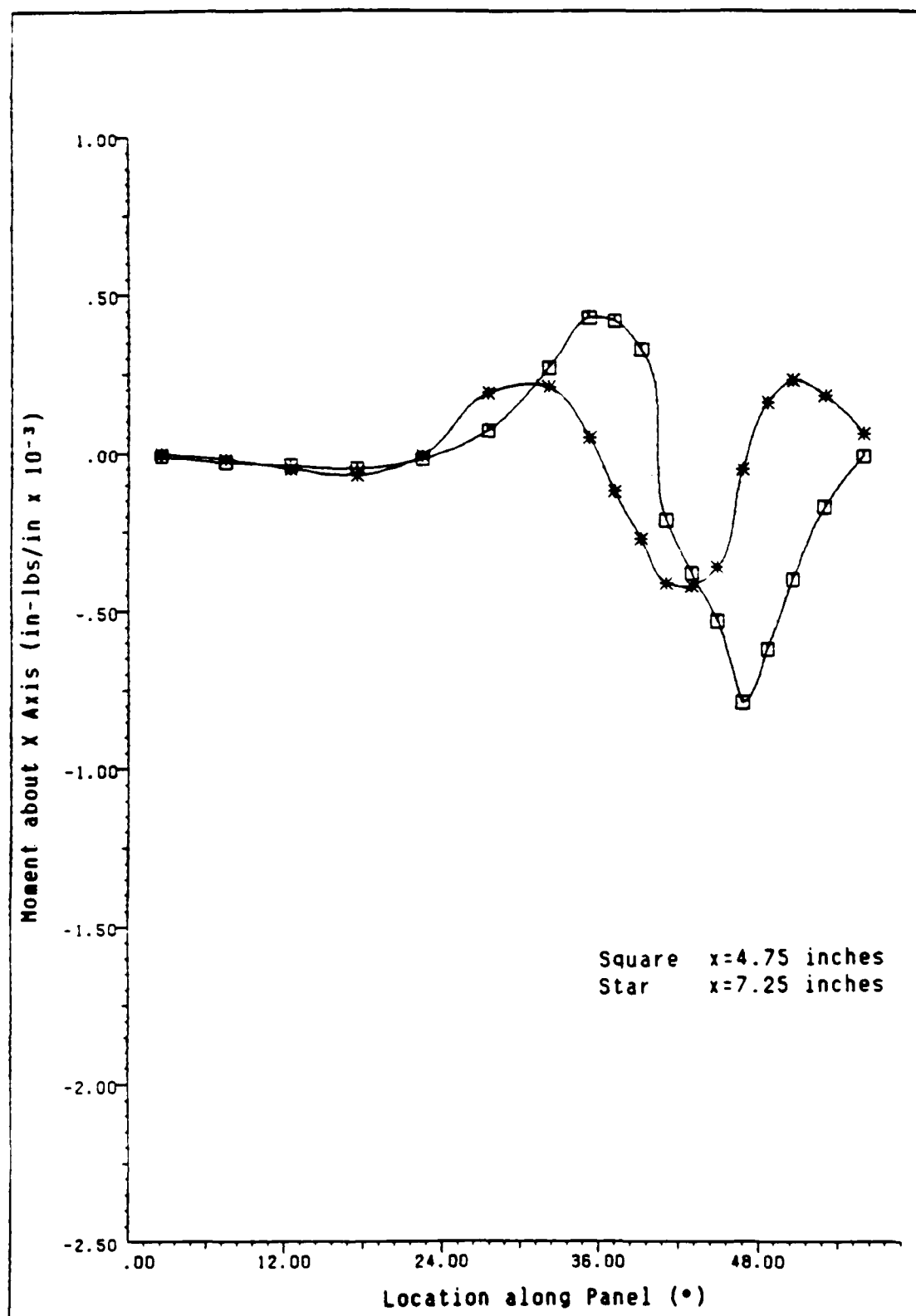


Fig. A4.17 Moment Profiles at $x = 4.750$ and $x = 7.250$ inches from the Loading Edge for Cutout D, -45 Second Ply, at Collapse Load of 147.2 lbs/in.

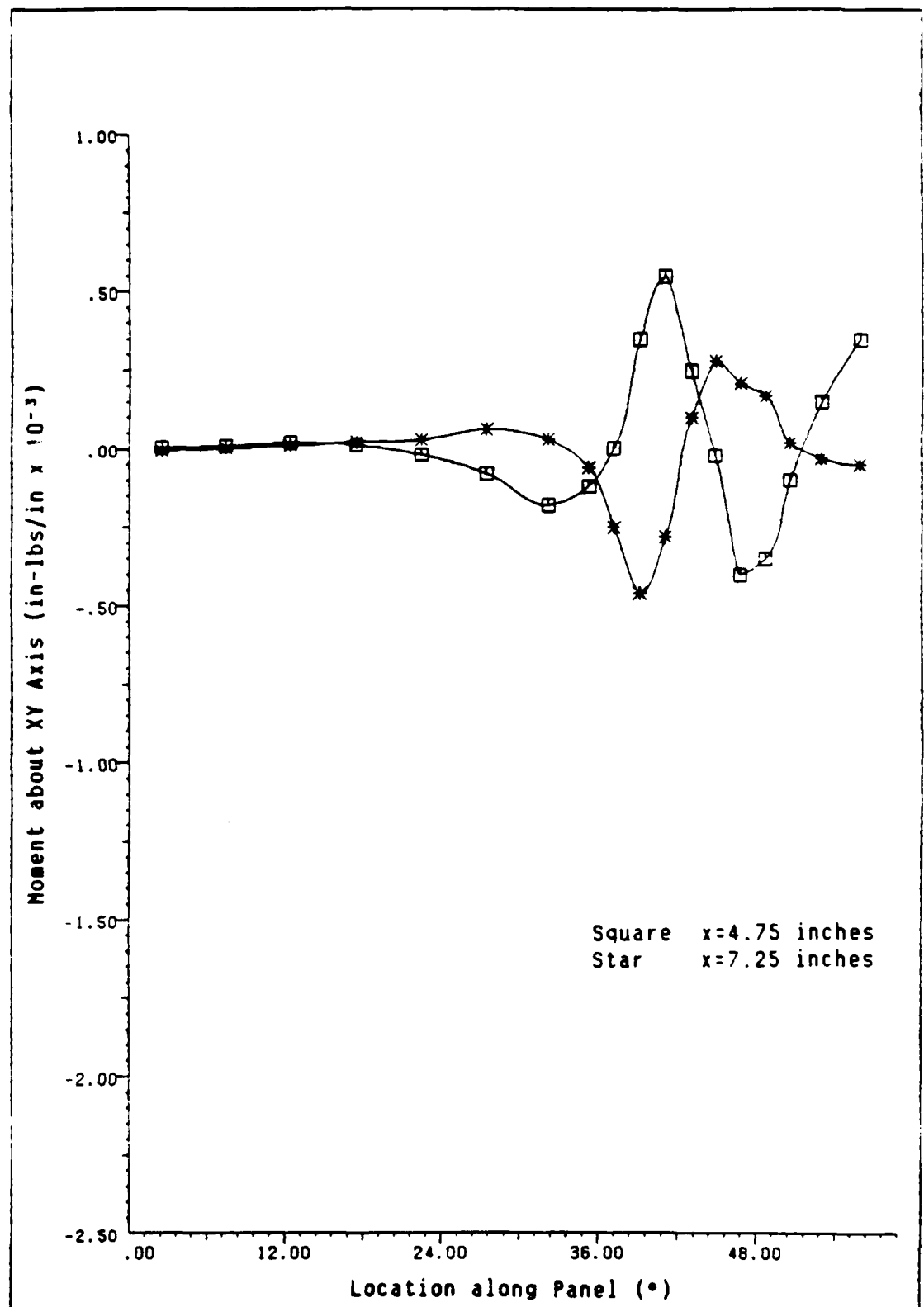


Fig. A4.18 Moment Profiles at $x=4.750$ and $x=7.250$ inches from the Loading Edge for Cutout D, -45 Second Ply, at Collapse Load of 147.2 lbs/in.

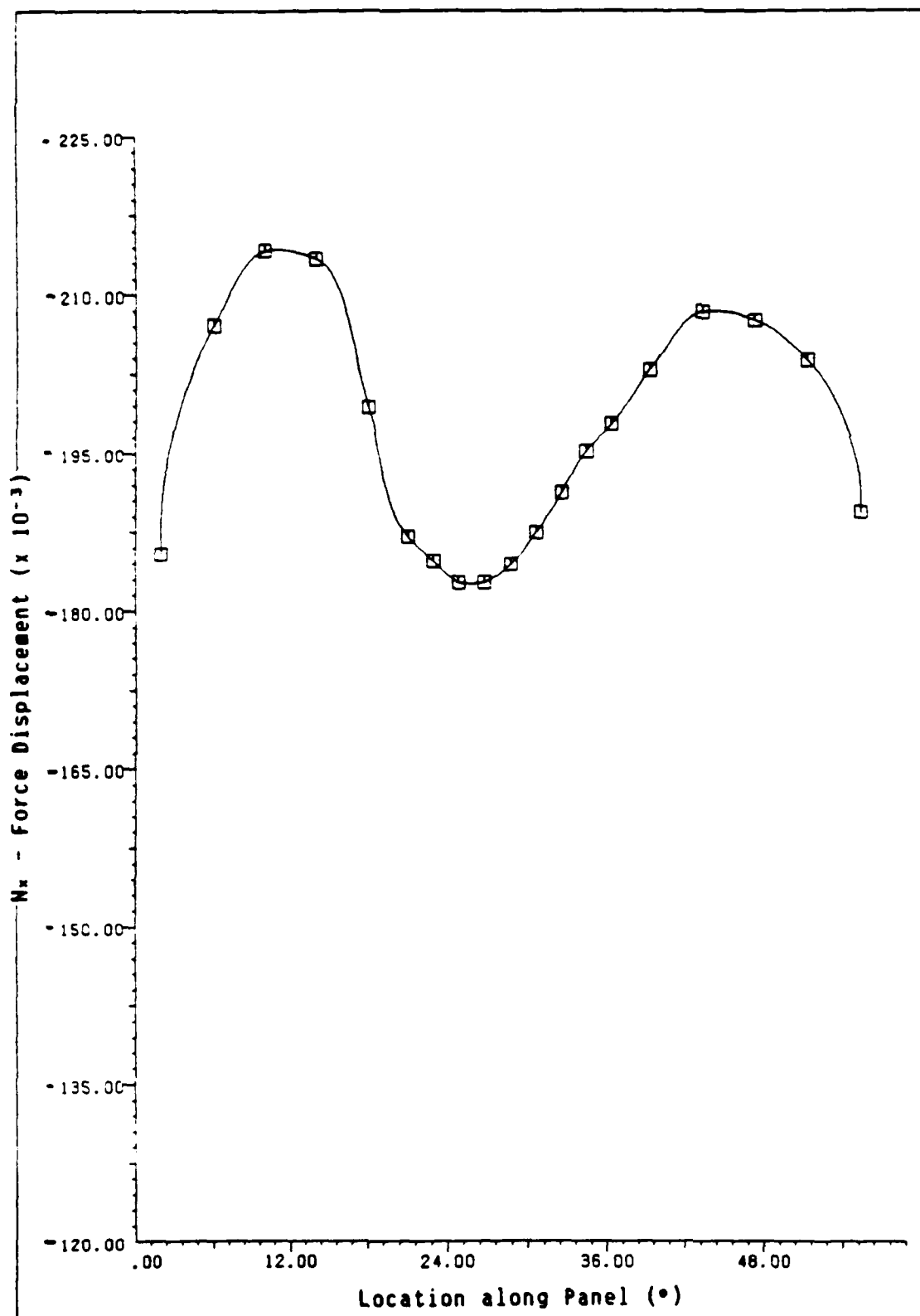


Fig. A4.19 N_x at the Loading Edge of the Panel at Collapse Load for Cutout A and +45 Second Ply

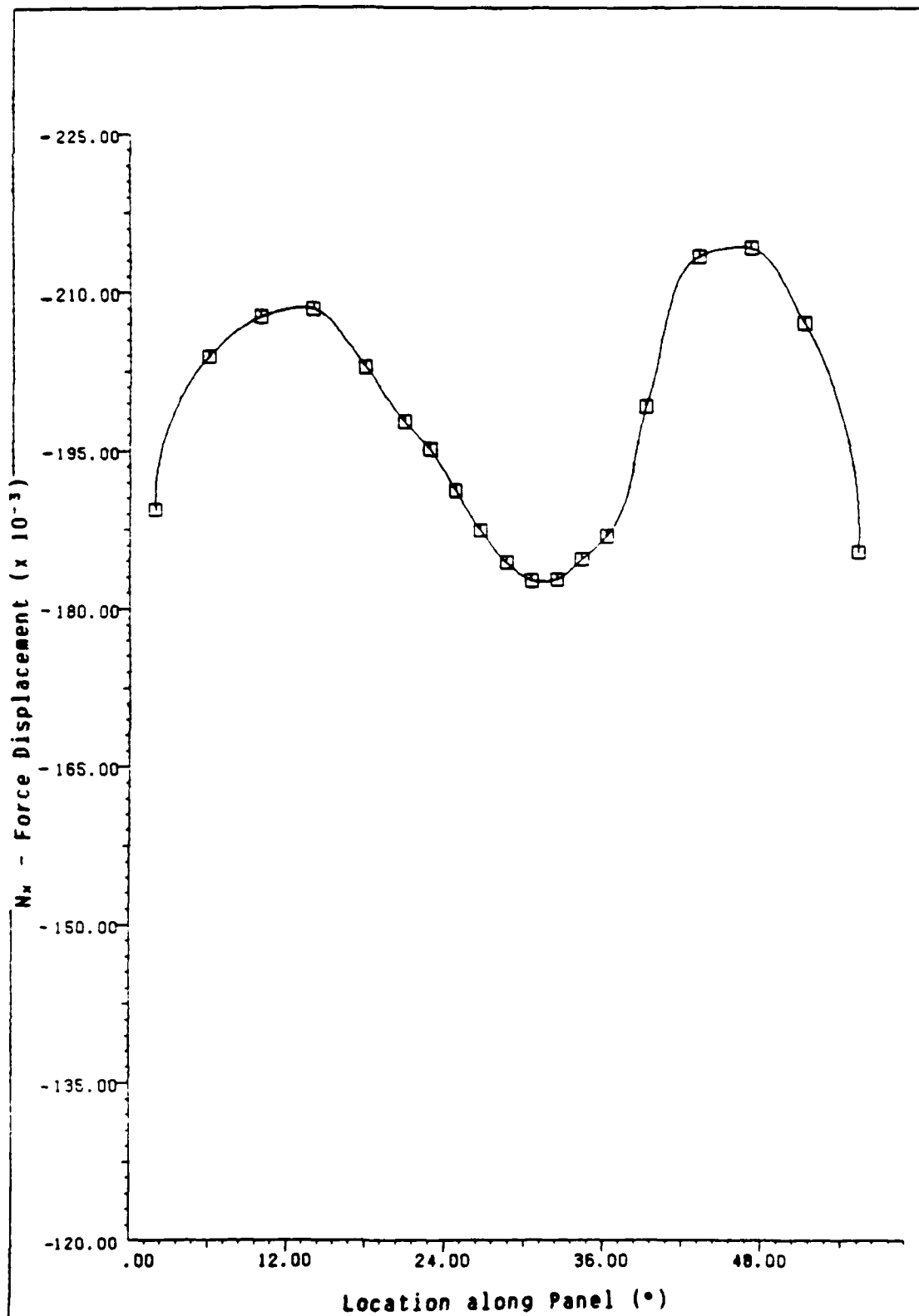


Fig. A4.20 N_x at the Loading Edge of the Panel at Collapse Load for Cutout A and -45 Second Ply

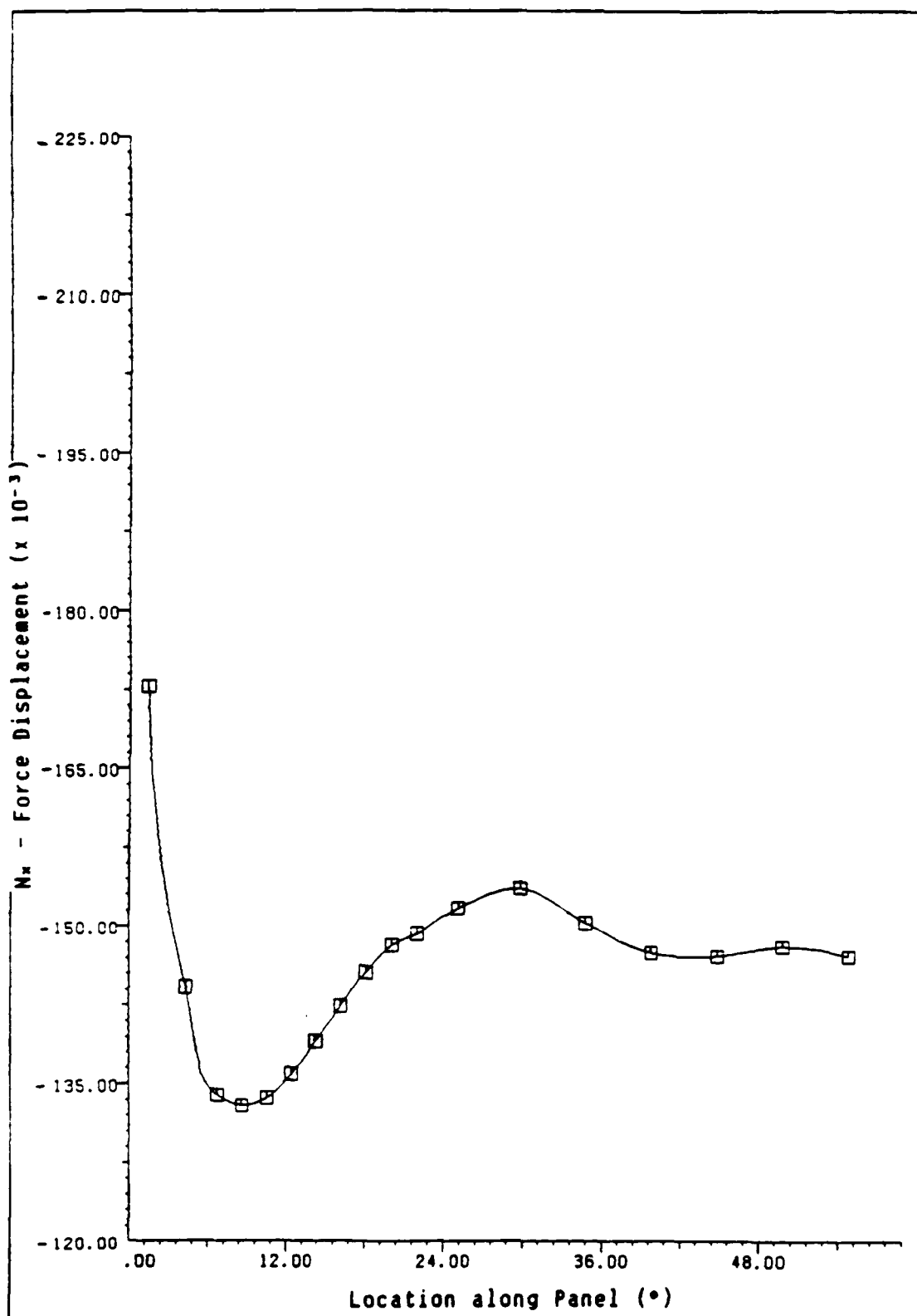


Fig. A4.21 N_x at the Loading Edge of the Panel at Collapse Load for Cutout C and +45 Second Ply

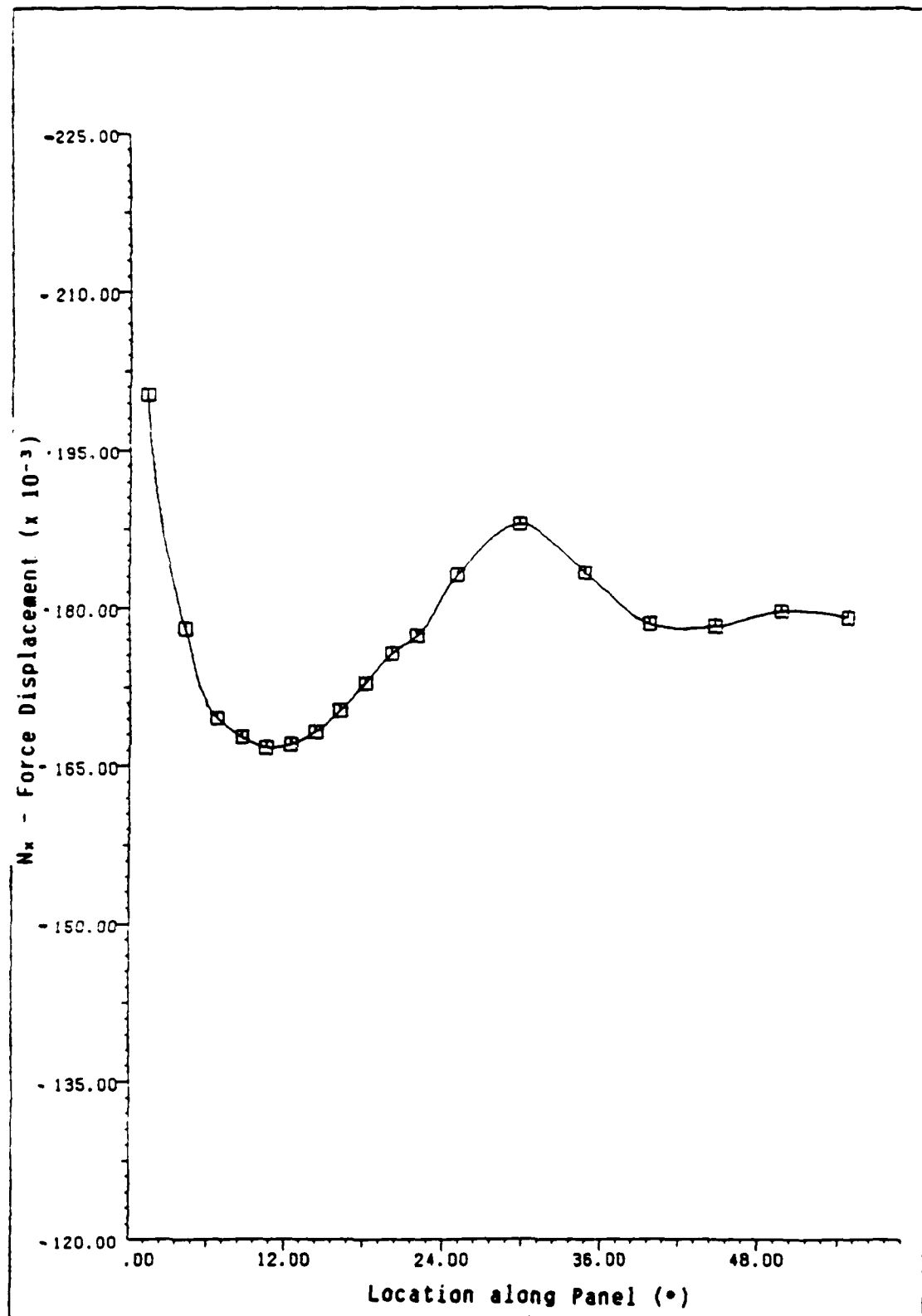


Fig. A4.22 N_x at the Loading Edge of the Panel at Collapse Load for Cutout C and -45 Second Ply

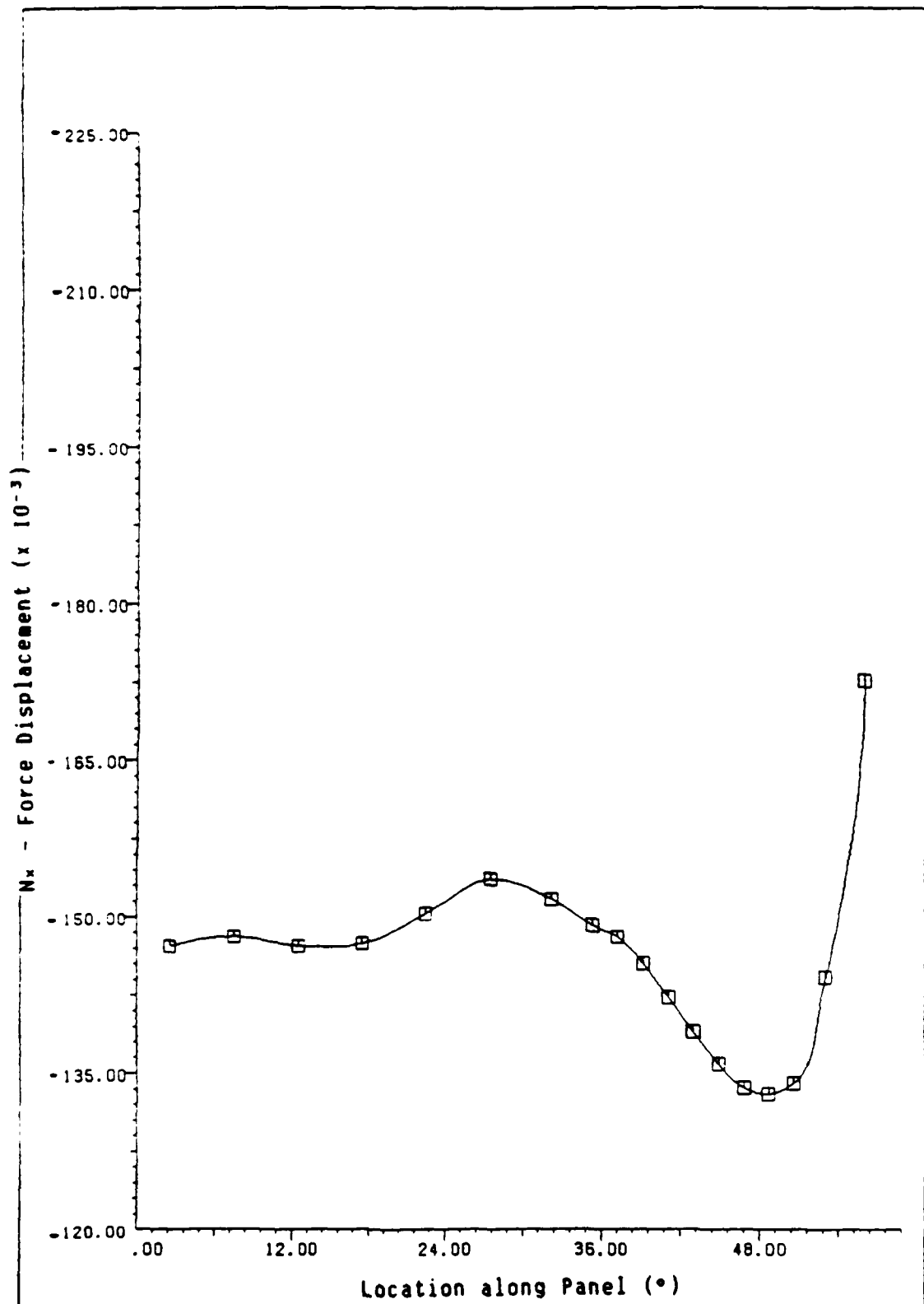


Fig. A4.23 N_x at the Loading Edge of the Panel at Collapse Load for Cutout D and +45 Second Ply

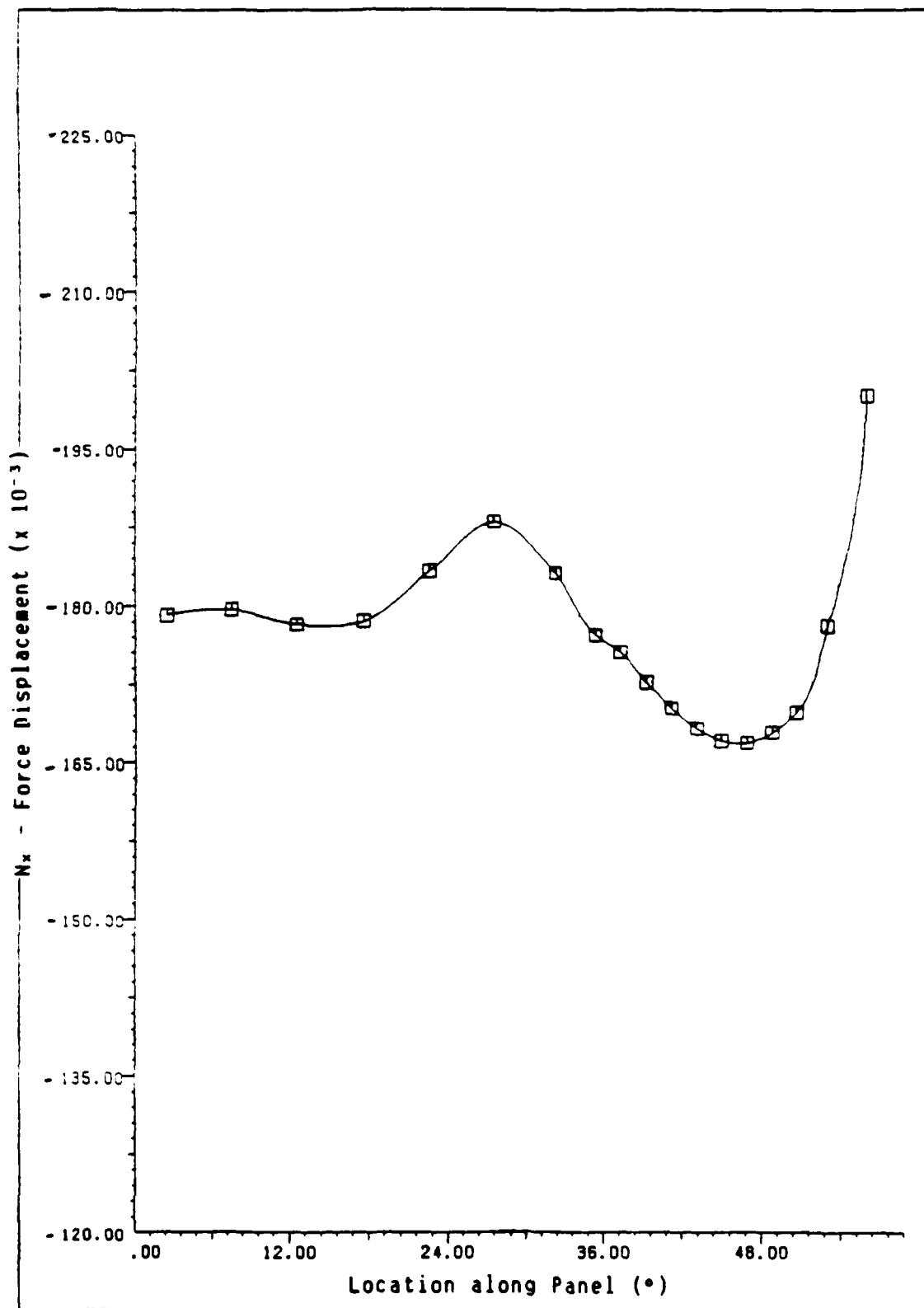


Fig. A4.24 N_x at the Loading Edge of the Panel at Collapse Load for Cutout D and -45 Second Ply

BIBLIOGRAPHY

1. Sobel, L. H., Weller, T., and Agarwal, B. L., "Buckling of Cylindrical Panels Under Axial Compression," Computers and Structures, 6: 29-35 (February 1976).
2. Andreev, L. V. et al. "Nonlinear Deformation of a Cylindrical Panel Under Axial Compression," Soviet Applied Mechanics, 17: 270-274 (September 1981).
3. Almroth, B. O. "Influence of Edge Conditions on the Stability of Axially Compressed Cylindrical Shells," AIAA Journal, 4: 134-140 (1966).
4. Rehfield, L. W. and Hallauer, W. L., Jr. "Edge Restraint Effect on Buckling of Compressed Curved Panels," AIAA Journal, 6: 187-189 (January 1968).
5. Becker, M. L., Palazotto, A. N., and Khot, N. S., "Instability of Composite Panels," Journal of Aircraft, 18: 739-743 (September 1981).
6. Tvergaard, V. "Buckling of Elastic-Plastic Cylindrical Panel Under Axial Compression," International Journal of Solid Structures, 13: 957-970, (1977).
7. Brogan, F. and Almroth, B. O., "Buckling of Cylinders with Cutouts," AIAA Journal, 8: 236-238 (February 1970).
8. Garashchuk, I. N. and Chernyshenko, I. S. "Numerical Investigation of the Stress State of a Cylindrical Shell with a Circular Hole," Soviet Applied Mechanics, 15: 484-488 (December 1979).
9. Almroth, B. O. and Holmes, A. M. C., "Buckling of Shells with Cutouts Experiment and Analysis," International Journal of Solid Structures, 8: 1057-1071 (August 1972).
10. Almroth, B. O. et al. "Stability of Cylinders with Circular Cutouts," AIAA Journal, 11: 1582-1584 (November 1973).
11. Almroth, B. O. and Brogan, F. A. "Bifurcation Buckling as an Approximation of the Collapse Load for General Shells," AIAA Journal, 10: 463-467 (April 1972).
12. Becker, M. L., Palazotto, A. N., and Khot, N. S., "Experimental Investigation of the Instability of Composite Cylindrical Panels," Experimental Mechanics, 22: 372-376 (October 1982).

13. Bauld, N. R., Jr. and Satyamurthy, K. Collapse Load Analysis for Plates and Shells. AFFDL-TR-79-3038. Air Force Flight Dynamics Laboratory, Wright-Patterson AFB OH, December 1970.
14. Harper, Lt James G. Buckling Analysis of Laminated Composite Circular Cylindrical Shells. MS Thesis, AFIT/GAE/AA/78D-8. School of Engineering, Air Force Institute of Technology (AU), Wright-Patterson AFB OH, December 1978 (AD-A081904).
15. Becker, Capt Marvin L. Analytical/Experimental Investigation of the Instability of Composite Cylindrical Panels. MS Thesis, AFIT/GAE/AA/79D-3. School of Engineering, Air Force Institute of Technology (AU), Wright-Patterson AFB OH, December 1979.
16. Herbert, Capt John S. Analytical/Experimental Linear Bifurcation of Curved Cylindrical Composite Panels. MS Thesis, AFIT/GAE/AA/82D-14. School of Engineering, Air Force Institute of Technology (AU), Wright-Patterson AFB OH, December 1982.
17. Janisse, T. C. and Palazotto, A. N., "Collapse Analysis of Cylindrical Composite Panel with Cutouts," AIAA Journal of Aircraft, 21: 731-733 (September 1984).
18. Lee, C. E. and Palazotto, A. N., "Nonlinear Collapse Analysis of Composite Cylindrical Panels with Small Cutouts or Notches," Composite Structures, 4: 217-229 (1985).
19. Snead, J. M. and Palazotto, A. N., "Moisture and Temperature Effects on the Instability of Cylindrical Composite Panels," AIAA Journal of Aircraft, 20: 777-783 (September 1983).
20. Environmental Effects on Advanced Composite Materials, 78th Annual Meeting American Society for Testing and Materials, ASTM, (June 1975).
21. Whitney, J. M. and Ashton, J. E., "Effects of Environment on the Elastic Response of Layered Composite Plates," AIAA Journal, 9: 1708-1712 (December 1971).
22. Browning, C. E. "The Mechanisms of Elevated Temperature Property Losses in High Performance Structural Epoxy Matrix Materials After Exposure to High Humidity Environments," Polymer Engineering and Science, 18, 16-24 (January 1978).
23. Browning, C. E., Husman, G. E. and Whitney, J. M., "Moisture Effects in Epoxy Matrix Composites," Composite Materials: Testing and Design (Fourth Conference), ASTM STP 617: 481-496, American Society for Testing and Materials (1977).
24. Tsai, S. W. and Hahn, H. T., Introduction to Composite Materials Westport, Connecticut: Technomic Publishing Company, 1980.

25. Jones, R. M. Mechanics of Composite Materials. New York: McGraw-Hill, 1975.
26. Almorh, B. O. et al. Structural Analysis of General Shells Volume II - User Instructions for STAGSC-1. LMSC-D633073 Applied Mechanics Laboratory, Lockheed Palo Alto Research Laboratory, Palo Alto CA, July 1979.
27. Sobel, L. H. and Thomas K. Evaluation of the STAGSC-1 Shell Analysis Computer Program. WARD - 10331 Westinghouse Advanced Reactors Division, Madison PA, August 1981.
28. Crank, J., The Mathematics of Diffusion (Second Edition), Clarendon Press, Oxford, 1975.
29. Weitsman, Y., "A Rapidly Convergent Scheme to Compute Moisture Profiles in Composite Materials under Fluctuating Ambient Conditions," Environmental Effects on Composite Materials, Volume 2, G. S. Springer Ed., Technomic, 1984, 170-177.
30. Cook, Robert D. Concepts and Applications of Finite Element Analysis (Second Edition). New York: John Wiley and Sons, 1981.
31. Brush, Don O. and Almorh, B. O. Buckling of Bars, Plates and Shells. New York: McGraw-Hill Book Company, 1975.
32. Bushnell, David. Computerized Buckling Analysis of Shells. AFWAL-TR-81-3049. Air Force Wright Aeronautical Laboratory, Wright-Patterson AFB OH, December 1981.
33. Cox, H. L. The Buckling of Plates and Shells. New York: Macmillan Company, 1963.
34. Higgs, D. L. and Vinson, J. R., "Elastic Stability of Generally Laminated Composite Plates Including Hygrothermal Effects," AFOSR-TR-1349, July 1977.
35. Almorh, B. O. and Brogan, F. A., "Numerical Procedures for Analysis of Structural Shells," AFWAL-TR-80-3129, March 1981.

VITA

Michael F. Hermsen was born on August 11, 1959 in Green Bay, Wisconsin. He attended high school at Preble High in Green Bay and completed his first undergraduate degree, B.S. Agricultural Engineering, from the University of Wisconsin - Platteville in December 1981. In March 1983, he entered the Air Force thru the OTS commissioning program. His first assignment was the Air Force Institute of Technology (AFIT). He completed AFIT's engineering conversion program with a B.S. Aeronautical Engineering in March 1985 and was immediately extended to the graduate program. Upon finishing the graduate program at AFIT, he will be stationed at Eglin AFB, Florida.

Permanent Address: 1713 Debra Lane

Green Bay, WI 54302

UNCLASSIFIED

SECURITY CLASSIFICATION OF THIS PAGE

REPORT DOCUMENTATION PAGE

1a REPORT SECURITY CLASSIFICATION UNCLASSIFIED			1b RESTRICTIVE MARKINGS	
2a SECURITY CLASSIFICATION AUTHORITY			3 DISTRIBUTION/AVAILABILITY OF REPORT Approved for public release; distribution unlimited	
2b DECLASSIFICATION/DOWNGRADING SCHEDULE			5. MONITORING ORGANIZATION REPORT NUMBER(S)	
4 PERFORMING ORGANIZATION REPORT NUMBER(S) AFIT/GAE-86M-2			7a. NAME OF MONITORING ORGANIZATION	
6a NAME OF PERFORMING ORGANIZATION School of Engineering		6b. OFFICE SYMBOL (If applicable) AFIT/ENA		7b. ADDRESS (City, State and ZIP Code)
6c ADDRESS (City, State and ZIP Code) Air Force Institute of Technology Wright-Patterson AFB OH 45433			9 PROCUREMENT INSTRUMENT IDENTIFICATION NUMBER	
8a NAME OF FUNDING/SPONSORING ORGANIZATION		8b. OFFICE SYMBOL (If applicable)		10 SOURCE OF FUNDING NOS
8c ADDRESS (City, State and ZIP Code)		PROGRAM ELEMENT NO.		PROJECT NO.
11 TITLE (Include Security Classification) See Box 19		TASK NO.		WORK UNIT NO.
12. PERSONAL AUTHOR(S) Michael F. Hermesen, B.S., 1Lt, USAF				
13a. TYPE OF REPORT MS Thesis		13b. TIME COVERED FROM _____ TO _____		14 DATE OF REPORT (Yr. Mo. Day) 1986 March
15. PAGE COUNT 154				
16. SUPPLEMENTARY NOTATION				
17 COSATI CODES			18 SUBJECT TERMS (Continue on reverse if necessary and identify by block number)	
FIELD	GROUP	SUB GR	Composites, Cylindrical Panel, Shell Analysis, Finite Elements, STAGSC-1, Material Degradation, Cutouts at Various Locations	
11	04			
19. ABSTRACT (Continue on reverse if necessary and identify by block number)				
Title: The Collapse of Composite Cylindrical Panels with Various Cutout Locations Considering Material Degradation				
Thesis Chairman: Dr. Anthony N. Palazotto				
Approved for public release: 1AW AFR 180-7. Lynn E. WOLAVER - 9 May 86 Dean for Research and Professional Development, Air Force Institute of Technology (AFIT), Wright-Patterson AFB OH 45433				
20 DISTRIBUTION/AVAILABILITY OF ABSTRACT CLASSIFIED/UNLIMITED <input checked="" type="checkbox"/> SAME AS RPT <input type="checkbox"/> DTIC USERS <input type="checkbox"/>			21 ABSTRACT SECURITY CLASSIFICATION UNCLASSIFIED	
22a NAME OF RESPONSIBLE INDIVIDUAL Dr. Anthony N. Palazotto			22b TELEPHONE NUMBER (Include Area Code) 513-255-3517	22c OFFICE SYMBOL AFIT/ENA

ABSTRACT

An analytical study, using the STAGSC-1 computer code, was conducted on a graphite/epoxy (AS4/3501) composite cylindrical panel acting under compressive loading considering cutouts positioned at critical locations within the panels surface area. The study also investigated the material degradation effects of temperature and moisture on the collapse load of these cylindrical panels. Two temperatures (80 and 250 °F), in both a symmetric and unsymmetric moisture condition, were investigated. The overall material degradation characteristics were investigated by degrading the E_2 and G_{12} moduli of the individual plies.

It was found that the effects of moisture and temperature (material degradation effects) can greatly reduce the collapse load of the cutout panel. A 15% decrease in the collapse load occurred at the saturated moisture conditions and elevated temperatures. The material degradation effects were found to produce the same results no matter where the cutout was located. The panel with cutouts was less affected, at the saturated moisture condition and elevated temperature, than that of a panel with no cutout.

It was also found that the collapse load, as expected, was dependent upon the location of the cutout within the panel. There was a decrease in the collapse load by as much as 26.2% when the cutout was moved from the center of the panel to a position closer to the side edge. There was very little change, 1%, when the cutout was positioned closer to the loading edge of the panel. Ply layup was also of great importance. There was a 21.3% increase or decrease in the collapse load if a certain ply layup (0/+45/90)_s, (symmetrically exchanging of the second and third plies) was chosen for the cutout positioned near the side supports.

END

10-86

DTIC